UNIVERSITÀ DEGLI STUDI DI MILANO

Department of Food, Environmental and Nutritional Sciences (DeFENS)

PhD Course in Food Systems

XXX Cycle

Food Packaging Innovations – Electrochemical Nanosensors for Primary Aromatic Amines Quantification

Supervisor: Dr. Stefano Farris

Masoud Ghaani

R10978

2018

CONTENTS

LIST OF FIGURES 5
LIST OF TABLES 8
ABSTRACT 9
RIASSUNTO 11

1. INTRODUCTION 13
1.1. Overview 14
1.2. Electrochemical Sensors 15
1.3. Electrodes in electrochemical sensors 15
1.3.1. Counter electrode 15
1.3.2. Reference electrode 15
1.3.3. Working electrode 16
1.4. Modified working electrodes 16
1.4.1. Selectivity 16
1.4.1.1. Enzymatic electrochemical biosensors 16
1.4.1.2. Molecularly imprinted polymers (MIP) based electrochemical sensor 17
1.4.2. Sensitivity 18
1.4.2.1. Nano modified electrodes 18
1.4.2.1.1. Nanoparticles 19
1.4.2.1.2. Nanofibers 20
1.4.2.1.3. Nanoplates 21
1.5. Applications of electrochemical sensors 23
1.5.1. Sensors in food industry 23
1.5.2. Sensors in food packaging 29
1.6. References 32
2. AIMS OF THE THESIS 43
3. CHAPTER 1: On the origin of primary aromatic amines in food packaging materials 44
3.1. Introduction 45
3.2. Fundamental chemistry underlying the formation of primary aromatic amines (PAAs) 49
3.3. Conclusions 54
3.4. References 56
4. CHAPTER 2: Determination of 2,4-diaminotoluene by a bionanocomposite modified glassy carbon electrode 58
4.1. Experimental part 59
4.1.1. Preparation of modified electrodes 59
4.1.2. Morphological characterization of the electrodes' surface 59
4.1.3. Real sample analysis 59
4.2. Results and discussion 60
4.2.1. Morphological characterization of modified GCEs 60

4.2.2. Electrochemical behavior of TDA on the electrode surface 61
4.2.3. Influence of scan rate 62
4.2.4. Effect of pH 66
4.2.5. Chronoamperometry measurements 67
4.2.6. Amperometric tests 68
4.2.7. Potential interference of other compounds 70
4.3. Real sample analysis 70
4.4. Conclusion 71
4.5. References 73
5. CHAPTER 3: Bionanocomposite modified glassy carbon electrode for the determination of 4,4'-methylene diphenyl diamine 74
5.1. Experimental part 75
5.1.1. Preparation of modified electrodes 75
5.2. Results and discussion 75
5.2.1. Characterization of the MWCNTs-CS-AuNPs composite 75
5.2.2. Electrochemical behavior of MDA on MWCNTs-CS-AuNPs/GCE 76
5.2.3. Effect of pH value 77
5.2.4. Electrocatalytic oxidation of MDA at the MWCNTs-CS-AuNPs/GCE 78
5.2.5. Chronoamperometric Measurements 81
5.2.6. Amperometric studies of electrocatalytic oxidation of MDA at the MWCNTs-CS-AuNPs/GCE surface 83
5.2.7. Real sample analysis 84
5.3. Conclusion 85
5.4. References 86
6. CHAPTER 4: Development of a new electrochemical sensor obtained by electropolymerization of nanocomposite molecularly imprinted biopolymer for determination of 4,4'-methylene diphenyl diamine 87
6.1. Experimental part 88
6.1.1. Fabrication of MWCNTs modified GCE 88
6.1.2. Preparation of MIP and non-imprinted modified electrodes 88
6.2. Result and discussion 88
6.2.1. Surface Morphology 88
6.2.2. Electrochemical responses 89
6.2.3. Optimization of analytical conditions 91
6.2.3.1. Effect of scan cycles 91
6.2.3.2. Effect of elution time 92
6.2.3.3. Effect of incubation time 93
6.2.3.4. Effect of mole ratio of template molecules to functional monomers 94
6.2.3.5. Effect of pH 95
6.2.4. Performance of the imprinted MIP/MWCNTs/GCE sensor 96
6.2.4.1. Sensitivity 96
6.2.4.2. Selectivity and reproducibility 97
6.2.5. Real sample analysis 98

6.3. Conclusion 99
6.4. References 100
7. Conclusions 101
8. Materials & Methods 102
8.1. Reagents 102
8.2. Apparatus and methods 102
Appendix 1: CONFERENCE ABSTRACTS 103
Appendix 2: PUBLICATIONS 109

LIST OF FIGURES

Introduction	
Figure 1. The ISO classification of nanoomaterials. Included as nano-objects are nanoparticles, nanofibers, and nanoplates. Figure adapted from (39).	19
Figure 2. Schematic representation of on-line sensors in a food-processing line. Figure adapted from (71).	24
Chapter 1	
Figure 1. (a) Schematic representation of a PU adhesive-based laminate packaging material (3-layer structure). (b) Sketch on the formation of poly(urea) in PU adhesive-based multilayer packaging materials wound in reels. Red-white spheres: water molecule; Ar-NCO: aromatic isocyanate monomers; Ar-NH_2: aromatic amines.	45
Figure 2. Schematic reaction mechanisms between: an isocyanic group and a hydroxyl group for the formation of an urethane linkage (scheme 1); an isocyanic monomer and a water molecule to yield a primary amine (scheme 2a); a primary amine and an isocyanic monomer to yield an urea (scheme 2b); an urethane group and an isocyanic monomer leading to an allophanate linkage (scheme 3); and an ureic group and an isocyanic monomer to yield a biuret linkage (scheme 4).	47
Figure 3. (a) Illustrative drawing of the formation of the isocyanic monomer from the thermal cleavage of the allophanate linkage. (b) Rendering image representing the potential migration of PAAs from the packaging to the food matrix. Red-white spheres: water molecules; black-blue spheres: representative aromatic amine; yellow arrows: migration of the isocyanic monomer; cyan arrows: washing-out effect of environmental moisture.	52
Chapter 2	
Figure 1. FE-SEM surface images of: (a) MWCNTs/GCE, (b) MWCNTs-CS/GCE, (c) AuNPs/GCE and (d) AuNPs/MWCNTs-CS/GCE.	60
Figure 2. Cyclic voltammograms in phosphate buffer (pH 7.0) at a 50 mV/s scan rate of (from down-right to up-left direction): (a) bare GCE, (b) MWCNTs/GCE, (c) MWCNTs-CS/GCE, and (d) AuNPs/MWCNTs-CS/GCE in the presence of 500 µM TDA.	62
Figure 3. Cyclic voltammograms of AuNPs/MWCNTs-CS/GCE in a phosphate buffer (pH 7.0) containing 500 µM TDA at different scan rates (100- 800 mV/s). The electrocatalytic peak current (I_p) variation as a function of the square root of sweep rate is shown in the inset.	63
Figure 4. Linear sweep voltammogram of AuNPs/MWCNTs-CS/GCE in a phosphate buffer solution (pH 7.0) containing 500 µM TDA at 100 mV/s. The Tafel plot derived from the linear sweep voltammogram is shown in the inset.	64
Figure 5. Experimental data (black dots) and linear regression of anodic peak potential (E_{pa}) versus natural logarithm of the scan rate [ln(v)].	65

Figure 6. Effect of the pH (solution containing 500 µM of TDA in 0.1 M Britton-Robinson buffer) on the anodic peak potential (E, –□–) and current (I, –●–) on the AuNPs/MWCNTs-CS/GCE. 66

Figure 7. Chronoamperograms obtained at AuNPs/MWCNTs-CS/GCE in PBS (pH 7.0) for different concentrations of TDA (0.04–4.0 mM) of TDA. The red-marked chronoamperogram is the blank (i.e., obtained in the absence of TDA). Insets: (a) Plots of I vs. $t^{-1/2}$ obtained from the chronoamperograms (TDA concentration 0.04–4.0 mM). (b) Plot of the slope of the straight lines against TDA concentration. (c) Dependence of I_{cat}/I_l on $t^{1/2}$ derived from the chronoamperograms (TDA concentration 0.04–4.0 mM). 68

Figure 8. Amperometric response at the rotating AuNPs/MWCNTs-CS/GCE at 570 mV in 20 mL phosphate buffer (pH 7) (TDA concentration 0.44–819.56 µM). The variation of the amperometric current against the TDA concentration is shown in insets (a) (0.44–53.60 µM) and (b) (53.60–819.56 µM). Inset (c) shows the stability of the response of the AuNPs/MWCNTs-CS/GCE for 1300 s (TDA concentration 550 µM). 69

Figure 9. Amperometric trace displaying the current response of the AuNPs/MWCNTs-CS/GC electrode after the sequential addition of the PAAs TDA, MDA, aniline, and the two additives Irganox® 1010 and Irgafos® 168. 71

Chapter 3

Figure 1. SEM images observed for (a) MWCNTs, (b) MWCNTs-CS and (c) MWCNTs-Cs-AuNPs 76

Figure 2. Cyclic voltammograms in B-R buffer (pH 10) at scan rate 50 mV/s in the presence of 500 µM MDA: (a) bare GCE, (b) MWCNTs/GCE, (c) MWCNTs-CS/GCE, (d) MWCNTs-CS-AuNPs/GCE. 77

Figure 3. Effect of pH on the oxidation peak current and oxidation peak potential in the response to 500 µM of MDA on the surface of MWCNTs-CS-AuNPs/GCE 78

Figure 4. 6 Cyclic voltammograms of MWCNTs-CS-AuNPs/GCE in a Britton-Robinson buffer solution (pH 10.0) containing 500 µM MDA at different scan rates (5–40 mV/s). The inset demonstrates the electrocatalytic peak current (I_p) variation as a function of the square root of sweep rate. 79

Figure 5. Linear sweep voltammogram of MWCNTs-CS-AuNPs/GCE in a Britton-Robinson buffer solution (pH 10.0) containing 500 µM MDA at 25–40 mV/s. Inset shows tafel plot derived from the linear sweep voltammograms. 80

Figure 6. Experimental data (black dots) and linear regression of anodic peak potential (E_{pa}) versus natural logarithm of the scan rate [ln(v)]. 81

Figure 7. Current response over time of the MWCNTs-CS-AuNPs/GCE in 0.1 M B-R buffer solution (pH 10.0) containing different concentrations of MDA (0.005 – 0.4 mM) during the chronoamperometric measurements (potential 700 mV). Numbers 1–8 correspond to the different MDA concentrations. Insets: (a) chronoamperograms of the intensity (I) as a function of the reciprocal square root of time ($t^{-1/2}$); (b) linear plot of the slopes of the eight straight lines in the inset (a) against the MDA concentration. 82

Figure 8. Amperometric responses at a rotating MWCNTs-CS-AuNPs/GCE held at 700 mV in different concentrations of 0.49 to 261.18 µM of MDA. The variation of amperometric current vs. MDA concentration in the range of 0.49–10.14 µM (inset a), 10.14–94.9 µM (inset b) and 94.90–261.18 µM (inset c). Inset d shows the stability of the response of MWCNTs-CS-AuNPs/GCE to 5 µM MDA during 3310 s. 84

Chapter 4

Figure 1. SEM image of Multi-walled carbon nanotubes modified glassy carbon electrode (MWCNTs/GCE) 89

Figure 2. DPV responses of the MIP/MWCNTs/GCE: (a) before extraction and (b) after extraction. 89

Figure 3. MIP/MWCNTs/GCE (a), NIP/MWCNTs/GCE (b), bare GCE (c), MIP/GCE (d) in 20 mL B-R buffer (pH 11) containing 500 µM MDA. 91

Figure 4. Effect of different number of cycles in electropolymerization process on the anodic peak currents of MDA (500 µM). 92

Figure 5. Effect of elution time (2 min, 5 min, 10 min, 15 min, and 20 min) on the current response of the sensor to MDA in the MIP layer. 93

Figure 6. Effect of incubation time (5 min, 10 min, 15 min, 20 min, and 30 min) on the current response of the sensor to MDA (500 µM). 94

Figure 7. Effect of different concentration of the MDA in electropolymerization process on the current response of the sensor to MDA (500 µM). 95

Figure 8. Effect of the pH solution. The pH effects on the anodic peak potentials and currents of 500 µM of MDA in Britton-Robinson buffer solution on the MIP/MWCNTs/GCE 96

Figure 9. (A) DPV responses of the MIP/MWCNTs/GCE. MDA concentrations: 0.5, 1, 10, 10, 25, 50, 60, 75 and 100 µM. (B) the calibration line of the response peak current vs. the MDA concentration. 98

LIST OF TABLES

Introduction	
Table 1. Application of electrochemical sensors in fish products.	24
Table 2. Application of electrochemical sensors in flour products.	25
Table 3. Application of electrochemical sensors in juice products.	25
Table 4. Application of electrochemical sensors in meat products.	26
Table 5. Application of electrochemical sensors in milk products.	27
Table 6. Substances possibly migrating from conventional non-plastic packaging materials to the food.	30
Table 7. Monomer/oligomer possibly migrating from plastic-based packaging materials to the food.	30
Chapter 1	
Table 1. Relative reactivity of active hydrogen compounds against isocyanate (data normalized according to the rate of the isocyanate/water reaction, adapted from 23).	50
Table 2. Thermal dissociation temperatures of linkages found in polyurethanes (adapted from 23, 31, and 32).	51
Chapter 2	
Table 1. Comparison of the electrocatalytic oxidation peak current (Ip) of TDA (500 µM) at pH 7.0 on the bare GC electrode and according with the different surface modifications (see the main text for details).	62
Table 2. Amount of added (spiked) and measured TDA at the AuNPs/MWCNTs-CS/GCE surface, with the resulting recovery percentage after the migration test using the acidic food simulant (simulant B) at typical sterilization conditions (121 ˚C for 20 minutes).	71
Chapter 3	
Table 1. Comparison of the electrocatalytic oxidation peak current (I_p) of MDA (500 µM) on various electrode surfaces at pH 10.0.	77
Table 2. Amount of added (spiked) and measured TDA at the MWCNTs-CS-AuNPs/GCE surface, with the resulting recovery percentage after the migration test using the acidic food simulant (simulant B) at typical sterilization conditions (121 ˚C for 20 minutes).	85
Chapter 4	
Table 1. Comparison of the electrocatalytic oxidation peak current (I_p) of MDA (500 µM) on various electrode surfaces at pH 11.0.	90
Table 2. Amount of added (spiked) and measured TDA at the MIP/MWCNTs/GCE surface, with the resulting recovery percentage after the migration test using the acidic food simulant (simulant B) at typical sterilization conditions (121 ˚C for 20 minutes).	99

ABSTRACT

Primary aromatic amines (PAAs) are substances that can be transferred from food packaging materials into foodstuffs and are "possibly carcinogenic to humans". The formation of PAAs from multilayer packaging materials consisting of aromatic polyurethane (PU) adhesives occurs from the reaction between residual isocyanic monomers (the most widely used of which are 2,4-toluene diisocyanate – TDI and 4,4'-methylene diphenyl diisocyanate – MDI) that have migrated to the surface of the inner layer of the package and water molecules making contact with the same plastic surface. However, for foods subjected to thermal treatments, an alternative formation of PAAs should also be taken into consideration. Due to the detrimental effect of the temperature, some secondary bonds (namely allophanate and biuret bonds) displaced on the main PU backbone may be disrupted, originating neo-formed isocyanic monomers (such as TDI and MDI). The migration of these monomers from the adhesive layer across the inner sealing film can lead to PAAs as soon as they come into contact with the water molecules of the liquid or high a_w packaged food. Although the existence and the mechanisms of the formation of allophanate and biuret linkages during the polymerization process with poly-isocyanates has been known for a long time, the negative impact on public health possibly arising from the migration of the neo-formed isocyanic monomers into the foods during thermal treatments seems to have not been fully perceived, with special regard to preservative heat treatments such as pasteurization and sterilization.

Regardless of the origin, the quantification of the risks associated with the potential formation of PAAs must be made by strict compliance with the provisions included in the current European legislation. However, both the non-selectivity of the widely adopted spectrophotometric method and the number of drawbacks associated with the more sophisticated techniques used at academic level and highly specialized laboratories impose the necessity for alternative analytical tools for the PAAs quantification.

In this thesis, after an introductive part on electrochemistry and the use of electrochemical sensors in food science, an in-depth review of the issues associated to the PAAs migration possibly occurring from food packaging materials is presented in chapter 1. In the following three chapters, the focus has been addressed to the implementation of electrochemical routes for the determination of PAAs by the development of modified electrochemical sensors characterized by high selectivity and sensitivity. More specifically, chapter 2 deals with the fabrication of a modified glassy carbon electrode (GCE) for the selective quantification of TDA. Different levels of complexity were investigated by modifying the electrode's surface

with multi-walled carbon nanotubes (MWCNTs), MWCNTs in chitosan (CS) and using gold nanoparticles (AuNPs).

In chapter 3 is described the development of a nanosensor for the MDA determination using multi-walled carbon nanotubes, chitosan, and gold nanoparticles for the modification of a glassy carbon electrode (MWCNTs-CS-Au/GCE).

In chapter 4, a new electrochemical sensor is proposed to determine MDA using a templating-based method known as ‘molecularly imprinted polymer’, together with multi-walled carbon nanotubes as conductive nanoparticles (MIP/MWCNTs/GCE). The three electrochemical sensors have been described in detailed fashion as far as both a polymer science perspective and analytical performance are concerned.

RIASSUNTO

Le ammine aromatiche primarie (AAP) sono sostanze cancerogene per l'uomo che possono migrare dai materiali destinati all'imballaggio all'alimento confezionato. La formazione delle AAP nei materiali di imballaggio riguarda in particolare le soluzioni multi-strato (materiali laminati) ottenuti mediante l'utilizzo di adesivi poliuretanici (PU). Secondo il meccanismo di reazione più noto, la formazione delle AAP avviene attraverso la reazione tra un monomero isocianico residuo di reazione (i due più rappresentativi sono il 2,4-toluene diisocianato – TDI e il 4,4'-metilene difenil diisocianato – MDI) e molecole di acqua che si trovano all'interno della confezione. Tuttavia, per quegli alimenti confezionati che subiscono trattamenti termici, è necessario considerare una via alternativa per la formazione di AAP. Infatti, a causa dell'elevata temperatura, alcuni legami secondari (biureti e ancor di più allofanati) presenti lungo la catena principale dell'adesivo PU possono essere spezzati, dando origine a monomeri isocianici di neo-formazione. La migrazione di tali monomeri dall'adesivo allo strato più interno della confezione (di solito polietilene, PE) può portare alla formazione di AAP non appena il monomero isocianico incontra le molecole di acqua presenti all'interno della confezione (soprattutto per alimenti ad elevata a_w). Nonostante la presenza dei legami allofanati e biureti lungo la catena poliuretanica sia nota da tempo, il potenziale impatto negativo sulla salute dei consumatori a causa di trattamenti termici impropri sembra non sia stato percepito adeguatamente, in particolare in merito a trattamenti di conservazione come pastorizzazione e sterilizzazione.

A prescindere dall'origine, la quantificazione del rischio associato alla formazione potenziale di AAP deve essere fatta rispettando le indicazioni contenute nel regolamento europeo 10/2011. Tuttavia, la non selettività dei metodi spettroscopici e il numero di problematiche associate alle più sofisticate tecniche usate a livello accademico o presso laboratori altamente specializzati, impone la necessità di individuare o sviluppare metodi analitici alternativi utili per la quantificazione delle AAP soprattutto a livello industriale.

In questa tesi di dottorato, dopo una parte introduttiva sull'elettrochimica e sull'uso di sensori elettrochmici nel settore alimentare, nel capitolo 1 è presentata un'ampia e approfondita recensione delle problematiche associate alla possibile migrazione delle AAP dai materiali di imballaggio. Nei tre capitoli successivi, l'attenzione è stata rivolta all'implementazione di strategie elettrochimiche per la determinazione delle AAP attraverso lo sviluppo di sensori elettrochimici modificati, caratterizzati dall'elevata sensibilità e selettività. Più specificatamente, il capitolo 2 presenta lo sviluppo di un elettrodo 'glassi-carbon' (GCE) per

la determinazione selettiva dell'ammina primaria nota come TDA. L'effetto di modificazioni superficiali a diverso grado di complessità è stato investigato impiegando diverse configurazioni, come ad esempio l'uso di nanotubi di carbonio 'multi-walled' (MWCNTs), nanotubi di carbonio 'multi-walled' in chitosano (CS) e utilizzando nanoparticelle d'oro (AuNPs).

Nel capitolo 3 si descrive, invece, lo sviluppo di un nanosensore specificatamente previsto per la determinazione della MDA, utilizzando lo schema presentato precedentemente per la determinazione della TDA.

Nel capitolo 4, invece, è presentata una strategia nuova e alternativa alle precedenti per la determinazione della MDA, ovvero un metodo di templaggio noto come 'molecularly imprinted polymers' (MIP), facendo uso simultaneo dei nanotubi di carbonio 'multi-walled', del chitosano come fase biopolimerica e nanoparticelle d'oro. I tre sensori elettrochimici descritti nella presente tesi di dottorato sono stati caratterizzati approfonditamente sia da un punto di vista polimerico che per quanto concerne la performance analitica.

1. INTRODUCTION

1.1. Overview

In the history of human, food always had a vital role for civilizations, thus food related aspects such as “quality” and “safety” are of primary importance since they may greatly affect people’s everyday lives’. Likewise, in the new era, one of the most important parameters that can attract customers’ trust is the endeavor of manufacturers to produce foodstuffs with high quality and safety. Hence, in the recent years, different chemical, physical, and microbiological analyses have been set up in the attempt to assess quantitatively the quality of food. Concerning chemical analyses and particularly chemical analytical analyses, the most adopted techniques include spectrophotometry (1), chromatography (2), titration (3), electrophoresis (4), chemiluminescence (5), and fluorimetric (6). Notwithstanding that each of these methods has its own peculiarities and advantages, they do not allow an easy and rapid monitoring due to intrinsic complexity, although to a different extent. In turns, this forces to seek for specialized operators. Other drawbacks are represented by extended time of analysis and expensive instrumentation. Therefore, the need for rapid, reliable, user-friendly, and low-cost approaches has recently been stressed, especially for quality control purposes within the food industry lines (7–9). Over recent years, the fabrication of smart sensors has gained much attention due to its potential to replace more sophisticated and complex techniques.

A sensor is a device or system with control and processing electronics, an interconnection network, and a software. Sensors are used to detect, locate, or quantify energy or matter, by giving a signal for the detection or measurement of a physical or chemical property to which the device responds. In practice, a sensor replies to a chemical or physical quantity to make a quantifiable output that is proportional to the measure. Most sensors are made up of four major components (Scheme 1). (i) The first is a receptor, i.e., the sensing part of the sensor, represented by a sampling area (generally a chemo-selective coating) where the surface chemistry occurs. Here, the analytical information is obtained from the adsorption of the target analyte on the recognition layer. The energy variation associated with detecting the analyte induces a change of a property of the receptor in terms of, for example, redox potential, pH, temperature, or light. (ii) The second is the transduction element, i.e., the measuring part of the sensor (e.g., an electrode), which is capable of transforming the energy variation and carrying the physical or chemical information into a useful analytical signal (e.g., electrical, optical, thermal, or chemical). Next are (iii) the signal processing electronics, and (iv) a signal display unit. The ideal sensor should possess the following characteristics: (i) specificity for the target

species (i.e., selectivity); (ii) sensitivity to changes in target-species concentrations; (iii) fast response time; (iv) extended lifetime of at least several months; and (v) small size (miniaturization), with the possibility of low-cost manufacture (10).

In recent years, different types of sensors intended for food applications have been developed, such as luminescence sensors (11,12) and electrochemical sensors (13–17). In luminescence sensors the emitted fluorescence, phosphorescence or chemiluminescence signals are measured after the analyte is immobilized in a suitable solid support, giving origin to the expression solid-phase luminescence (SPL) or to its equivalent solid-matrix luminescence (SML). Under certain conditions, these analytical signals can be related to the concentration of analyte in the sample. Due to great importance of electrochemical sensors in food related fields, this branch of sensors is investigated more deeply in the following section (10).

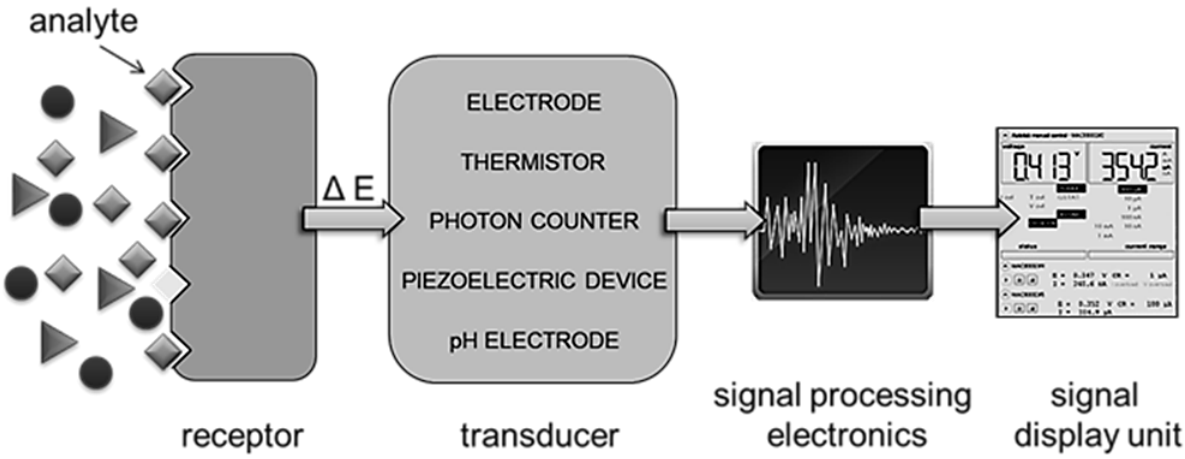

Scheme 1. Representation of the working principle and components of a sensor.

1.2. Electrochemical Sensors

Electrochemistry is the branch of chemistry concerned with the interrelation of electrical and chemical effects. A large part of this field deals with the study of chemical changes caused by the passage of an electric current and the production of electrical energy by chemical reactions (18). Electrochemical sensors represent an important subclass of chemical sensors that work based on the electrochemistry principles. In this type of sensors, the transducer is the electrode (19). A typical electrochemical sensor consists of 3 main electrodes, sensing (working electrode), counter, and reference electrodes, which are all connected to a potentiostat device. The working principle of electrochemical sensors is based on redox reactions that take place at the electrode/analyte interface upon applying a voltage by means of a potentiostat. The

electrons transfer between electrode and electroactive species gives origin to a current that is proportional to the concentration of the analyte. The potentiostat is generally connected to a display unit that usually is a computer. This computer is used to display the variations of the current and voltage during the experiment and to control the device by a dedicated software with a special electrochemical method (10,18,20,21). An overall view of an electrochemical sensor is shown in Scheme 2.

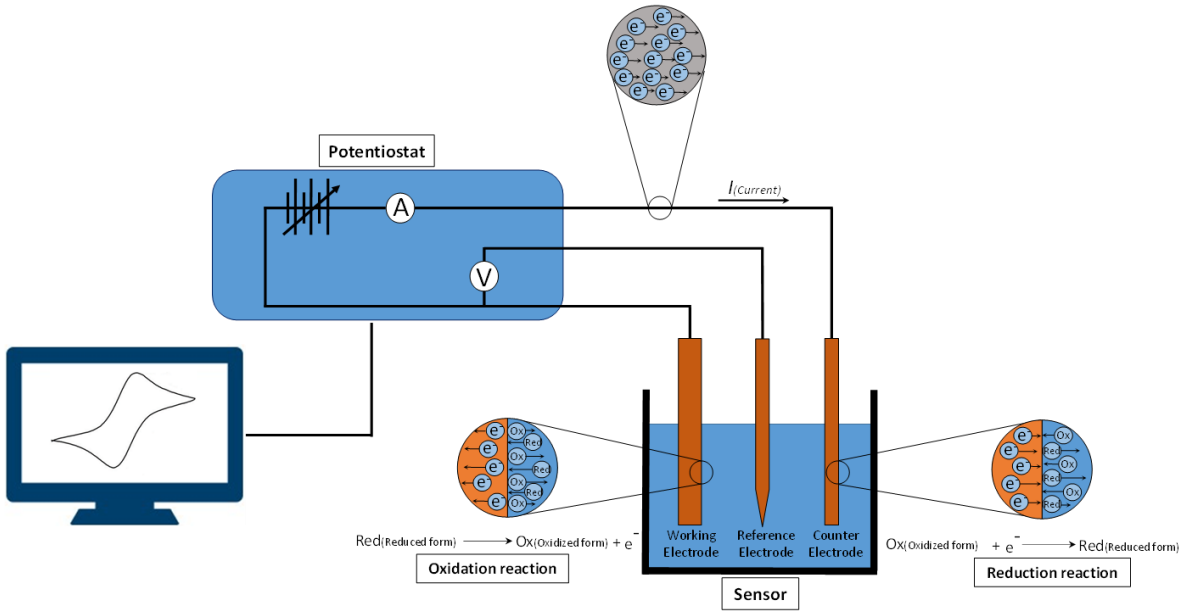

Scheme 2. Schematic representation of an electrochemical sensor.

1.3. Electrodes in electrochemical sensors

As mentioned previously, an electrode in electrochemical sensors works as a transducer. Nowadays, most of electrochemical sensors consist of three main electrodes, that is, counter, reference, and working electrodes.

1.3.1. Counter electrode

A closed electric circuit is an essential prerequisite to measure an electric entity (22). In an electrolysis cell (including all 2- and 3-electrode cells) a current flows through the working electrode and the counter electrode. Generally, a counter electrode is be made up of a conducting and inert material, for instance graphite or noble metals like platinum (23).

1.3.2. Reference electrode

Measuring the actual (experimental) potential must be done against a reference potential, which must be stable and well known. A proper reference electrode must have some fundamental properties, such as a stable potential and chemical reaction, a well-known half

reaction (i.e., either the oxidation or the reduction reaction component of a redox reaction), ease of construction, and must not interfere with the measurement of the analyte. There are few half reactions that have these properties and consequently there the number of available reference electrodes is limited. The most widely used are silver–silver chloride (Ag-AgCl) electrode and the saturated calomel (Hg_2Cl_2) electrode (24).

1.3.3. Working electrode

The working electrode monitors the redox reaction that occurs at the working electrode/analyte interface after applying a voltage by the potentiostat (Scheme 2). The electrons transfer between electrode and electroactive species gives origin to a current that is proportional to the concentration of the analyte (10). A number of working electrodes have been used in electrochemical sensors, such as mercury, glassy carbon, carbon paste, platinum, and gold electrodes. Due to two the restricted selectivity and sensitivity of bare working electrodes, various modifications (both chemical and physical) have been suggested during the last years to enhance the ultimate analytical performance of the electrode. In the following sections, different types of modified electrodes and modifiers are briefly surveyed.

1.4. Modified working electrodes

Modified working electrodes are generally modified via an extra layer that eventually leads to higher sensitivity and selectivity of the electrochemical device (19).

1.4.1. Selectivity

In the current years, in order to increase the selectivity of sensors, different chemical and biological compounds have been used for the electrode modification. Here, two main groups of these compounds are described:

1.4.1.1. Enzymatic electrochemical biosensors

Enzymes are biological macromolecules consisting of a sequence of amino acids with a catalyst function, that is, they accelerate chemical reactions. One of the most interesting properties of enzymes is the inherent selectivity for special compounds (in a more specific way, enzymes exhibit high specificity for a given substrate). Due to this special property, enzymes have been largely used over the last years for modifying the surface of working electrodes to boost the selectivity of the sensors (25). For instance, Dervisevic et al. tried to control the freshness of fish products by using a new xanthine biosensor. They immobilized the enzyme xanthine oxidase on the polymeric mediator/MWCNT nanocomposite layer for constructing the sensor. Using the xanthine oxidase as a modifier had a great impact on the selectivity of the

sensor (linear range: $2 \times 10^{-6} – 48 \times 10^{-6}$ M; limit of detection: 0.12×10^{-6} M). The authors also specified that the modified biosensor had high storage stability and acceptable anti-interference capability (26). In another project, Apetrei et al. immobilized the enzyme tyrosinase on the carboxyl functionalized single-walled carbon nanotubes modified electrode for tyramine determination. They used differential pulse voltammetry for calculating the linear range and the limit of detection of the sensor ($5 \times 10^{-6} – 180 \times 10^{-6}$ M and 6.2×10^{-7} M, respectively) and applied the sensor to determine tyramine in pickled and smoked fish samples. The authors also specified that this sensor had an excessive ability for selective, sensitive and rapid determination of tyramine in other food samples (27). Nasirizadeh et al. used the enzyme catalase to fabricate an electrochemical biosensor based on a modified gold electrode for the determination of hydrogen peroxide in different beverage samples. In this research, the authors used differential pulse voltammetry to calculate two linear ranges ($1.0 \times 10^{-6} – 21.5 \times 10^{-6}$ M and $21.5 \times 10^{-6} – 115.0 \times 10^{-6}$ M) and the limit of detection (0.25×10^{-6} M) of the sensor. The authors reported that the sensor exhibited high sensitivity, good repeatability, and a wide linear range in compared to other similar works on the quantification of hydrogen peroxide in real samples (17).

1.4.1.2. Molecularly imprinted polymers (MIP)-based electrochemical sensors

Molecularly imprinted polymers (MIPs) are referred to as those polymers that have been produced by polymerization and templated (imprinted) with a template agent represented by the analyte that, after polymerization, is then removed (thereby originating the templated structure). The final MIP polymer contains cavities that are complementary to the template molecules. The high specificity and stability of MIPs make them a promising alternative to enzymes, antibodies and other natural receptors usually used in the sensor technology. MIP-modified electrodes have been used as the main transducer in several researches (28,29). For instance, Cui et al. developed an electrochemical sensor for detecting trace amounts of propyl gallate. As the first step, they modified the surface of the glassy carbon electrode by PtAu bimetallic nanoparticles-capped graphene-carbon nanotubes composites, then they deposited a MIP layer via electropolymerization of an o-phenylenediamine membrane in the presence of propyl gallate molecules as template. To increase the performance of the sensor, various parameters, such as scan cycles, incubation time, molar ratios of template molecules to functional monomers, and extraction time were optimized. In this project, the authors reported a limit of detection of 2.51×10^{-8} M and a linear range of $7 \times 10^{-8} – 1 \times 10^{-5}$ M. Moreover, the application of the proposed sensor in real sample was assessed in three different kinds of

vegetable oils. The results demonstrated that the sensor is able to provide reliable information even in multi-components real samples (30). Pacheco et al. fabricated a selective and sensitive MIP electrochemical sensor for the detection of ochratoxin A (OTA). In this project the researchers used a glassy carbon electrode as the main working electrode, which was modified using multiwalled carbon nanotubes (MWCNTs) and polypyrrole (PPy) MIP layer, respectively. The imprinted PPy film was prepared by electropolymerization of pyrrole in the presence of OTA as the template molecule via cyclic voltammetry (CV). The OTA molecules have been removed later by using 1% trimethylamine solution (in methanol). The researchers reported an ultimate linear range of 0.05×10^{-6} to 1.0×10^{-6} M and a limit of detection of 0.0041×10^{-6} M. In the last part of their work, the proposed sensor has been used successfully to measure the concentration of the analyte in beer and wine. The authors stated that the recoveries of the sensor were between 84 and 110% (16).

1.4.2. Sensitivity

Sensitivity, i.e. the measure of a signal magnitude, is a relevant parameter for all types of analytical methods, including electrochemical sensors. It allows characterizing the analytical performance of the sensor, while making possible to define its detection limit, a measure of the smallest concentration that can be determined with a specified precision or reproducibility, described as signal-to-noise ratio (S/N). Improving the sensitivity of electrochemical sensors is a goal for many different applications, because this would allow to detect smaller amount of the targeted analyte. Among different strategies, using nano-sized entities (e.g., nanoparticles) to modify the electrode surface is one of the most common approaches to increase the sensitivity of the sensor.

1.4.2.1. Nano-modified electrodes

Accordingly to the most widely accepted (though non-exhaustive) definition, nanotechnology relates to objects having at least one dimension between 1 and 100 nm. In the sizes below 100 nm, especially lower than 10 nm, these materials show some novel properties different from the bulk sized materials, such as enhanced reactivity and catalytic activity, faster electron/ion transport, pronounced changes in thermal and optical properties, enhanced plasticity, negative refractivity and novel quantum mechanical properties (31). These special properties are not only because of the size of the nanomaterials. Nanostructures are deeply different forms of matter than simple chemicals. Their size and organization frequently take advantage of the quantum mechanical properties of these structures to have unique properties.

A simple example is the extraordinary fluorescence property and photostability of the so called "quantum dots", which cannot be explained in terms of the elemental composition alone (32). Since nano-sized materials have a wide spectrum of application in different fields like chemistry, physics, biology, and engineering, it can be concluded that nanotechnology is an interdisciplinary discipline (33). In the current years, nanotechnology also had a huge influence in the field of analytical chemistry. The search in the literature demonstrated that different kinds of nano-objects, such as silver nanoparticles (34), gold nanoparticles (35), carbon nanotubes (36), gold nanowires (37), and graphene with its derivatives (38) have a great potential for applications in the analytical chemistry field, including electrochemical sensors. The main reason of using nano-objects is to improve the overall efficiency of the sensors by specifically increasing their sensitivity.

Nano-objects can be grouped in three different subclasses depending on their shape: i) nanoparticles, ii) nanofibers, and iii) nanoplates (Figure 1).

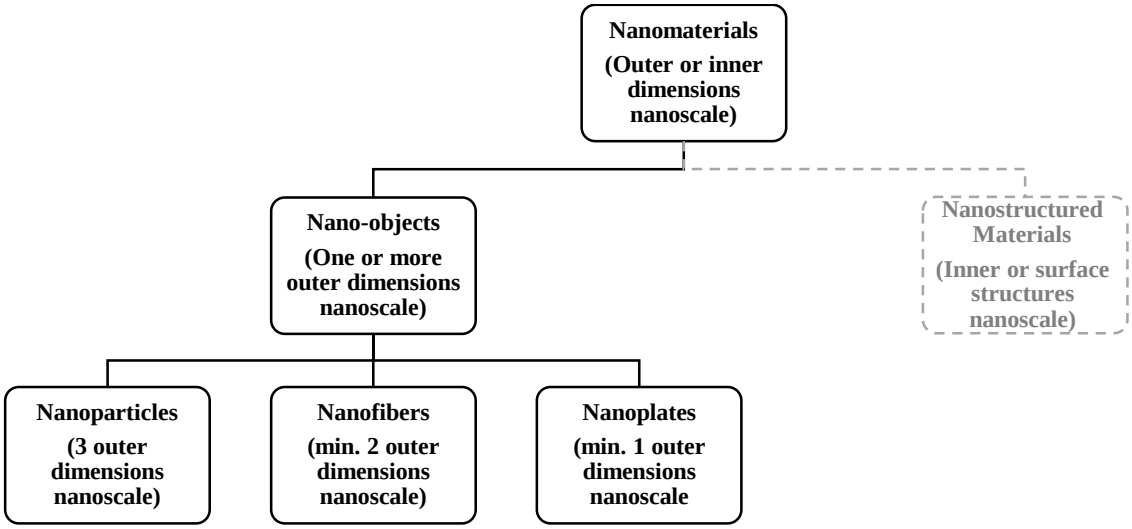

Figure 1. The ISO classification of nanomaterials. Included as nano-objects are nanoparticles, nanofibers, and nanoplates. Figure adapted from (39).

1.4.2.1.1. Nanoparticles

Generally speaking, nanparticles are intended as three-dimensional, spherical objects having a diameter less than 100 nm. Nanoparticles with a clearly ordered arrangement of atoms (or ions) are called nanocrystallites, and nanoparticles with a clear-cut discrete electronic energy levels are often referred to as "quantum dots" or "artificial atoms"; most often, they have compositions of typical semiconductor materials, but not always (40). Currently, these kinds of nanoobjects attracted a lot of attention because of their unique properties. Indeed, because of the higher surface-to-volume ratio and higher available surface area of these nano-entities

compared to bulk materials, they have extraordinary physical (e.g., plasmonic resonance, fluorescence) and chemical (e.g., catalytic activity) properties (41). In spite of some peculiarities strictly belonging to each specific nanoparticle, some common features can be outlined, such as enhancement of the electron transfer; suitability to act as reactants and for the immobilization of biomolecules, labeling biomolecules and catalysis of electrochemical reactions (42).

Various types of nanoparticles have recently been used for the electrode modification, such as semiconductor nanoparticles (43), metal nanoparticles (44), and oxide nanoparticles (45). For instance, in a very fascinating research, Anusha et al. compared two different types of sensors for glucose determination: one based on an electrode, modified with gold, chitosan, and glucose oxidase (limit of detection = 1.5×10^{-6} M); the other one only differing by the replacement of chitosan polymer with chitosan nanoparticles (limit of detection = 1.1×10^{-6} M). Their experiments indicated the positive effect of nanoparticles on sensitivity and efficiency of the sensor (46). Sophia et al. fabricated a novel non-enzymatic electrochemical sensor for the determination of hydrogen peroxide by modifying the surface of the working electrode with copper nanoparticles. They reported that the fabricated sensor exhibited swift response time, wide linear range, and low detection limit (3.45×10^{-6} M) with good reproducibility and stability (47).

1.4.2.1.2. Nanofibers

One-dimensional nano-objects are known as “nanofibers”, with the length being the relevant dimension. There are three main subclasses of nanofibers: nanotubes, which are hollowed nanofibers; nanorods, namely rigid nanofibers; and nanowires, i.e., electrically conducting nanofibers (48,49). Beside the naturally-occurring nanofibers (e.g., those arising from cellulose), the most common method for fabrication of nanofibers is electrospinning, although new methods have been brought to the front in recent years for the obtainment of nanofibers, such as interfacial polymerization (48,50), hydrothermal synthesis (51), and phase separation (52). For other synthetic nanofibers such as the allotropes of carbon named carbon nanotubes (CNTs), more complicated approaches (e.g., laser ablation, arc discharge, and chemical vapor deposition) are necessary.

CNTs have found wide application to modify electrochemical sensors. CNTs are made up of sp2 carbon units with many microns in length and nanometers in diameter. This type of nanofibers can behave like metals or semiconductors based on their diameter and degree of helicity (53). CNTs are generally divided in two main subclasses: i) single-walled carbon

nanotubes (SWNTs) and multi-walled carbon nanotubes (MWNTs). SWNTs are composed of a single rolled graphene sheet with an internal diameter of the tube of 1–2 nm. MWCNTs consist of multiple rolled layers (concentric tubes) of graphene with a diameter of 2–50 nm and the distance between sheets of approximately 0.34 nm (54). Muhammad et al. fabricated a new electrochemical sensor for sensing thiamphenicol residues in milk. To increase the sensitivity of the sensor, the authors modified the electrode by the simultaneous use of carbon nanotubes and gold nanoparticles. A wide linear calibration range (0.1×10^{-6} – 30×10^{-6} M) and a very low detection limit (0.003×10^{-6} M) were eventually determined for this sensor. They also stated that the proposed sensor had high sensitivity and good repeatability, and the sensor can be used to sense the thiamphenicol in bovine milk samples perfectly (55). In another work, Wang et al. modified a glassy carbon electrode using carboxylated MWNTs and gold nanoparticles, followed by a molecular imprinting method to make the sensor selective for olaquindox. Their novel MIP sensor offered a 2.7×10^{-9} M of detection limit for olaquindox. The same authors showed that the proposed sensor was able to detect olaquindox in complex real samples (56).

1.4.2.1.3. Nanoplates

Two-dimensional nano-objects looking as tiny tiles are known as nanoplates. These kinds of nano-objects have a thickness in the nanoscale (~ 1 nm), with the length and width often being in the "micron" scale (39). In the recent years, different nanoplates have been used for the modification of electrochemical sensors. Among others, graphene and graphene oxide have attracted much attention.

Especially at laboratory scale, the most widely adopted method to obtain graphene from the parental graphite is the chemical method. This method consists of a preliminary oxidation of graphite to obtain graphite oxide. Graphene oxide can be thus obtained from graphite oxide by thermal or mechanical exfoliation of graphite oxide (57). Eventually, graphene can be obtained from graphene oxide by reduction, which can take place by thermal expansion, using some reducing agents (hydrazine, $NaBH_4$, etc.), and carrying out an electrochemical reduction (58).

Graphene is the building unit of graphite, which is a two-dimensional material, composed of a single planar sheet of sp^2-bonded carbon atoms packed in a honeycomb crystal lattice (59). Graphene has various appealing properties, such as huge specific area, high electrical conductivity, mobility of charge carriers (~200 000 $cm^2 V^{-1} s^{-1}$), high Young's modulus (~1000 GPa), excellent thermal conductivity (~5000 W $m^{-1} K^{-1}$), impressive fracture strength (~125 GPa), and high chemical stability (58,60). Due to these unprecedented properties, graphene is

thought to have a great potential for fabricating high-performance electrochemical sensors (61). For instance, Xu et al. developed an imprinted sol-gel electrochemical sensor based on a composite of graphene and single walled carbon nanotubes for the determination of propyl gallate. They claimed that the proposed sensor exhibited good specificity and selectivity towards template molecules as well as excellent reproducibility, regeneration, and stability. They also reported that the sensor could be used for the determination of analytes in real samples, such as cookies, instant noodles, and edible oils with satisfactory results (62). In another research, Deng et al. developed a graphene–polyvinyl pyrrolidone composite film-modified acetylene black paste electrode to investigate the electrochemical behavior of vanillin. They concluded that the graphene–polyvinyl pyrrolidone composite exhibits a high electrochemical activity for promoting the direct electron transfer of vanillin. The same authors used the proposed electrode as a sensor for the determination of vanillin and they calculated a very good limit of detection for this sensor. The successfull application of the sensor in various food samples was also demonstrated (63).

Graphene oxide is the oxidized form of graphene. This nanoplate can be synthesized through strong acid/base attack of graphite crystals to introduce oxygen-containing groups in the graphite stacks, after which a full exfoliation of the oxidized solid into nanosheets is necessary (64). Due to the oxygen-containing groups on its edges GO is water soluble, though its conductivity is lower than the bare graphene. GO has different special properties that can be advantageously used for a variety of applications, such as sensing, energy-related, and new optoelectronic applications (65). In the field of electrochemistry applications, GO can be used to make easier the electron transfer rate of active species at the surface of electrode (66). Qiu et al. designed an electrochemical sensor modified with GO and multi-walled carbon nanotubes for the simultaneous determination of sunset yellow and tartrazine, taking advantage of the excellent electronic and antifouling properties of multi-walled carbon nanotubes and the signal amplification properties of GO. They reported a great analytical performance of the sensor for simultaneous determination of sunset yellow and tartrazine, claiming an excellent sensing capability of the analytes in orange juice (36). Adekunle et al. fabricated an electrochemical nanosensor based on iron(III) oxide (Fe_2O_3), GO and prussian blue nanoparticles for the determination of nitrite (NO_2^-) and nitric oxide (NO) on a platinum (Pt)-modified electrode. This sensor was proposed as a new, simple, and cost-effective analytical device that can possibly be used in water, food, biological, and environmental samples (67).

1.5. Applications of electrochemical sensors

Electrochemical sensors have been widely used in different fields, such as clinical (68,69), industrial (17), and environmental (70). Besides these, one of the most important field of application of electrochemical sensors is the food sector and its related sciences and technologies.

1.5.1. Sensors in the food industry

The development of electrochemical sensor in the food industry has most often been aimed at solving some of the main drawbacks associated to conventional spectrometric and chromatographic techniques. Indeed, these approaches, while offering high sensitivity and selectivity, suffer from high costs, time-consuming procedures, difficult sample preparation, and specialized personnel. Moreover, they are destructive. For these reasons, spectrometric and chromatographic techniques very seldom find use for on-line quality control of food products.

In fact, the food industry needs analytical devices that can satisfy the following requirements:

- simple to operate
- real-time
- no hygiene risk
- physically robust and stable
- sensitive
- nondestructive.

In addition, recent advances in materials chemistry and physics and in the field of information processing led to the design of new sensors in the form of an array for multiple analytes detection. The sensor array can also be formed by non-selective sensors, which provide a response pattern that can be analyzed by sophisticated methods of multivariate statistics. In principle, the appropriate sensor or sensors array can be placed along all the food chain as schematically shown in Figure 2 (71). A non-exhaustive list of the applications of electrochemical sensors in the food sector is displayed in Tables 1–5.

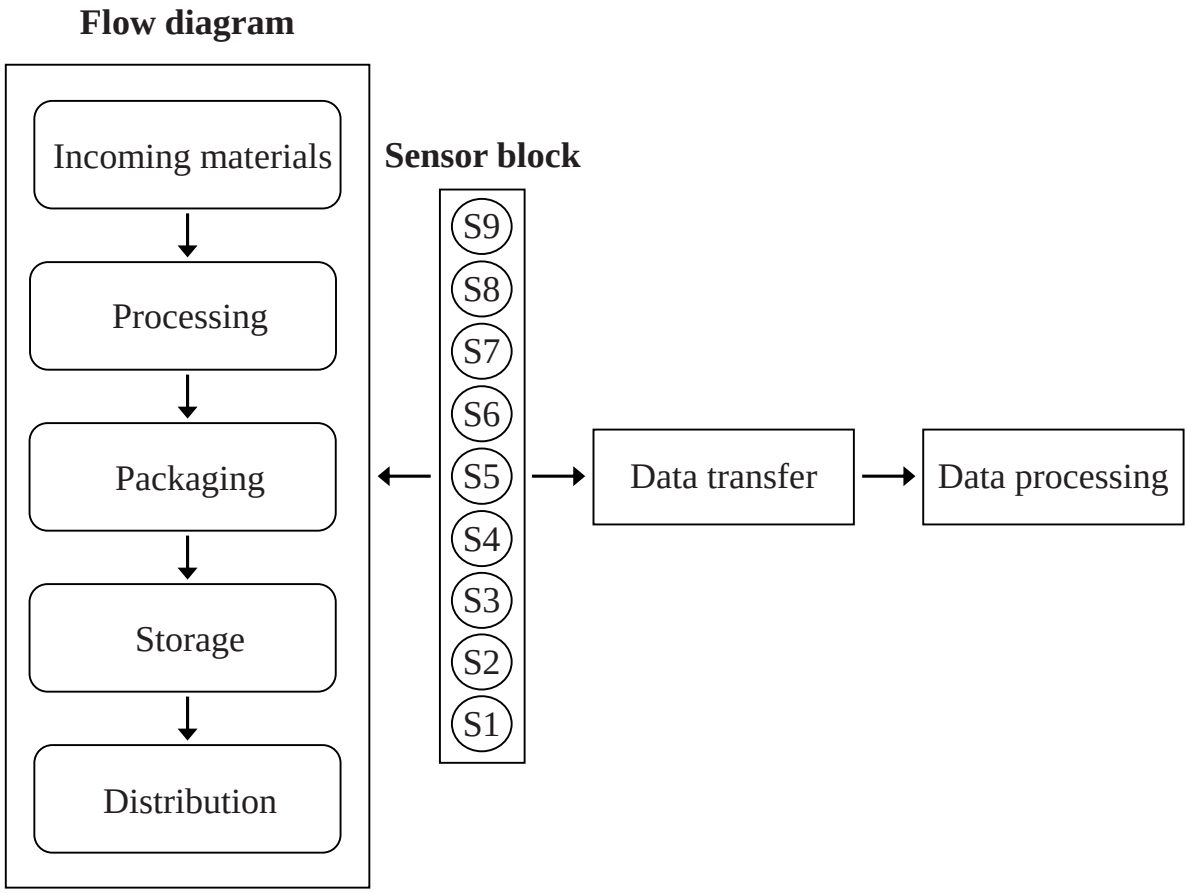

Figure 2. Schematic representation of on-line sensors in a food-processing line. Figure adapted from (71).

Table 1. Application of electrochemical sensors in Fish products

Modifier	Analyte	Linear range	LOD	REF
MIP, Graphene, CNTs	Tetrabromobisphenol A	1.0×10^{-11} – 1.0×10^{-8} M	3.7×10^{-12} M	72
MIP, MWCNTs	Metronidazole	1.71×10^{-4} – 2.05×10^{-1} mg L^{-1}	4.92×10^{-5} mg L^{-1}	73
MIP, Ni nanoparticles	Phenobarbital	1.4×10^{-7} – 1.3×10^{-4} M	8.2×10^{-9} M	74
Graphene, Gold nanoparticles	Nitric oxide	36×10^{-9} – 20×10^{-6} M	18×10^{-9} M	75
Polystyrene, Graphene oxide	Histamine	0.1×10^{-6} – 3×10^{-6} M	0.03×10^{-6} M	76
ß-Cyclodextrin, Graphene oxide-SO_3H	Cadaverine	50×10^{-9} M – 500×10^{-9} M	20×10^{-9} M	77
Manganese oxide, Chitosan	Xanthine	1×10^{-6} M – 500×10^{-6} M	1.31×10^{-6} M	78
Graphitized mesoporous carbon	Uric acid, Xanthine, Hypoxanthine	20×10^{-6} M – 400×10^{-6} M, 20×10^{-6} M – 320×10^{-6} M, 20×10^{-6} M – 240×10^{-6} M	110×10^{-9} M, 388×10^{-9} M, 351×10^{-9} M	79
Oligonucleotide, Dendritic gold nanoparticles, Reduced graphene	Listeria monocytogenes	1.0×10^{-12} – 1.0×10^{-6} M	2.9×10^{-13} M	80
Polyaniline	Cadmium	3.30×10^{-8} – 7.12×10^{-8} mol dm^{-3}	4×10^{-9} mol dm^{-3}	81
Carbon nanofibers	Xanthine	0.03×10^{-6} M – 21.19×10^{-6} M	20×10^{-9} M	82

MWCNTs	Uric acid, Xanthine, Hypoxanthine	up to 700×10^{-6} M, up to 200×10^{-6} M, up to 150×10^{-6} M	141×10^{-9} M, 134×10^{-9} M, 2.87×10^{-6} M	83
Phthalocyanines	Trimethylamin, NH_3	$2 \times 10^{-4} – 2 \times 10^{-3}$ M	4×10^{-4} M, 3×10^{-4} M	84
CNTs, DNA	Caffeine	0.1 – 12 mg L^{-1}	0.068 mg L^{-1}	85
MWCNTs	Malachite green	$5.0 \times 10^{-8} – 8.0 \times 10^{-6}$ M	6.0×10^{-9} M	86
Preanodized nontronite	Uric acid, Xanthine, Hypoxanthine	$2 \times 10^{-6} – 40 \times 10^{-6}$ M, $2 \times 10^{-6} – 40 \times 10^{-6}$ M, $4 \times 10^{-6} – 30 \times 10^{-6}$ M	0.42×10^{-6} M, 0.07×10^{-6} M, 0.34×10^{-6} M	87
Nafion, lead, ruthenium oxide pyrochlore	Hypoxanthine	up to 120×10^{-6} M	0.75×10^{-6} M	88

Table 2. Application of electrochemical sensors in Flour products

Modifier	Analyte	Linear range	LOD	REF
Gold nanoparticles, Reduced graphene oxide, polyvinylpyrrolidone	Butylated hydroxyanisole	$0.2 \times 10^{-6} – 100.0 \times 10^{-6}$ M	0.04×10^{-6} M	89
Palladium nanoparticles, Graphene oxide nanosheets	Bromate	$1 \times 10^{-6} – 10 \times 10^{-6}$ M, $10 \times 10^{-6} – 1000 \times 10^{-6}$ M	1.05×10^{-7} M	90
bi-enzyme: Agarose, Corn flour, Gelatin, β(1→3)-d-glucanase, Glucose oxidase, Gold nanoparticles tri-enzyme sensor: Agarose, Corn flour, Gelatin, β(1→3)-d-glucanase , Glucose oxidase, Peroxidase, Gold nanoparticles	β(1→3)-d-Glucan	bi-enzyme: 100 –1000 ng mL^{-1} tri-enzyme: 100 –1000 ng mL^{-1}	bi-enzyme: 30 ng mL^{-1} tri-enzyme: 50 ng mL^{-1}	91
Bentonite, Porphyrin	Mn(II)	$6.0 \times 10^{-7} – 5.0 \times 10^{-4}$ M	1.07×10^{-7} M	92

Table 3. Application of electrochemical sensors in Juice products

Modifier	Analyte	Linear range	LOD	REF
Polypyrrole doped with 8- Hydroxyquinoline-5-Sulfonic acid	Cu (II)	$1.0 \times 10^{-5} – 1.0 \times 10^{-1}$ M	1.0×10^{-5} M	93
Cytochrome C	Hydrogen peroxide	$5 \times 10^{-7} – 0.12$ M	2×10^{-7} M	94
MIP	Ascorbic Acid	$0.45 \times 10^{-6} – 13.52 \times 10^{-6}$ M, $13.52 \times 10^{-6} – 409.10 \times 10^{-6}$ M	0.11×10^{-6} M	95
Carboxylic group functionalized poly(3,4-ethylenedioxythiophene)	Bactericide Carbendazim	$1.2 \times 10^{-8} – 1 \times 10^{-5}$ M	3.5×10^{-9} M	96
Gold nanoparticals, Graphene sheets	Guaiacol	$1.0 \times 10^{-7} – 1.5 \times 10^{-5}$ M	5.4×10^{-8} M	97
Titanium dioxide, Pt(II)-Porphyrin complex	Quercetin	0.002 – 50 mg L^{-1}	0.8×10^{-3} mg L^{-1}	98
Graphene nanosheets, Silver nanoparticles	Thiourea	$1 \times 10^{-6} – 3000 \times 10^{-6}$ M	0.7×10^{-6} M	99
Mesoporous silica, Multiwalled carbon nanotubes	Carbendazim	$0.2 \times 10^{-6} – 4.0 \times 10^{-6}$ M	0.056×10^{-6} M	100
MIP	Ascorbic Acid	$1 \times 10^{-4} – 100 \times 10^{-4}$ M	36.4×10^{-6} M	101
Nickel oxide nanoparticles, (9,10-dihydro-9,10-ethanoanthracene-11,12-dicarboximido), 4-ethylbenzene-1,2-diol (DEDED)	Ascorbic Acid, Sudan I	$0.01 \times 10^{-6} – 600 \times 10^{-6}$ M, $0.5 – 1{,}000 \times 10^{-6}$ M	0.006×10^{-6} M, 0.2×10^{-6} M	102
Gold nanoparticle, Ethylenediamine, Multi walled Carbon nanotube	Myricetin	$5.0 \times 10^{-8} – 4.0 \times 10^{-5}$ M	1.2×10^{-8} M	103
MIP	Diphenylamine	$4.95 \times 10^{-6} – 115 \times 10^{-6}$ M	3.9×10^{-6} M	104
MWCNTs, Poly(diallyldimethylammonium chloride), Gold nanoparticles composite	Sulfite	0.1 – 200 mg L^{-1}	0.03 mg L^{-1}	105
Guanin, Graphene nanoribbon	Total Antioxidant capacities	0.1 – 4 mg L^{-1}	0.05 mg L^{-1}	106

4-Aminophenylboronic acid, Graphene oxide	Fructose, Mannose, Glucose	$0.2 \times 10^{-6} – 60 \times 10^{-6}$ M, $1 \times 10^{-6} – 60 \times 10^{-6}$ M, $1 \times 10^{-6} – 60 \times 10^{-6}$ M	100×10^{-9} M, 800×10^{-9} M 800×10^{-9} M	107
Copper oxide nanoparticles	Thiourea	0.05 – 20 mg L^{-1}	0.02 mg L^{-1}	108
MIP , MWCNTs	Sucrose	$0.01 \times 10^{-3} – 10 \times 10^{-3}$ M	3×10^{-6} M	109
Reduced Graphene oxide	Pb^{2+}	5 – 200 ppb	1 ppb	110
P-Aminophenol - MWCNTs	Vitamin C	$2 \times 10^{-7} – 1.2 \times 10^{-7}$ M	8×10^{-8} M	111
Graphene oxide, Chitosan	Ascorbate	$0.01 \times 10^{-3} – 3.00 \times 10^{-3}$ M	13×10^{-9} M	112
ZnO, CNTs	Ascorbic Acid	$0.1 \times 10^{-6} – 450 \times 10^{-6}$ M	0.07×10^{-6} M	113
Electrode 1: Nanostructured CeO2 Electrode 2: Gold sononanoparticles, Nanostructured CeO2	Ascorbic Acid	Electrode 1: $1.5 \times 10^{-6} – 4.0 \times 10^{-6}$ M Electrode 2: $1.5 \times 10^{-6} – 4.0 \times 10^{-6}$ M	Electrode 1: 1.59×10^{-6} M Electrode 2: 2.93×10^{-6} M	114
MIP	Parathion	$1 \times 10^{-7} – 1 \times 10^{-5}$ M	5.4×10^{-8} M	115
Cytochrome C, Nickel oxide nanoparticles, Carboxylated MWCNTs, Polyaniline	Hydrogen peroxide	$3 - 700 \times 10^{-6}$ M	0.2×10^{-6} M	116
Amino-functionalized exfoliated graphite nanoplatelet, Bismuth	Lead	$5 \times 10^{-6} – 45 \times 10^{-6}$ mg L^{-1}	1×10^{-6} mg L^{-1}	117
Gold sononanoparticles	Ascorbic acid	$1.5 \times 10^{-6} – 4.0 \times 10^{-3}$ M	3.71×10^{-6} M	118
Gold nanoparticles, Chitosan, MWCNTs, Polyaniline	Sulfite	$0.75 \times 10^{-6} – 400 \times 10^{-6}$ M	0.5×10^{-6} M	119
MIP	Metolcarb	$0.5 \times 10^{-4} – 3.5 \times 10^{-4}$ M	1.34×10^{-8} M	120
Alcohol oxidase	Ethanol	$0.10 \times 10^{-3} – 30 \times 10^{-3}$ M	9.9×10^{-6} M	121
Cobalt phthalocyanine	Citric acid	$12 \times 10^{-3} – 2$ M	2×10^{-4} M	122
Gold nanoparticles dispersed in an ionic liquid 1-butyl-3-methylimidazolium hexafluorophosphate, Binuclear nickel(ii) complex immobilized on functionalized silica	Fisetin	$0.28 \times 10^{-6} – 1.39 \times 10^{-6}$ M, $2.77 \times 10^{-6} – 19.50 \times 10^{-6}$ M	0.05×10^{-6} M	123
Copper hexacyanoferrate film	Ascorbate	$0.15 \times 10^{-3} – 5 \times 10^{-3}$ M	2.1×10^{-6} M	124
Polyaniline	L-Ascorbic	$0.4 \times 10^{-6} – 2 \times 10^{-3}$ M	0.4×10^{-6} M	125

Table 4. Application of electrochemical sensors in Meat products

Modifier	Analyte	Linear range	LOD	REF
Au, Reduced graphene oxide, Poly(diallydimethylammonium chloride)	Nitrite	$0.5 \times 10^{-6} – 8.5 \times 10^{-6}$ M	0.04×10^{-6} M	126
Anti-E. coli O157–Magnetic beads conjugate (MBs–pECAb), AuNPs modified with secondary antibodies (AuNPs–sECAb)	Escherichia coli O157: H7	$10^2 – 10^5$ CFU ml^{-1}	Buffer solution: 148 CFU ml^{-1}, Minced beef: 457 CFU ml^{-1}, Tap water: 309 CFU ml^{-1}	127
Ractopamine–Tetraphenylborate complexed nanoparticles	Ractopamine	$1.0 \times 10^{-7} – 0.1$ M	7.4×10^{-8} M	128
MIP, Poly(pyrrole), Graphene oxide, Binuclear phthalocyanine cobalt (II) sulphonate	Quinoxaline-2-Carboxylic acid	$1.0 \times 10^{-8} – 1.0 \times 10^{-4}$, $1.0 \times 10^{-4} – 5.0 \times 10^{-4}$	2.1×10^{-9} M	129
Mn(II) Phthalocyanine, Carbon Ceramic SiO_2/C	Nitrite	$0.79 \times 10^{-6} – 15.74 \times 10^{-6}$ M	0.02×10^{-6} M	130
Fe and Zn modified montmorillonite	Tetracycline	$0.30 \times 10^{-6} – 52.0 \times 10^{-6}$ M	0.10×10^{-6} M	131
MIP, MWCNTs, Chitosan	Quinoxaline-2-Carboxylic acid	$2.0 \times 10^{-6} – 1.0 \times 10^{-3}$ M	4.4×10^{-7} M	132
Poly taurine, Zirconia nanoparticles	Ractopamine, Salbutamol	$1 \times 10^{-6} – 28 \times 10^{-6}$ M, $5 \times 10^{-6} – 220 \times 10^{-6}$ M	0.15×10^{-6} M, 0.02×10^{-6} M	133
Reduced graphene oxide, Gold nanoparticles	Dopamine	$10 \times 10^{-6} – 1000 \times 10^{-6}$ M	6.0×10^{-8} M	134
Neomycin antibody, poly-[2,5-di-(2-thienyl)-1H-pyrrole-1-(p-benzoic acid)]	Neomycin	$10 \times 10^{-3} – 250 \times 10^{-3}$ mg L^{-1}	$6.76\pm0.17 \times 10^{-3}$ mg L^{-1}	135

Poly alizarin red S, MWCNTs	Nitrite	$30 \times 10^{-9} – 1.1 \times 10^{-3}$ M	2×10^{-9} M	136
Anti-calpastatin antibody, Mercaptoundecanoic acid, Protein A from Staphylococcus aureus	Calpastatin	$20 \times 10^{-3} – 160 \times 10^{-3}$ mg L^{-1}	-	137
Monoclonal anti-S. typhimurium antibody	Salmonella typhimurium	$10 – 10^{7}$ CFU ml^{-1}	20 CFU ml^{-1}	138
Cholesterol esterase, Cholesterol oxidase, Glutaraldehyde, Bovine Serum Albumin	Cholesterol	$2 \times 10 – 50 \times 10$ mg L^{-1}	-	139
Molybdenum oxide layer	Nitrite	$5 \times 10^{-6} – 1000 \times 10^{-6}$ M	1×10^{-6} M	140
MIP	Clenbuterol	$0.004 \times 10^{-3} – 25 \times 10^{-3}$ M	20×10^{-9} M	141

Table 5. Application of electrochemical sensors in Milk products

Modifier	**Analyte**	**Linear range**	**LOD**	**REF**
MIP, Cubic gold nanoparticles , 2-aminoethanethiol functionalized graphene oxide	Tyrosine	$1.0 \times 10^{-9} – 2.0 \times 10^{-8}$ M	1.5×10^{-10} M	142
Block polyelectrolyte composite films, MWCNTs	Bisphenol A	$4.56 \times 10^{-2} – 2.28 \times 10$ mg L^{-1}	2.28×10^{-3} mg L^{-1}	143
TiO_2 nanoparticles, CdSe nanoparticles, N-hydroxysuccinimide/1-ethyl-3-(3-dimethylaminopropyl) carbodiimide hydrochloride, OTA antibody, Bovine serum albumin	Ochratoxin A	$10 \times 10^{-9} – 50 \times 10^{-6}$ mg L^{-1}	2.0×10^{-9} mg L^{-1}	144
Nano gold particle, Cysteamine, Mono-tosyl-b-cyclodextrin	Diethylstilbestrol	$1.00 \times 10^{-6} – 100 \times 10^{-6}$ mg L^{-1}	0.30×10^{-6} mg L^{-1}	145
MIP	Sulfadimethoxine	$0.15 \times 10^{-3} – 3.7 \times 10^{-3}$ M	70×10^{-6} M	146
Nano iron oxide, CNTs	Hydrogen peroxide	$1.2 \times 10^{-6} – 21.6 \times 10^{-6}$ M	3.7×10^{-9} M	147
Chitosan, Calcium oxide nanoparticles, Ionic liquids	Melamine	$9.6 \times 10^{-15} – 9.6 \times 10^{-3}$ M	9.6×10^{-16} M	148
Mixed monolayer of p-nitrophenyl and phenyl - Graphene nanosheets - Rabbit-anti Botulinum neurotoxin type-E antibody	Botulinum neurotoxin type-E	$10 \times 10^{-6} – 10 \times 10^{-3}$ mg L^{-1}	5.0×10^{-6} mg L^{-1}	149
Cytochrome C nitrite reductase, Carbon ink	Nitrite	$0.7 \times 10^{-6} – 370 \times 10^{-6}$ M	1.2×10^{-6} M	150
Fe_3MoO_4	Hydrogen peroxide	$1 \times 10^{-6} – 1.6 \times 10^{-3}$ M	0.5×10^{-6} M	151
MWCNTs, Molybdenum disulfide	Hydrogen peroxide	$10 \times 10^{-9} – 100 \times 10^{-6}$ M	5.0×10^{-9} M	152
Anti-penicillin G, Bilayer lipid membrane (s-BLM), Gold nanoparticles	Penicillin G	$3.34 \times 10^{-9} – 3.34 \times 10^{-3}$ mg L^{-1}	2.7×10^{-10} mg L^{-1}	153
MIP, Fe_3O_4 magnetic nanoparticles	Dimetridazole	$1.0 \times 10^{-8} – 1.0 \times 10^{-6}$ M, $1.0 \times 10^{-6} – 1.0 \times 10^{-4}$ M	3.6×10^{-9} M	154
MWCNTs, Azure A, Gold nanoparticle	Ascorbic acid, Dopamine, Uric acid, Tryptophan	$300 \times 10^{-6} – 10000 \times 10^{-6}$ M, $0.5 \times 10^{-6} – 50 \times 10^{-6}$ M, $0.5 \times 10^{-6} – 50 \times 10^{-6}$ M, $1 \times 10^{-6} – 100 \times 10^{-6}$ M	16×10^{-6} M, 0.01×10^{-6} M, 0.01×10^{-6} M, 0.3×10^{-6} M	155
Gold nanoparticles functionalized with 3-mercaptophenyl boronic acid, Bamboo-like multiwall carbon nanotubes dispersed in hyperbranched polyethyleneimine , Glucose oxidase	Glucose	2.5×10^{-4} M – 5×10^{-3} M	0.8×10^{-6} M	156
RuO_2, Nafion, Gold nanoparticle; SnO_2, Nafion, Gold nanoparticle; ZrO_2-Nafion-Gold nanoparticle	Hydrogen peroxide	$0.1 \times 10^{-9} – 30 \times 10^{-3}$ M, $1.3 \times 10^{-3} – 39 \times 10^{-3}$ M, $1 \times 10^{-9} – 1000 \times 10^{-3}$ M	-	157
MIP	Melamine	$5 \times 10^{-9} – 100 \times 10^{-9}$ M	1.4×10^{-9} M	158
Zinc sulfur, Poly (3,4-ethylenedioxythiophene), Reduced graphene oxide	Adenine, Guanine, Thymine	$0.5 \times 10^{-6} – 150 \times 10^{-6}$ M, $0.5 \times 10^{-6} – 150 \times 10^{-6}$ M,	0.141×10^{-6} M, 0.116×10^{-6} M,	159

		$5.0 \times 10^{-6} – 600 \times 10^{-6}$ M	2.57×10^{-6} M	
MWCNTs, Mesoporous carbon, Three-dimensional porous graphene	Chloramphenicol	$5 \times 10^{-9} – 5 \times 10^{-7}$ M, $5 \times 10^{-7} – 4 \times 10^{-6}$	1×10^{-10} M	160
MIP	Anthelmintic drug oxfendazole	$0.05 \times 10^{-6} – 0.50 \times 10^{-6}$ M	DPV: 0.025×10^{-6} M SWV: 0.015×10^{-6} M	161
Bi_2WO_6 nanoplates	Diethylstilbestrol, Bisphenol A	$50 \times 10^{-9} – 2100 \times 10^{-9}$ M, $70 \times 10^{-9} – 1300 \times 10^{-9}$ M	15×10^{-9} M, 20×10^{-9} M	162
Silver nanoparticles, PAMAM dendrimer	Nitrite	4.0×10^{-6} M – 1.44×10^{-3} M	0.4×10^{-6} M	163
Graphene oxide doped eggshell membrane, Prussian blue	Hydrogen peroxide	$125 \times 10^{-9} – 195 \times 10^{-6}$ M	31×10^{-9} M	164
Cu2O/Cu nanocomposite	Hydrogen peroxide	$4.0 \times 10^{-7} – 1.0 \times 10^{-2}$ M	2.0×10^{-7} M	165
Mesoporous carbon, Trimetallic nanorattle (Au-core/AgPt-shell nanorattles), Zearalenone antibody	Zearalenone	$0.005 \times 10^{-3} – 15 \times 10^{-3}$ mg L^{-1}	1.7×10^{-6} mg L^{-1}	166
MWCNTs, Cetyltrimethylammonium bromide, Poly(diphenylamine)	Chloramphenicol	$1 \times 10^{-8} – 1 \times 10^{-5}$ M	2×10^{-9} M	167
Ordered mesoporous carbon, Nafion	Melamine	$5 \times 10^{-8} – 7 \times 10^{-6}$ M	2.4×10^{-9} M	168
$Ni(OH)_2$, Electroreduced graphene oxide, MWCNTs	Glucose, Hydrogen peroxide	$0.01 \times 10^{-3} – 1.5 \times 10^{-3}$ M, $0.01 \times 10^{-3} – 9.05 \times 10^{-3}$ M	2.7×10^{-6} M, 4×10^{-6} M	169
Copper nanoparticles, SiO_2-pro-NH_2; Copper nanoparticles, SiO_2-pro-NH-cyanuric-NH_2	Hydrogen peroxide	$5.14 \times 10^{-6} – 1250 \times 10^{-6}$ M, $1.14 \times 10^{-6} – 1120 \times 10^{-6}$ M	0.85×10^{-6} M, 0.27×10^{-6} M	170
Not modified	Melamine	$5 \times 10^{-6} – 90 \times 10^{-6}$ M	0.85×10^{-6} M	171
Anti Listeria monocytogenes monocolnal antibody	Listeria monocytogenes	10^2 CFU ml^{-1} – 10^6 CFU ml^{-1}	-	172
Polyaniline nano-gold composite, Dimethyl-3-butylimidazolium hexafluorophosphate, Staphylococcal enterotoxin B immuno-magnetosomes, Bovine serum albumin	Staphylococcal enterotoxin B	$0.05 \times 10^{-3} – 5 \times 10^{-3}$ mg L^{-1}	0.017×10^{-3} mg L^{-1}	173
MWCNTs	L-tryptophan	$0.6 \times 10^{-6} – 9.0 \times 10^{-6}$ M, $10.0 \times 10^{-6} – 100.0 \times 10^{-6}$ M	$(3.30 \pm 0.37) \times 10^{-8}$ M	174
MIP	Sulfadiazine	$0.2 \times 10^{-6} – 20 \times 10^{-6}$, $20 \times 10^{-6} – 100 \times 10^{-6}$ M	0.13×10^{-6} M	175
MWCNTs, MIP	Bovine serum albumin	$1.99 \times 10^{-3} – 30.91 \times 10^{-3}$ mg L^{-1}	0.40×10^{-3} mg L^{-1}	176
Magnetic bead, Nano gold particle, MIP	Streptomycin	$0.05 \times 10^{-3} – 20 \times 10^{-3}$ mg L^{-1}	10×10^{-9} mg L^{-1}	177
MIP, Chitosan, Silver nanoparticles, Graphene, MWCNTs	Neomycin	$9 \times 10^{-9} – 7 \times 10^{-6}$ M	7.63×10^{-9} M	178
Amino-functionalized graphene, Chitosan, Au nanoparticles, Mesoporous silica, Diethylstilbestrol antibody	Diethylstilbestrol	$0.01 \times 10^{-3} – 20 \times 10^{-3}$ mg L^{-1}	3.4×10^{-9} mg L^{-1}	179
MWCNTs , Chitosan, HRP labled penicillin polyclonal antibody	Penicillin	$0.05 \times 10^{-3} – 5.0 \times 10^{-3}$ mg L^{-1}	1.05×10^{-3} mg L^{-1}	180
MIP	Tobramycin	$5.0 \times 10^{-10} – 5.0 \times 10^{-8}$ M	1.4×10^{-10} M	181
Nafion, graphene oxide, Co_3O_4 nanocomposite	Hydrogen peroxide	$1 \times 10^{-6} – 5000 \times 10^{-6}$ M	0.3×10^{-6} M	182
Ag@Cu nanowires, Nafion	Hydrogen peroxide	$1 \times 10^{-3} – 10 \times 10^{-3}$ M	3×10^{-6} M	183
MWCNTs, Mg-Al-CO_3 layered double hydroxide	L-Tryptophan	$3 \times 10^{-6} – 90 \times 10^{-6}$ M, $90 \times 10^{-6} – 1000 \times 10^{-6}$ M	6.8×10^{-9} M	184
MWCNTs, Polyhistidine, Glucose oxidase	Glucose	$0.25 \times 10^{-3} – 5.00 \times 10^{-3}$ M	2.2×10^{-6} M	185
Magnetic MIP	Metronidazole	$5.0 \times 10^{-8} – 1.0 \times 10^{-6}$ M	1.6×10^{-8} M	186
Lysine oxidase, Gold nanoparticles, Platinum nanoparticles	Lysine	$1.0 \times 10^{-6} – 600 \times 10^{-6}$ M	1.0×10^{-6} M	187
-	Salmonella	$10^3 – 10^6$ cells mL^{-1}	143 cells mL^{-1}	188

DNA probe	Peanut allergen Ara h 1	$10 \times 10^{-15} – 10 \times 10^{-10}$ M	0.35×10^{-15} M	189
β-Cyclodextrin, Reduced graphene oxide	Diethylstilbestrol	0.01×10^{-6} M – 13×10^{-6} M	4×10^{-9} M	190
MIP, Chitosan, Platinum nanoparticles, Graphene, Gold nanoparticles	Erythromycin	$7.0 \times 10^{-8} – 9.0 \times 10^{-5}$ M	2.3×10^{-8} M	191
Monoclonal antibodies of Aflatoxin M1	Aflatoxin M1	$6.25 \times 10^{-6} – 100 \times 10^{-6}$ mg L^{-1}	1×10^{-6} mg L^{-1}	192
Polyaniline, MWCNTs, Gold nanoparticles	Hydrogen peroxide	3.0 μM × $10^{-6} – 600 \times 10^{-6}$ M	0.3×10^{-6} M	193
MIP	Melamine	$4.0 \times 10^{-6} – 0.45 \times 10^{-3}$ M	0.36×10^{-6} M	194
MnO_2, MWCNTs	Hydrogen peroxide	$1.2 \times 10^{-6} – 1.8 \times 10^{-3}$ M	8.0×10^{-7} M	195
Nafion, MWCNTs	Adenine	$1.0 \times 10^{-7} – 7.0 \times 10^{-5}$ M	3.3×10^{-8} M	196
-	Riboflavin	$0.8 \times 10^{-9} – 110 \times 10^{-9}$ M, $110 \times 10^{-9} – 1000 \times 10^{-9}$ M	0.1×10^{-9} M	197
-	Melamine	$1.0 \times 10^{-8} – 5.0 \times 10^{-6}$ M	3.0×10^{-9} M	198
Poly-5,2′-5′,2″-terthiophene-3′-carboxyli c acid , MWCNTs, Lactate dehydrogenase, Oxidized form of nicotinamide adenine dinucleotide	Lactate	$5 \times 10^{-6} – 90 \times 10^{-6}$ M	1×10^{-6} M	199
Melamine antibody, Chloro-phenanthroline binuclear copper , Horseradish peroxidase, Fe_3O_4/Au colloid nano-particles	Melamine	$1 \times 10^{-3} – 40 \times 10^{-3}$ mg L^{-1}, $60 \times 10^{-3} – 100 \times 10^{-3}$ mg L^{-1}	0.25×10^{-3} mg L^{-1}	200
MWCNTs, Core-shell organosilica, Horseradish peroxidase, Chitosan	Hydrogen peroxide	$7.0 \times 10^{-7} – 2.8 \times 10^{-3}$ M	2.5×10^{-7} M	201
New methylene blue, Horseradish peroxidase, Penicillin polyclonal antibody	Penicillin	$0.25 \times 10^{-3} – 3.0 \times 10^{-3}$ mg L^{-1}	0.298×10^{-3} mg L^{-1}	202

1.5.2. Sensors in food packaging

Packaging is a crucial element in food manufacturing. Despite the well-established advantages that packaging offers to the consumer, it has been the subject of many debates concerning both the environmental impact and the health issues associated to the use of packaging materials. Due to the increasing awareness of consumers toward the potential risks in terms of food contact materials (FCMs), the assessment of the migration of the substances from the packaging materials to the food attracted the interest of both the scientific community and the legislative agencies. Table 6 and Table 7 show some of the most relevant substances that can possibly migrate from conventional food packaging materials to the food (203):

Table 6. Substances possibly migrating from conventional non-plastic packaging materials to the food.

Packaging material	Migrated substance
Wooden Packaging	1-propanol
Tin	DGEBA
Recycled Paper & board	DIPNs
Cans coated with lacquer	Epichlorohydrin
Paper cardboard & board	Metals (Zn, Sn, Al, Mn, Ba)
Cartons (Al-laminated)	Al
Aseptic	H_2O_2
Aluminum Foil paper laminates	Phthalate esters (DBP, BBP, DEHP)
Cans	BADGE (lacquer)
Aluminum	Al
Paper based food packaging	2378-TCDD/ 2378-TCDF (polychlorinated dibenzofurans)
Ceramic containers	Pb, Cd
Aluminum	Al
Paper & board	4,4-bis(dimethylamino benzophenone) (MK) 4,4-bis-(diethylamino benzophenone) (DEAB)

Table 7. Monomer/oligomer possibly migrating from plastic-based packaging materials to the food.

Packaging material	Migrated substance
PS	Styrene
Polyester cookware	Benzene
PVC films	DEHA, Dioctyladipate
LDPE	Irganox 1010 (I-1010), Naphthalene
HDPE	Irganox 1076 (I-1076)
Coating material (poly(vinyl alcohol) based liquid plast emulsion	Monomers of HA-LA plast
PP cups	2-decanone
PS + ABS + waxed paperboard	Mineral hydrocarbons
Wax coatings	Mineral hydrocarbons
PP	monomers
ABS	Mineral hydrocarbons
PC	Bisphenol-A

Especially because of legal obligations, companies dealing with food packaging, both manufacturers and converters, are increasingly looking to new devices/analytical tools enabling the determination of hazardous substances that can migrate from the packaging material to the food. The common analytical methods that are used by packaging companies are mainly spectrophotometric/colorimetric and chromatographic methods. However, due to the aforementioned disadvantages, packaging companies most often prefer to outsource the FCM

procedures on their production. Electrochemical sensors, because of sensitivity, selectivity, lower cost, and ease to use compared to conventional analytical instrumentation, probably represent the most promising solution for the years to come. To this scope, researchers strove to develop new electrochemical sensors for detecting hazardous analytes in food packaging materials (204–207).

One of the most dangerous substances that can be possibly transferred from multilayer packaging materials consisting of aromatic polyurethane (PU) adhesives into foodstuffs is represented by the isocyanic monomers. Once these monomers come into contact with the water molecules inside of the package, primary aromatic amines (PAAs) will be formed. Because of the risk associated to PAAs (they are carcinogenic substances), it becomes clear the importance of investigating comprehensively the formation, migration, and mechanisms of control of PAAs from food packaging materials.

1.6. References

1- W. Li, Y. Wang, L. Huang, T. W., H. Hu, Y. Du. Luminescence. 30, (2015), 872–877.

2- C. Ni, B. Zhu, N. Wang, M. Wang, S. Chen, J. Zhang, Y. Zhu. Food Chemistry. 194, (2016), 555–560.

3- I. Burgos-Luján, A. Z. Tong. Food Analytical Methods. 8, (2015), 1836–1841.

4- F. Gatea, E. D. Teodor, G. Paun, A. O. Matei, G. L. Radu. Food Analytical Methods. 8, (2015), 1335–1340.

5- W.-B. Shim, H. Mun, H.-A. Joung, J. A. Ofori, D.-H. Chung, M.-G. Kim. Food Control. 36, (2014), 30–35.

6- W. Kong, J. Xiong, H. Yue, Z. Fu. Analytical Methods. 87, (2015), 9864–9868.

7- A. Rehman, N. Iqbal, P. A. Lieberzeit, F. L. Dickert. Monatshefte für Chemie - Chemical Monthly. 140, (2009), 931–939.

8- S. Viswanathan, J. Radecki. Polish journal of food and nutrition sciences. 58, (2008), 157–164.

9- G. Campanella, M. Ghaani, G. Quetti, S. Farris. Trends in Food Science & Technology. 46, (2015), 137–143.

10- M. Ghaani, C. A. Cozzolino, G. Castelli, S. Farris. Trends in Food Science & Technology. 51, (2016), 1–11.

11- S.-H. Fan, J. Shen, H. Wu, K.-Z. Wang, A.-G. Zhang. Chinese Chemical Letters. 26, (2015), 580–584.

12- C. Pénicaud, S. Guilbert, S. Peyron, N. Gontard, V. Guillard. Food Chemistry. 123, (2010), 1275–1281.

13- L. A. Goulart, F. Cruz de Moraes, L. H. Mascaro. Materials Science and Engineering C. 58, (2016), 768–773.

14- F. Gao, D. Zheng, H. Tanaka, F. Zhan, X. Yuan, F. Gao, Q. Wang. Materials Science and Engineering C. 57, (2015), 279–287.

15- B. Liu, B. Xiao, L. Cui, M. Wang. Materials Science and Engineering C. 55, (2015), 457–461.

16- J. G. Pacheco, M. Castro, S. Machado, M. F. Barroso, H. P.A. Nouws, C. Delerue-Matos. Sensors and Actuators B. 215, (2015), 107–112.

17- N. Nasirizadeh, S. hajihosseini, Z. Shekari, M. Ghaani. Food Analytical Methods. 8, (2015), 1546–1555.

18- A. J. Bard, L. R. Faulkner, (2001). Electrochemical Methods: Fundamentals and Applications. United States of America: John Wiley & Sons.

19- J. Wang, (2001). Analytical Electrochemistry. New Jersey: John Wiley & Sons.
20- L. Rassaei, M. Amiri, C. Mihai Cirtiu, M. Sillanpaa, F. Marken, M. Sillanpaa. Trends in Analytical Chemistry. 30, (2011), 1704–1715.
21- T. T. Ngo (Ed.), (1987). Electrochemical Sensors in Immunological Analysis. New York: Springer Science+Business Media.
22- L. M. Moretto, K. Kalcher (Eds.), (2014). Environmental Analysis by Electrochemical Sensors and Biosensors Volume 1: Fundamentals. New York: Springer Science+Business Media.
23- A. J. Bard, G. Inzelt, F. Scholz (Eds.), (2008). Electrochemical Dictionary. Berlin Heidelberg: Springer-Verlag.
24- J. R. Allen. Laboratory medicine. 34, (2013), 544–547.
25- X. Zhang, H. Ju, J. Wang (Eds.), (2008). Electrochemical Sensors, Biosensors and Their Biomedical Applications. United States of America: Elsevier.
26- M. Dervisevic, E. Custiuc, E. Çevik, M. Senel. Food Chemistry. 181, (2015), 277–283.
27- I. M. Apetrei, C. Apetrei. Journal of Food Engineering. 149, (2015), 1–8.
28- S. A. Piletsky, A. P. F. Turner. Electroanalysis. 14, (2002), 317–323.
29- T.-P. Huynh, W. Kutner. Biosensors and Bioelectronics. 74, (2015), 856–864.
30- M. Cui, J. Huang, Y. Wang, Y. Wu, X. Luo. Biosensors and Bioelectronics. 68, (2015), 563–569.
31- S. Vaddiraju, I. Tomazos, D. J. Burgess, F. C. Jain, F. Papadimitrakopoulos. Biosensors and Bioelectronics. 25, (2010), 1553–1565.
32- J. F. Leary. Canadian Journal of Ophthalmology. 45, (2010), 449–456.
33- S. Neethirajan, D. S. Jayas. Food Bioprocess Technology. 4, (2011), 39–47.
34- V. Erady, R. J. Mascarenhasa, A. K. Satpati, S. Detriched, Z. Mekhalif, J. Dalhalle, A. Dhason. Journal of Electroanalytical Chemistry. 806, (2017), 22–31.
35- Z. Bai, W. Dong, Y. Ren, C. Zhang, Q. Chen. Langmuir. 34, (2018), 2235−2244.
36- X. Qiu, L. Lu, J. Leng, Y. Yu, W. Wang, M. Jiang, L. Bai. Food Chemistry. 190, (2016), 889–895.
37- R. Chauhan, P. R. Solanki, J. Singh, I. Mukherjee, T. Basu, B.D. Malhotra. Food Control. 52, (2015), 60–70.
38- N. Chen, Y. Cheng, C. Li, C. Zhang, K. Zhao, Y. Xian. Microchim Acta. 182, (2015), 1967–1975.
39- P. Linkov, M. Artemyev, A. E. Efimov, I. Nabiev. Nanoscale. 5, (2013), 8781–8798.

40- S. P. Gubin (Ed.), (2009). Magnetic Nanoparticles. Weinheim: WILEY-VCH Verlag GmbH & Co. KGaA.
41- S. Galdiero, A. Falanga, M. Vitiello, M. Cantisani, V. Marra, M. Galdiero. Molecules. 16, (2011), 8894-8918.
42- X. Luo, A. Morrin, A. J. Killard, M. R. Smyth. Electroanalysis. 18, (2006), 319–326.
43- S. Hooshmand, Z. Es'haghi. Analytica Chimica Acta. 972, (2017), 28–37.
44- W. Liu, K. Hiekel, R. Hübner, H. Sun, A. Ferancova, M. Sillanpää. Sensors and Actuators B. 255, (2018), 1325–1334.
45- J. B. Raoof, N. Teymoori, M.A. Khalilzadeh. Food Analytical Methods. 8, (2015), 885–892.
46- J. R. Anusha, C. J. Raj, B.-B. Cho, A. T. Fleming, K.-H. Yu, B. C. Kim. Sensors and Actuators B. 215, (2015), 536–543.
47- J. Sophia, G. Muralidharan. Materials Research Bulletin. 70, (2015), 315–320.
48- L. T. H. Nguyen, S. Chen, N. K. Elumalai, M. P. Prabhakaran, Y. Zong, C. Vijila, S. I. Allakhverdiev, S. Ramakrishna. Macromolecular Materials and Engineering. 298, (2013), 822–867.
49- J. Ramsden, (2011). Nanotechnology: An Introduction. United States of America: Elsevier.
50- C. Chen, Y. Yu, K. Li, M. Zhao, L. Liu, J. Yang, J. Liu, D. Sun. Cellulose. 22, (2015), 3929–3939.
51- Y. Yu, Z. Ren, M. Li, S. Gong, S. Yin, S. Jiang, X. Li, X. Wei, G. Xu, G. Shena, G. Han. CrystEngComm. 17, (2015), 1024–1029.
52- S.-h. Hsu, S. Huang, Y.-C. Wang, Y.-C. Kuo. Acta Biomaterialia. 9, (2013), 6915–6927.
53- A. J. S. Ahammad, J.-J. Lee, M. A. Rahman. Sensors. 9, (2009), 2289–2319.
54- B. S. Sherigara, W. Kutner, F. D'Souza. Electroanalysis. 15, (2003), 753–772.
55- A. Muhammad, R. Hajian, N. A. Yusof, N. Shams, J. Abdullah, P. M. Woi, H. Garmestani. RSC Advances. 8, (2018), 2714–2722.
56- H. Wang, S. Yao, Y. Liu, S. Wei, J. Su, G. Hu. Biosensors and Bioelectronics. 87, (2017), 417–421.
57- Y. Wang, Z. Li, J. Wang, J. Li, Y. Lin. Trends in Biotechnology. 29, (2011), 205–212.
58- T. Gan, S. Hu. Microchim Acta. 175, (2011), 1–19.
59- I. Uysal Unalan, G. Cerri, E. Marcuzzo, C. A. Cozzolinoa, S. Farris. RSC Advances. 4, (2014), 29393–29428.

60- L. Kui, Z. Guixia, W. Xiangke. Chinese Science Bulletin. 57, (2012), 1223–1234.
61- M. Pumera, A. Ambrosi, A. Bonanni, E. L. K. Chng, H. L. Poh. Trends in Analytical Chemistry. 29, (2010), 954–965.
62- G. Xu, Y. Chi, L. Li, S. Liu, X. Kan. Food Chemistry. 177, (2015), 37–42.
63- P. Deng, Z. Xu, R. Zeng, C. Ding. Food Chemistry. 180, (2015), 156–163.
64- S. Basu, P. Bhattacharyya. Sensors and Actuators B. 173, (2012), 1–21.
65- C. Galande, W. Gao, A. Mathkar, A. M. Dattelbaum, T. N. Narayanan, A. D. Mohite, P. M. Ajayan. Particle & Particle Systems Characterization. 31, (2014), 619–638.
66- D. Chen, H. Feng, J. Li. Chemical reviews. 112, (2012), 6027−6053.
67- A. S. Adekunle, S. Lebogang, P. L. Gwala, T. P. Tsele, L. O. Olasunkanmi, F. O. Esther, D. Boikanyo, N. Mphuthi, J. A. O. Oyekunle, A. O. Ogunfowokan, E. E. Ebenso. RSC Advances. 5, (2015), 27759–27774.
68- M. Azimzadeh, M. Rahaiea, N. Nasirizadeh, K. Ashtari, H. Naderi-Manesh. Biosensors and Bioelectronics. 77, (2016), 99–106.
69- M. Azimzadeh, M. Rahaie, N. Nasirizadeh, H. NaderiManesh. Analytical Methods. 7, (2015), 9495–9503.
70- L. A. Pradela-Filho, B. C. Oliveira, R. M. Takeuchi, A. L. Santos. Electrochimica Acta. 180, (2015), 939–946.
71- A. Escarpa, M. C. Gonzalez, M. A. Lopez (Eds.), (2015). Agricultural and Food Electroanalysis. United Kingdom: John Wiley & Sons.
72- Z. Zhang, R. Cai, F. Long, J. Wang. Talanta. 134, (2015), 435–442.
73- Y. Liu, J. Liu, H. Tang, J. Liu, B. Xu, F. Yu, Y. Li. Sensors and Actuators B. 206, (2015), 647–652.
74- H. C. Yu, X. Y. Huang, F. H. Lei, X. C. Tan, Y. C. Wei, H. Li. Electrochimica Acta. 141, (2014), 45–50.
75- Y. Wang, B. Song, J. Xu, S. Hu. Microchim Acta. 182, (2015), 711–718.
76- L. Saghatforoush, M. Hasanzadeh, N. Shadjou. Chinese Chemical Letters. 25, (2014), 655–658.
77- L. Saghatforoush, M. Hasanzadeh, N. Shadjou. Journal of Electroanalytical Chemistry. 714-715, (2014), 79–84.
78- K. Kamil Reza, N. Singh, S. K. Yadav, M. K. Singh, A.M. Biradar. Biosensors and Bioelectronics. 62, (2014), 47–51.
79- R. Thangaraj, A. S. Kumar. Analytical Methods. 4, (2012), 2162–2171.

80- W. Sun, X. Qi, Y. Zhang, H. Yang, H. Gao, Y. Chen, Z. Sun. Electrochimica Acta. 85, (2012), 145–151.
81- M. Oliveira, S. Viswanathan, S. Morais, C. Delerue-Matos. Chemical Papers. 66, (2012), 891–898.
82- X. Tang, Y. Liu, H. Hou, T. You. Talanta. 83, (2011), 1410–1414.
83- A. S. Kumar, R. Shanmugam. Analytical Methods. 3, (2011), 2088–2094.
84- M.L. Rodríguez-Méndez, M. Gay, C. Apetrei, J.A. De Saja. Electrochimica Acta. 54, (2009), 7033–7041.
85- S. Y. Ly, C. H. Lee, Y. S. Jung. Neuromolecular Medicine. 11, (2009), 20–27.
86- H. Yi, W. Qu, W. Huang. Microchim Acta. 160, (2008), 291–296.
87- J.-M. Zen, Y.-Y. Lai, H.-H. Yang, A. Senthil Kumar. Sensors and Actuators B. 84, (2002), 237–244.
88- J.-M. Zen, Y.-Y. Lai, G. Ilangovan, A. Senthil Kumar. Electroanalysis. 12, (2000), 280–286.
89- L. Wang, R. Yang, H. Wang, J. Li, L. Qu, P. d. B. Harrington. Talanta. 138, (2015) 169–175.
90- M. R. Majidi, S. Ghaderi, K. Asadpour-Zeynali, H. Dastangoo. Food Analytical Methods. 8, (2015), 2011–2019.
91- D. Bagal-Kestwal, R. M. Kestwal, B.-C. Hsieh, R. L.C. Chen, T.-J. Cheng, B.-H. Chiang. Biosensors and Bioelectronics. 26, (2010), 118–125.
92- B. Rezaei, M. Ghiaci, M. E. Sedaghat. Sensors and Actuators B. 131, (2008), 439–447.
93- M. Sharifian, N. Ashraf, M. H. Arbab Zavar, M. Chamsaz, F. Afzali. Journal of The Electrochemical Society. 162, (2015), 57–61.
94- N. Akhtar, S. A. El-Safty, M. Khairy, W. A. El-Said. Sensors and Actuators B. 207, (2015), 158–166.
95- X. Zhao, W. Zhang, H. Chen, Y. Chen, G. Huang. Food Analytical Methods. 7, (2014), 1557–1563.
96- Y. Yao, Y. Wen, L. Zhang, Z. Wang, H. Zhang, J. Xu. Analytica Chimica Acta. 831, (2014), 38–49.
97- X. Yang, F. Zhang, Y. Hu, D. Chen, Z. He, L. Xiong. International Journal of Electrochemical Science. 9, (2014), 5061–5072.
98- L. Tian, B. Wang, R. Chen, Y. Gao, Y. Chen, T. Li. Microchim Acta. 182, (2015), 687–693.

99- A. Safavi, R. Ahmadi, F. Aghakhani Mahyari, M. Tohidi. Sensors and Actuators B. 207, (2015), 668–672.

100- C. A. Razzino, L. F. Sgobbi, T. C. Canevari, J. Cancino, S. A. S. Machado. Food Chemistry. 170, (2015), 360–365.

101- Y. Kong, X. Shan, J. Ma, M. Chen, Z. Chen. Analytica Chimica Acta. 809, (2014), 54–60.

102- H. Karimi-Maleh, M. Moazampour, M. Yoosefian, A. L. Sanati, F. Tahernejad-Javazmi, M. Mahani. Food Analytical Methods. 7, (2014), 2169–2176.

103- R. Hajian, N. A. Yusof, T. Faragi, N. Shams. PLOS ONE. 9, (2014), 96686.

104- V. L.V. Granado, M. Gutiérrez-Capitán , C. Fernández-Sánchez , M. T. S. R. Gomes , A. Rudnitskaya, C. Jimenez-Jorquera. Analytica Chimica Acta. 809, (2014), 141–147.

105- M. Amatatongchai, W. Sroysee, S. Chairam, D. Nacapricha. Talanta. 133, (2015), 134–141.

106- Y. Yang, J. Zhou, H. Zhang, P. Gai, X. Zhang, J. Chen. Talanta. 106, (2013), 206–211.

107- Q. Wang, I. Kaminska, J. Niedziolka-Jonsson, M. Opallo, M. Li, R. Boukherroub, S. Szunerits. Biosensors and Bioelectronics. 50, (2013), 331–337.

108- L. Tian, Y. Gao, L. Li, W. Wu, D. Sun, J. Lu, T. Li. Microchim Acta. 180, (2013), 607–612.

109- H. Shekarchizadeh, A. A. Ensafi, M. Kadivar. Materials Science and Engineering C. 33, (2013), 3553–3561.

110- J.-M. Jian, Y.-Y. Liu, Y.-L. Zhang, X.-S. Guo, Q. Cai. Sensors. 13, (2013), 13063–13075.

111- S. Gheibi, H. Karimi-Maleh, M. A. Khalilzadeh, H. Bagheri. Journal of Food Science and Technology. 52, (2015), 276–284.

112- R. Celiešiūtė, G. Grincienė, Š. Vaitekonis, T. Venckus, T. Rakickas, R. Pauliukaitė. Chemija. 24, (2013), 296–306.

113- M. Bijad, H. Karimi-Maleh, M. A. Khalilzadeh. Food Analytical Methods. 6, (2013), 1639–1647.

114- M. Y. M. Abdelrahim, S. R. Benjamin, L. M. Cubillana-Aguilera, I. Naranjo-Rodríguez, J. L. H.-H. d. Cisneros, J. J. Delgado, J. M. Palacios-Santander. Sensors.13, (2013), 4979–5007.

115- C. Li, G. Zhan, M. Ma, Z. Wang. Colloids and Surfaces B: Biointerfaces. 90, (2012), 152–158.

116- S. Lata, B. Batra, N. Karwasra, C. S. Pundir. Process Biochemistry. 47, (2012), 992–998.

117- I. Ion, A. C. Ion. Sensors and Actuators B. 166–167, (2012), 842–847.

118- C. Ajaero, M. Y. M. Abdelrahim, J. M. Palacios-Santander, M. L. A. Gil, I. Naranjo-Rodríguez, J. L. H.-H. d. Cisneros, L. M. Cubillana-Aguilera. Sensors and Actuators B. 171–172, (2012), 1244–1256.

119- R. Rawal, S. Chawla, T. Dahiya, C. S. Pundir. Analytical and Bioanalytical Chemistry. 401, (2011), 2599–2608.

120- M.-F. Pan, G.-Z. Fang, B. Liu, K. Qian, S. Wang. Analytica Chimica Acta. 690, (2011), 175–181.

121- M. Hämmerle, K. Hilgert, M. A. Horn, R. Moos. Sensors and Actuators B. 158, (2011), 313–318.

122- K. C. Honeychurch, L. Gilbert, J. P. Hart. Analytical and Bioanalytical Chemistry. 396, (2010), 3103–3111.

123- D. Brondani, I. C. Vieira, C. Piovezan, J. M. Ramos da Silva, A. Neves, J. Dupont, C. W. Scheeren. Analyst. 135, (2010), 1015–1022.

124- R. Pauliukaite, M. E. Ghica, C. M. A. Brett. Analytical and Bioanalytical Chemistry. 381, (2005), 972–978.

125- P. J. O'Connell, C. Gormally, M. Pravda, G. G. Guilbault. Analytica Chimica Acta. 431, (2001), 239–247.

126- S. Jiao, J. Jin, L. Wang. Sensors and Actuators B. 208, (2015), 36–42.

127- A.-R. H. Abdel-Azzem Hassan, A. D. L. Escosura-Muñiz, A. Merkoçi. Biosensors and Bioelectronics. 67, (2015), 511–515.

128- J. Zhang, X. Shao, J. Yue, D. Li, Z. Chen. Nanoscale Research Letters. 9, (2014), 639–645.

129- Y. Yang, G. Fang, X. Wang, M. Pan, H. Qian, H. Liu, S. Wang. Analytica Chimica Acta. 806, (2014), 136–143.

130- A. Rahim, L. S. S. Santos, S. B. A. Barros, L. T. Kubota, R. Landers, Y. Gushikem. Electroanalysis. 26, (2014), 541–547.

131- T. Gan, Z. Shi, J. Sun, Y. Liu. Talanta. 121, (2014), 187–193.

132- Y. Yang, G. Fang, G. Liu, M. Pan, X. Wang, L. Kong, X. He, S. Wang. Biosensors and Bioelectronics. 47, (2013), 475–481.

133- M. Rajkumar, Y.-S. Li, S.-M. Chen. Colloids and Surfaces B: Biointerfaces. 110, (2013), 242–247.

134- J. Yang, J. R. Strickler, S. Gunasekaran. Nanoscale. 4, 2012, 4594–4602.

135- Y. Zhu, J. I. Son, Y.-B. Shim. Biosensors and Bioelectronics. 26, (2010), 1002–1008.

136- W. Yue, D. Zheng, C. Hu, S. Hu. Journal of Nanoscience and Nanotechnology. 10, (2010), 6586–6593.

137- K. Zór, R. Ortiz, E. Saatci, R. Bardsley, T. Parr, E. Csöregi, M. Nistor. Bioelectrochemistry. 76, (2009), 93–99.

138- F. Salam, I. E. Tothill. Biosensors and Bioelectronics. 24, (2009), 2630–2636.

139- A. K. Basu, P. Chattopadhyay, U. Roychoudhuri, R. Chakraborty. Bioelectrochemistry. 70, (2007), 375–379.

140- J. Â. R. C. Rocha, L. Â. Kosminsky, T. R. L. C. Paixa Äo, M. Bertotti. Electroanalysis. 13, 2001, 155–160.

141- A. Pizzariello, M. Stred'ansky, S. Stred'anska, S. Miertus. Sensors and Actuators B. 76, (2001), 286–294.

142- M. Lütfi Yola, T. Eren, N. Atar. Sensors and Actuators B. 210, (2015), 149–157.

143- J. Yi, S. Tang, Z. Wang, Y. Yin, S. Yang, B. Zhang, S. Shu, T. Liu, L. Xu. International Journal of Environmental Analytical Chemistry. 95, (2015), 158–174.

144- J. Yang, P. Gao, Y. Liu, R. Li, H. Ma, B. Du, Q. Wei. Biosensors and Bioelectronics. 64, (2015), 13–18.

145- Z. Yan, P. Xiong, N. Gan, J. He, N. Long, Y. Cao, F. Hu, T. Li. Journal of Electroanalytical Chemistry. 736, (2015), 30–37.

146- A. Turco, S. Corvaglia, E. Mazzotta. Biosensors and Bioelectronics. 63, (2015), 240–247.

147- K. Thandavan, S. Gandhi, N. Nesakumar, S. Sethuraman, J. B. Balaguru Rayappan, U. M. Krishnan. Sensors and Actuators B. 215, (2015), 166–173.

148- K. Rovina, S. Siddiquee, N. K. Wong. Sensing and Bio-Sensing Research. 4, (2015), 16–22.

149- J. Narayanan, M. K. Sharma, S. Ponmariappan, Sarita, M. Shaik, S. Upadhyay. Biosensors and Bioelectronics. 69, (2015), 249–256.

150- T. Monteiro, P. R. Rodrigues, A. L. Gonçalves, J. J. G. Moura, E. Jubete, L. Añorga, B. Piknova, A. N. Schechter, C. M. Silveira, M. G. Almeida. Talanta. 142, (2015), 246–251.

151- H. Liu, C. Gu, D. Li, M. Zhang. Materials Research Bulletin. 64, (2015), 375–379.

152- Y. Lin, X. Chen1, Y. Lin, Q. Zhou, D. Tang. Microchim Acta. 182, (2015), 1803–1809.

153- H. Li, B. Xu, D. Wang, Y. Zhou, H. Zhang, W. Xia, S. Xu, Y. Li. Journal of Biotechnology. 203, (2015), 97–103.

154- C. Hu, J. Deng, X. Xiao, X. Zhan, K. Huang, N. Xiao, S. Ju. Electrochimica Acta. 158, (2015), 298–305.

155- H. Filik, A. Aslıhan Avan, S. Aydar. Arabian Journal of Chemistry. 9, (2016), 471–480.

156- M. Eguílaz, R. Villalonga, J. M. Pingarrón, N. F. Ferreyra, G. A. Rivas. Sensors and Actuators B. 216, (2015), 629–637.

157- V. Dharuman, C. Anjalidevi, P. N. Manikandan, H. Imran. Analytical Methods. 7, (2015), 3454–3460.

158- J. Deng, S. Ju, Y. Liu, N. Xiao, J. Xie, H. Zhao. Food Analytical Methods. 8, (2015), 2437–2446.

159- X. Ye, Y. Du, K. Duan, D. Lu, C. Wang, X. Shi. Sensors and Actuators B. 203, (2014), 271–281.

160- G. Yang, F. Zhao. Biosensors and Bioelectronics. 64, (2015), 416–422.

161- A.-E. Radi, A.-E. El-Naggar, H. M. Nassef. Journal of Electroanalytical Chemistry. 729, (2014), 135–141.

162- L. Peng, S. Dong, H. Xie, G. Gu, Z. He, J. Lu, T. Huang. Journal of Electroanalytical Chemistry. 726, (2014), 15–20.

163- D. Ning, H. Zhang, J. Zheng. Journal of Electroanalytical Chemistry. 717-718, (2014), 29–33.

164- R. Mohammad-Rezaei, H. Razmi, S. Dehgan-Reyhan. Colloids and Surfaces B: Biointerfaces. 118, (2014), 188–193.

165- B. Luo, X. Li, J. Yang, X. Li, L. Xue, X. Li, J. Gu, M. Wang, L. Jiang. Analytical Methods. 6, (2014), 1114–1120.

166- L. Liu, Y. Chao, W. Cao, Y. Wang, C. Luo, X. Pang, D. Fan, Q. Wei. Analytica Chimica Acta. 847, (2014), 29–36.

167- K. Kor, K. Zarei. Journal of Electroanalytical Chemistry. 733, (2014), 39–46.

168- Z. Guo, X.-f. Xu, J. Li, Y.-w. Liu, J. Zhang, C. Yang. Sensors and Actuators B. 200, (2014), 101–108.

169- W. Gao, W. W. Tjiu, J. Wei, T. Liu. Talanta. 120, (2014), 484–490.

170- A. A. Ensafi, N. Zandi-Atashbar, M. Ghiaci, M. Taghizadeh, B. Rezaei. Materials Science and Engineering C. 47, (2015), 290–297.

171- W. R. de Araujo, T. R. L. C. Paixão. Electrochimica Acta. 117, (2014), 379–384.

172- C. Cheng, Y. Peng, J. Bai, X. Zhang, Y. Liu, X. Fan, B. Ning, Z. Gao. Sensors and Actuators B. 190, (2014), 900–906.

173- L. Wu, B. Gao, F. Zhang, X. Sun, Y. Zhang, Z. Li. Talanta. 106, (2013), 360–366.

174- T. Thomas, R. J. Mascarenhas, O. J. D'Souza, P. Martis, J. Dalhalle, B.E. K. Swamy. Journal of Colloid and Interface Science. 402, (2013), 223–229.

175- S. Sadeghi, A. Motaharian. Materials Science and Engineering C. 33, (2013), 4884–4891.

176- B. B. Prasad, A. Prasad, M. Prasad Tiwari. Biosensors and Bioelectronics. 39, (2013), 236–243.

177- B. Liu, D. Tang, B. Zhang, X. Que, H. Yang, G. Chen. Biosensors and Bioelectronics. 41, (2013), 551–556.

178- W. Lian, S. Liu, J. Yu, J. Li, M. Cui, W. Xu, J. Huang. Biosensors and Bioelectronics. 44, (2013), 70–76.

179- R. Li, H. Yu, Y. Li, R. Feng, X. Li, H. Li, Q. Wei, B. Du. Analytical Methods. 5, (2013), 5534–5540.

180- J.-L. Li, D.-D. Pan, H.-J. Zhu, L. Liu. Modern Food Science and Technology. 29, (2013), 2294–2299.

181- V. K. Gupta, M. Lütfi Yola, N. Özaltın, N. Atar, Z. Ü., L. Uzun. Electrochimica Acta. 112, (2013), 37–43.

182- A. A. Ensafi, M. Jafari–Asl, B. Rezaei. Talanta. 103, (2013), 322–329.

183- J. S. Easow, T. Selvaraju. Electrochimica Acta. 112, (2013), 648–654.

184- O. J. D'Souza, R. J. Mascarenhas, T. Thomas, I. N.N. Namboothiri, M. Rajamathi, P. Martis, J. Dalhalle. Journal of Electroanalytical Chemistry. 704, (2013), 220–226.

185- P. R. Dalmasso, M. L. Pedano, Gustavo A. Rivas. Biosensors and Bioelectronics. 39, (2013), 76–81.

186- D. Chen, J. Deng, J. Liang, J. Xie, C. Hu, K. Huang. Sensors and Actuators B. 183, (2013), 594–600.

187- N. Chauhan, J. Narang, Sunny, C.S. Pundir. Enzyme and Microbial Technology. 52, (2013), 265–271.

188- A. Afonso, B. Pe´rez-Lo´pez, R. C. Faria, L. H.C. Mattoso, M. Herna´ndez-Herrero, A. X. Roig-Sague´s, M. Maltez-da Costa, A. Merkoci. Biosensors and Bioelectronics. 40, (2013), 121–126.

189- X. Sun, L. Guan, X. Shan, Y. Zhang, Z. Li. Journal of Agricultural and Food Chemistry. 60, (2012), 10979−10984.

190- D. Lu, S. Lin, L. Wang, X. Shi, C. Wang, Y. Zhang. Electrochimica Acta. 85, (2012), 131–138.

191- W. Lian , S. Liu, J. Yu, X. Xing, J. Li, M. Cui, J. Huang. Biosensors and Bioelectronics. 38, (2012), 163–169.

192- G. Bacher, S. Pal, L. Kanungo, S. Bhand. Sensors and Actuators B. 168, (2012), 223–230.

193- J. Narang, N. Chauhan, C. S. Pundir. Analyst. 136, (2011), 4460–4466.

194- Y. T. Liu, J. Deng, X. L. Xiao, L. Ding, Y. L. Yuan, H. Li, X. T. Li, X. N. Yan, L. L. Wang. Electrochimica Acta. 56, (2011), 4595–4602.

195- B. Xu, M.-L. Ye, Y.-X. Yu, W.-D. Zhang. Analytica Chimica Acta. 674, (2010), 20–26.

196- M. Xi, Y. Duan, X. Li, L. Qu, W. Sun, K. Jiao. Microchimica Acta. 170, (2010), 53–58.

197- A. Safavi, N. Maleki, H. Ershadifar, F. Tajabadi. Analytica Chimica Acta. 674, (2010), 176–181.

198- Q. Cao, H. Zhao, Y. He, N. Ding, J. Wang. Analytica Chimica Acta. 675, (2010), 24–28.

199- M. M. Rahman, M. J.A. Shiddiky, M. Aminur Rahman, Y.-B. Shim. Analytical Biochemistry. 384, (2009), 159–165.

200- N. Gan, F. Wang, L.-Y. Wang, T.-H. Li, X. Yang. Chinese Journal of Sensors and Actuators. 22, (2009), 456–460.

201- S. Chen, R. Yuan, Y. Chai, B. Yin, W. Li, L. Min. Electrochimica Acta. 54, (2009), 3039–3046.

202- H. Wu, W. Yang, J. Ma. Chemistry Bulletin / Huaxue Tongbao. 71, (2008), 394–397.

203- I. S. Arvanitoyannis, L. Bosena. Critical Reviews in Food Science and Nutrition. 44, (2004), 63–76.

204- M. Khanna, S. Roy, R. Kumar, S. Wadhwa, A. Mathur, A. K. Dubey. IEEE Sensors Journal. 18, (2018), 2206–2210.

205- C. Fu, C. Liu, Y. Li, Y. Guo, F. Luo, P. Wang, L. Guo, B. Qiu, Z. Lin. Analytical chemicstry. 88, (2016), 10176−10182.

206- F. Long, Z. Zhang, J. Wang, L. Yan, B. Zhou. Electrochimica Acta. 168, (2015), 337–345.

207- A. I. Zia, A. Rao, S. C. Mukhopadhyay, (2015). In S. C. Mukhopadhyay (Ed.), Next Generation Sensors and Systems. (pp. 55–79). Switzerland: Springer.

2. AIMS OF THE THESIS

The goal of this 3-year PhD project was to provide a new, alternative analytical tool for the determination of primary aromatic amines (PAAs) that can possibly migrate from food packaging materials to the food. More specifically, the new device has been thought as a new tool for in-line quality control operations within the packaging companies' plants, with special reference to those converters that make use of polyurethane adhesives (PUs) to obtain multi-layer packaging materials.

To achieve this goal, we first decided to review the fundamental mechanisms underlying the formation of PAAs, in order to reconsider mechanisms of formation that were somehow underestimated or neglected in the past years. In a second part of the work, we focused on the development of electrochemical sensors specifically designed for the selective quantification of PAAs. In particular, TDA and MDA (the two most important PAAs that can originate from PU-based adhesive systems) were selected as PAAs. The high selectivity and sensitivity aimed for the electrochemical sensors were conceived as a result of the synergism arising from electrochemistry, polymer science, and nanotechnology concepts.

3. CHAPTER 1

On the origin of primary aromatic amines in food packaging materials

This chapter specifically focuses on the formation of PAAs arising from the cleavage of secondary bonds (namely allophanate and biuret bonds) on the main PU backbone due to the effect of high temperatures. Such high temperatures can be due to both typical preservative thermal treatments (e.g., pasteurization and sterilization) and pre-consumption operations (e.g., vacuum-cooking, microwaving, etc.) on packaged foods. However, because greater attention is generally posed to the "in service" life of packaged food, we deliberately focused on the heat treatments occurring before the food reaches the market shelves. After highlighting the chemical basis of the PAAs formation, we describe the physical aspects associated with their migration, in order to better clarify the potential risks that might arise from an underestimation of the overall phenomenon. We have finally stressed the importance of strictly complying with the current legislation on food contact materials through an adequate setting of the assessment procedures for the quantification of PAAs migrating from the packaging to the food after thermal treatments.

3.1. Introduction

Multilayer packages consist of several layers of different materials (generally from two layers up to 15 layers) on top of one another to yield an aggregate thickness defined, by convention, to be less than 250 μm (thicker structures are typically identified as “sheet” materials) (1). The combination of different plastic materials, sometimes including metal or cellulosic substrates, underlies the rapid popularity of laminated structures, as they allow for fine-tuning the final performance of the ultimate package to precisely match the food’s requirement for an extended shelf life.

Several converting operations concern multilayered packaging materials, namely printing, coating, laminating, and finishing. Lamination, in particular, is the operation that allows for the holding together of different layers for the entire life cycle of the package. Although extrusion lamination and coextrusion are widely adopted processes, the lamination mediated by an adhesive (often called “tie” layer) finds application in most converting lines due to the ease of manufacturing and the low cost involved (2) (Figure 1a). Among the wide assortment of adhesive systems commercially available, polyurethane (PU) adhesives are well-known for superior flexibility, mechanical and adhesion properties, and weathering resistance (3), which play an important role when severe processing/environmental conditions (e.g., high temperature of retort processing, aggressive chemicals, or high-moisture environments) may affect the package performance and the quality of the food inside it.

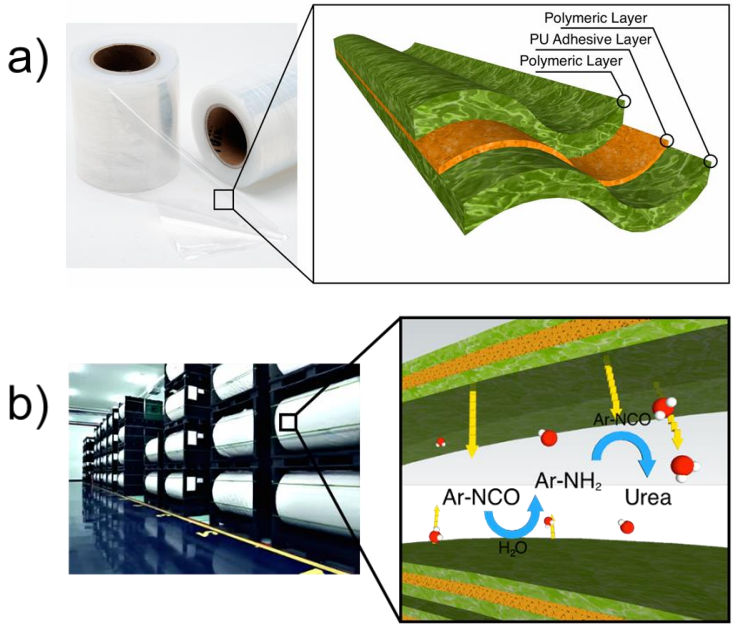

Figure 1. (a) Schematic representation of a PU adhesive-based laminate packaging material (3-layer structure). (b) Sketch on the formation of poly(urea) in PU adhesive-based multilayer packaging materials wound in reels. Red-white spheres: water molecule; Ar-NCO: aromatic isocyanate monomers; Ar-NH_2: aromatic amines.

PU adhesives come from reactive systems usually including two main components, one carrying isocyanic moieties (NCO-terminated) and the other containing hydroxyl groups (OH-terminated). These components, when mixed together, undergo chemical reactions (i.e., chain extension) that bind the applied materials into a solid layer of high molecular weight PU adhesive (Figure 2, scheme 1). The adhesive components react after lamination, further increasing the molecular weight of the PU adhesive to achieve the required performance (4). Because the adhesives are made of reactive chemicals that are expected to polymerize by linear extension and/or cross-link, government food-safety-related agencies (e.g., the Food and Drug Administration [FDA] in the United States and the European Food Safety Authority [EFSA]) have established a strict legislative body to control the risk associated with the potential migration of toxic substances from the adhesives to the food (e.g., unreacted residuals), which in turn might also have harmful effects on the consumers' health (5). In the case of multilayer packaging materials (e.g., pouches, trays, bags, wrappers, etc.), in particular, one of the main issues related to PU adhesive systems is the potential presence of primary aromatic amines (PAAs) in the food matrix (6). The potential risk associated with PAAs arises from the suspected carcinogenic activity of some of them that can affect humans (e.g., 2,4 and 2,6-diaminotoluene and 4,4-methylenedianiline), as stated by the International Agency for Research on Cancer (7).

Unlike the U.S. regulation, which has banned the aromatic-based PU adhesives to the advantage of fully aliphatic systems (8), the European legislation establishes that "…plastic materials and articles shall not release primary aromatic amines in a detectable quantity into food or food simulant. The detection limit is 0.01 mg of substance per kg of food or food stimulant (namely, 10 ng g^{-1} of food). The detection limit applies to the sum of primary aromatic amines released (expressed as aniline)" (9). Excluded from this provision are the species reported in Table 1 of Annex I of the same regulation (e.g., 1,3-phenylenediamine and 1,3-benzenedimethanamine).

The most popular method for the quantification of PAAs is the spectrophotometric method, developed by the German Federal Institute for Health Protection of Consumers and Veterinary Medicine (BgVV) (10). This method is based on the derivatization with N-(1-naphthyl)ethylene-1,2-diamine dihydrochloride (NEDA) of the amines present in the aqueous food simulant (acetic acid 3%, w/v) after the migration test. The final colored compound is then measured spectrophotometrically at 550 nm (i.e., the maximum absorbance of the aniline derivative). Quantification of PAAs is expressed as equivalent to aniline. The main drawback associated with this method is its non-selectivity, which may lead to an overestimation of the total amount of PAAs found in the aqueous simulant (11). To overcome this issue, several methods have been developed during the last decade (11–15). Most modern analytical techniques based on mass spectrometry and advances in ionization processes for non-volatile compounds have made use of UHPLC–MS and their hyphenated techniques such as

UHPLC–MS/TQ and, most recently, UHPLC–Q-TOF/MS (16,17). All of these methods, besides targeting increasing sensitivity, demonstrate that the unequivocal identification of all compounds present in food packaging materials, including the non-intentionally added substances (NIAS), can be achieved.

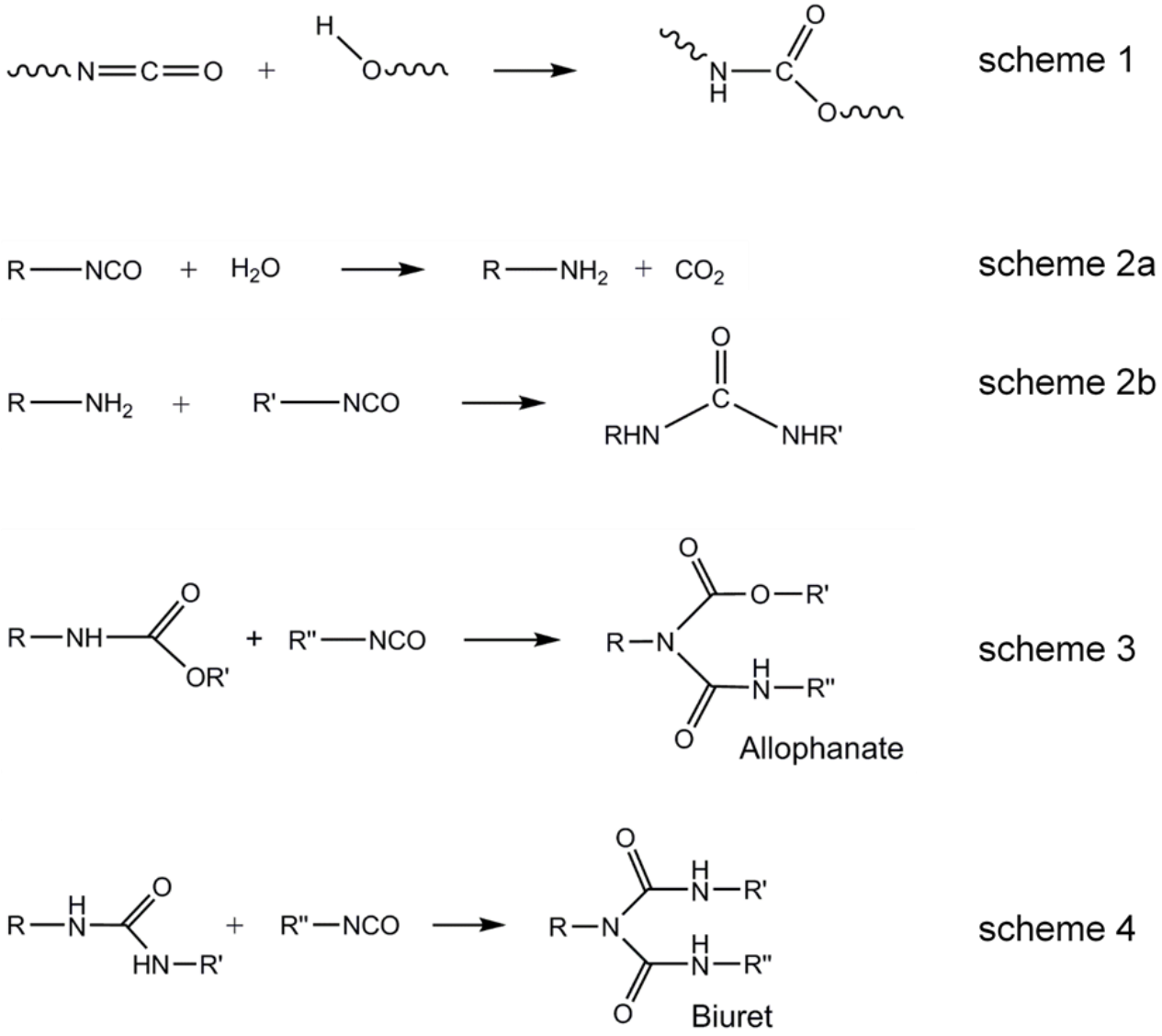

Figure 2. Schematic reaction mechanisms between: an isocyanic group and a hydroxyl group for the formation of an urethane linkage (scheme 1); an isocyanic monomer and a water molecule to yield a primary amine (scheme 2a); a primary amine and an isocyanic monomer to yield an urea (scheme 2b); an urethane group and an isocyanic monomer leading to an allophanate linkage (scheme 3); and an ureic group and an isocyanic monomer to yield a biuret linkage (scheme 4).

The origin of PAAs is primarily linked to residual (unreacted) isocyanic monomers that migrate across the sealing layer, which is generally highly amorphous low-density polyethylene (LDPE) or

cast polypropylene (C-PP) (18) from the PU adhesive to the surface of the laminate. Within this specific time span, i.e. immediately following the lamination process and before the packaging operations, the possibly migrated isocyanic monomer can uniquely come in contact with the air (thus, in contact with the surrounding environmental moisture) between two adjacent coils of the laminated material wound in a reel. The reaction between the residual isocyanic monomer and water molecules leads to the formation of primary amines (Figure 2, scheme 2a). In practice, this issue is commonly addressed by storing the reels of the laminate materials for the time necessary to consume the free isocyanic monomer by: i) further reaction with the main adhesive system, or ii) reacting, after migration, with the water molecules of the environmental humidity always present in traces between the coils of the laminate (19,20). In the latter case, the isocyanic monomers will first react with the water molecules to form primary amines (Figure 2, scheme 2a), which in turn will react with newly-migrated isocyanic molecules to generate (poly)urea (Figure 2, scheme 2b), a whitish, solid, and non-toxic compound that, due to a high melting point, may affect the sealing of packaging materials negatively when present on the surface of the sealing layer in a high amount. Consequently, in the case of a multilayer film wound in a reel, there would never be the formation of primary amines, but only (poly)urea, as schematically depicted in Figure 1b. However, if the same multilayer material were used shortly after lamination to pack a high a_w food, PAAs would be solubilized in the surrounding moisture as soon as they get formed, with consequent diffusion from the internal surface of the laminate to the interior of the package, i.e. to the food. In compliance with the quality management procedures for good manufacturing practice for materials and articles intended to come into contact with food (regulation 2023/2006) (19), laminate manufacturers (e.g., the *converters*) define experimentally (e.g., spectrophotometrically) for each multilayer system the time necessary after lamination to achieve the complete migration of the isocyanic monomer, i.e. the time after which the formation of PAAs no longer occurs (this time is often called *PAAs decay*). Such a time span, which is assumed as the minimum time required before using the packaging material in a safe way, depends on many variables, such as the environmental conditions (e.g., temperature), the PU adhesive system (e.g., type of isocyanic, polyol component, amount of free isocyanic monomer, presence of catalysts, chain extenders, etc.), and the plastic layer between the adhesive and the food matrix (e.g. type of polymer, film thickness, presence of additives such as plasticizer, etc.) (21). Therefore, there will reasonably be a specific PAAs decay for each specific packaging system.

As demonstrated by our literature survey, much less attention has been paid so far to the potential formation of PAAs from alternative routes (e.g., secondary reactions) that, although being quantitatively less significant than the main pathway seen before, could lead to exceed the maximum concentration of PAAs allowed by the current regulations on packaging materials intended to come in contact with food.

3.2. Fundamental chemistry underlying the formation of primary aromatic amines (PAAs)

The isocyanic group (–NCO) can react with a number of compounds containing free functional groups with mobile hydrogen atoms. The reactivity depends on the characteristics of the functional group, as summarized in Table 1. As mentioned in the previous section, the reaction between an isocyanic group and a hydroxyl group has long since been exploited to obtain the urethane linkage. In particular, PU adhesive systems are mainly obtained using aromatic di-isocyanates, the most widely used being methylene diphenyl diisocyanate (MDI) and toluene diisocyanate (TDI) (4). In the presence of water, the reaction to an aromatic isocyanic group leads to the formation of an aromatic amine, with carbamic acid as an instable intermediate and CO_2 as a side product.

While the amines formation is immediately followed by the formation of (poly)ureas through an immediate reaction with the next migrating isocyanic monomer in multi-layer flexible films wound in a reel, a potential safety issue may occur when the same materials are in service. As explained before, the problem is practically overcome by proper handling of the laminates, i.e., by the assessment of the minimum time needed to allow complete migration of the isocyanic monomer from the adhesive layer to the surface that will come into contact with the food. However, this approach only accounts for the potential risk associated with the unreacted isocyanic monomers, thus neglecting any neo-formed PAAs possibly arising from post-treatments of packaged foods. Thermal treatments on packaged foods find applications as a method of cooking, e.g., in vacuum cooking and microwave ovens. However, heat treatments are most often used in the food industry to preserve the packaged foods from microbial spoilage and contamination, thus extending the shelf life. This is achieved through a proper setting of the temperature and the time of the thermal treatment. While pasteurization aims to control the microbial growth with light thermal treatments (e.g., 90°C for 60 minutes), sterilization aims to kill all micro-organisms in the food with the combined use of high temperatures and pressures for a specific amount of time. Typical conditions are 121 °C × 30 minutes or 134 °C × 3 minutes (22)

Table 1. Relative reactivity of active hydrogen compounds against isocyanate (data normalized according to the rate of the isocyanate/water reaction, adapted from 23).

Hydrogen Active Compound	Formula	Relative Reactivity Rate (non-catalyzed, 25 °C)
primary aliphatic amine	$R\text{-}NH_2$	1000
secondary aliphatic amine	$R_2\text{-}NH$	200-500
primary aromatic amine	$Ar\text{-}NH_2$	2-3
primary hydroxyl	$RCH_2\text{-}OH$	1
water	H_2O	1
secondary hydroxyl	$R_2CH\text{-}OH$	0.3
urea	R-NH-CO-NH-R	0.15
tertiary hydroxyl	$R_3C\text{-}OH$	0.005
phenolic hydroxyl	Ar-OH	0.001-0.005
urethane	R-NH-COOR	0.001

Because the binding energy of the urethane bond can withstand these conditions, the cleavage of this linkage due to preservative thermal treatments has to be excluded (24,25). It is likely that there may be some chemical breakdown of the main polymeric chain (depolymerization), with the consequent formation of chains with a lower molecular weight, but in any case, not low enough to allow their migration (26). Conversely, these thermal treatments may disrupt some secondary bonds displaced on the main PU backbone, such as allophanate and biuret bonds (27–29). Allophanates and biurets are formed after addition-type reactions between isocyanic monomers and urethane and ureic groups, respectively (Figure 2, schemes 3 and 4). The amount of allophanate and biuret bonds found in a PU adhesive polymer chain depends, among other factors, on the reaction molar ratio between the polyisocyanic component and polyol component—that is, the higher the amount (in moles) of polyisocyanate, the higher the amount of the above bonds formed (30). In addition, the polymerization temperature may affect the formation of allophanate and biuret bonds, because higher temperatures will lead to a greater formation of allophanate and biuret linkages. On the other hand, the presence of the catalyst and its concentration can also influence the amount of these linkages, reducing the required temperature for their formation (31).

Table 2. Thermal dissociation temperatures of linkages found in polyurethanes (adapted from 23,31,32).

Linkage	Onset of dissociation (°C)
Aromatic urethane[a]	~ 200
Aliphatic urethane[b]	~ 250
Aromatic urea	140-180
Aliphatic urea	160-200
Aromatic biuret	100-110
Aliphatic biuret	115-125
Aromatic allophanate	85-105
Aliphatic allophanate	100-120
Disubstituted urea	235-250

[a]*Formed by reaction between an aryl isocyanate and an alkyl alcohol*

[a]*Formed by reaction between an alkyl isocyanate and an alkyl alcohol*

Due to the higher amount of urethane groups compared to the ureic ones, the allophanate bonds exceed the biuret ones on the main PU adhesive backbone. As shown in Table 2, the thermostability of the above linkages follows the order: urethane > urea > biuret > allophanate. In addition, among allophanate bonds, those obtained from aromatic isocyanic monomers are thermally less stable than those obtained from aliphatic isocyanic monomers (see Table 2). As a consequence, the low thermal stability of allophanates and, to a lesser extent, biurets, can be indicated as the main cause of "re-formation" of isocyanic monomers when laminate structures obtained with aromatic polyurethane adhesive systems are used. The cleavage of the allophanate and biuret bonds begins at approximately 70 °C, and the rate of the "re-formation" of the monomer increases with an increase in temperature, until it can be considered complete for temperatures above 105 °C (29,33,34).

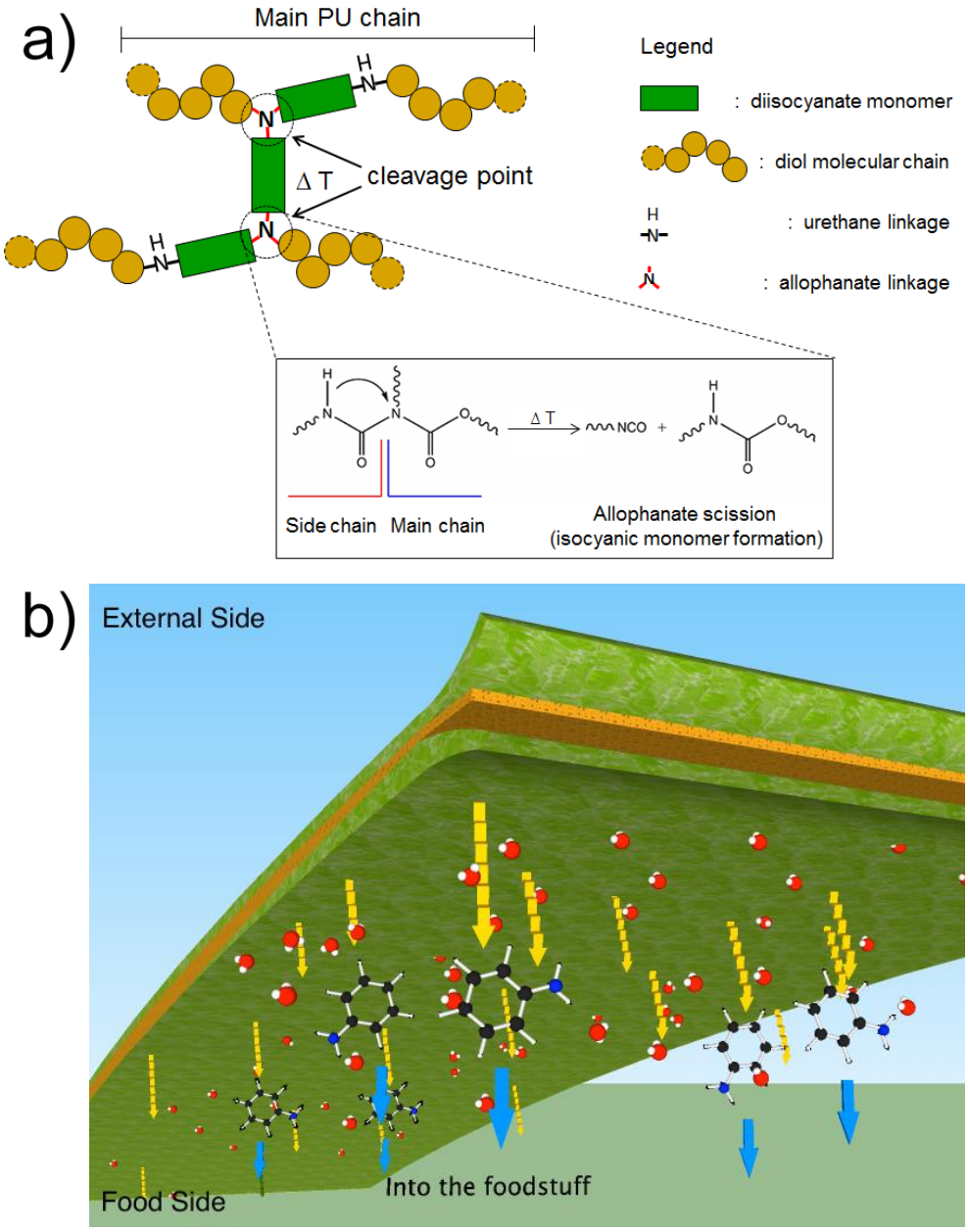

Figure 3. (a) Illustrative drawing of the formation of the isocyanic monomer from the thermal cleavage of the allophanate linkage. (b) Rendering image representing the potential migration of PAAs from the packaging to the food matrix. Red-white spheres: water molecules; black-blue spheres: representative aromatic amine; yellow arrows: migration of the isocyanic monomer; cyan arrows: washing-out effect of environmental moisture.

When a multilayer packaging system obtained using a polyurethane adhesive is subjected to a preservative thermal cycle, there will always be the re-formation of isocyanic monomers due to the cleavage of allophanate linkages as a result of the thermal energy input and the duration of the heating process (Figure 3a). It should also be noted that the migration of the newly formed isocyanic monomer is not so unlikely, due to two main reasons: i) the low molecular weight (MW) of isocyanates,

especially when TDI (MW = 174.2 g mol^{-1}) and MDI (MW = 250.5 g mol^{-1}) are used; and ii) the increased relaxation of the molecular chains of the inner plastic layer (i.e., the sealing layer, which is most often a polyolefin such as low-density polyethylene, LDPE or cast polypropylene, C-PP) due to the high temperature used, which is well above the glass transition temperature (T_g LDPE ~ –125 °C) and, in some circumstances, close to the melting temperature of the polymer (T_m LDPE ~ 105–125 °C) (35).

As anticipated in the previous section, the potential re-formation of isocyanic monomers becomes a crucial point for liquid foods (e.g., retort pouches containing soups) or high water activity (a_w) foods. In fact, when the isocyanic monomers encounter water molecules, the formation of PAAs readily occurs due to the high reactivity of the –NCO group to water at the preservative thermal cycle temperature (36). Provided that the above chemical pathway will find experimental evidence, PAAs can be classified as non-intentionally added substances (NIAS). In addition, because the internal moisture of the package contributes to washing out the freshly formed PAAs from the inner surface of the package (i.e., the sealing layer), the migration of the isocyanic monomers will continuously take place as long as they are consumed through the PAAs formation. In other words, the internal moisture triggers the formation of PAAs, which will thus migrate continuously from the inner packaging layer to the food matrix (Figure 3b).

The most effective counteraction to tackle this issue would be not to use the aromatic isocyanates as starting molecules in the adhesive formulation. However, the use of aliphatic adhesive systems is generally deemed unprofitable. This is because first of all, aliphatic adhesive systems are more costly than polyurethane adhesive systems exclusively based on aromatic isocyanates (aromatic adhesive systems). Secondly, aliphatic adhesive systems have a much lower reactivity compared to the aromatic ones (37). The low reactivity of aliphatic adhesive systems forces converters to extend the storage time of the multilayer reels in the climatic rooms in order to guarantee an adequate degree of polymerization that, in turn, will dramatically affect the ultimate sealing and thermal performance of the PU adhesive. Therefore, the use of aliphatic isocyanates may negatively impact the overall throughput due to evident logistic problems. For all those applications, envisaging the use of aromatic adhesive systems, an assessment of the risk associated with the formation of PAAs "post-thermal treatments" (i.e., after subjecting the packaging materials to preservative thermal cycles) is of utmost importance. Actually, the ongoing European legislation on food contact materials (regulation 10/2011) provides clear provisions for the migration tests on food packaging materials subjected to thermal treatments, inspired by the basic principle that "…the risk assessment should cover the potential migration under worst foreseeable conditions of use and the toxicity" (9). Accordingly, assuming a thermal cycle between 121 °C and 130 °C × 0.5 to 1 hour, the migration test should be carried out at 130 ° C × 1 hour using the simulant B (water solution of acetic acid 3%, w/v). As

confirmed by the work of Pezo and co-workers, the conditions set out by the legislation guarantee a reliable quantification of the PAAs possibly formed after the thermal treatment (17). The main question thus becomes: Do converters take care of quantifying the neo-formed PAAs possibly coming from the preservative thermal treatments of liquid/high a_w foods? Based on an informal survey we conducted throughout the year 2014, out of 52 companies (20 located in Italy, 32 across the European Union), only five (i.e. less than 10%) declared that they consciously complied with the current legislation. This means that they performed the quantification of PAAs accounting for any "*worst foreseeable conditions*," possibly occurring from lamination to service, namely, also considering the preservative thermal cycles (e.g., pasteurization and sterilization). The remaining "outlaw" companies (which of course will be kept undisclosed), though aware of the existence of a specific legislation, admitted to do what many companies do: only quantify the PAAs decay time after lamination. Although the sample we considered cannot be considered as an absolute depiction of the facts, and we cannot generalize the outcome of our survey, it is, however, indicative of a potential scenario among converters. The seriousness of this matter imposes a careful consideration of the risks for public health associated with a potential underestimation of PAAs that may contaminate some types of packaged food. On the other hand, all of the interviewed subjects stated that the quantification of PAAs (both "pre-thermal treatments" and "post-thermal treatments") is performed by the spectrophotometric method (which is in accordance with the requirements of Article 11 of regulation 882/2004 of the European Commission), as equivalent to aniline, probably because it represents a user-friendly, low-cost, and time saving approach compared to most sophisticated and complex techniques (e.g., chromatography analyses). However, it has been pointed out that this colorimetric method is not selective and can overestimate the total amount of PAAs (11,17,18). Therefore, in addition to a greater sensibility of all stakeholders (from the converters to the surveillance authorities) to prevent consumers from potential contamination of foods due to the migration of PAAs above the legislation limits, new easy-to-use, cost-effective, and accurate analytical methods should take over as mandatory procedures for a reliable assessment of the PAAs that migrated from the package to the food. This appears in accordance with the same regulation 10/2011 of the European Commission (forward 45), which clearly states, "Certain migration testing rules should be updated in view of new scientific knowledge. Enforcement authorities and industry need to adapt their current testing regime to these updated rules […]" (9).

3.3. Conclusions

The migration of primary aromatic amines from food-packaging materials represents a serious risk to public health as PAAs are potentially carcinogenic substances. Although the main source of PAAs is represented by residues of aromatic isocyanates arising from incomplete curing of the main

polyurethane adhesive, the thermal effect of heat treatments from ~ 70 °C on, both before reaching the market (e.g., preservative thermal treatments) and after being put in service (e.g., vacuum cooking), may contribute to a significant increase of PAAs migrating into the food. This is the crucial point: Who, among the stakeholders (especially converters), really knows about the potential formation of PAAs possibly caused by thermal treatments on packaged foods, especially before going to the market shelves? The risk is that without this knowledge, the worst foreseeable conditions will not be properly set, leading to a consequent underestimation of the PAAs possibly reaching the food. Based on our experience, the interpretation of the legislation by converters is often wrong, as they tend to consider the "*worst foreseeable conditions*" as only those occurring after the packaged food has been placed on the shelves. However, the legislation indeed includes all the treatments that the package may experience before it enters the market. As long as this aspect remains not totally understood, the risks for public health associated with a potential migration of PAAs that may contaminate some types of packaged food will be high.

At the same time, an "updating" of the analytical tools is necessary for a reliable quantification of PAAs possibly migrating from the packaging materials to the food. In particular, the spectrophotometric/colorimetric method (as equivalent to aniline) does not seem to provide accurate results compared to, for example, chromatography techniques, which are, however, more complicated and expensive, and thus less willingly adopted by most converters.

3.4. References

1- T. Dunn, (2009). Multilayer flexible packaging. In K. L. Yam (Ed.), The Wiley Encyclopedia of Packaging Technology, 3rd ed. (pp. 799–806). Hoboken (NJ): Wiley & Sons.

2- D. V. Rosato, (1998). Extruding Plastics: A Practical Processing Handbook. Berlin: Springer.

3- G. Malucelli, A. Priola, F. Ferrero, A. Quaglia, M. Frigione, C. Carfagna. International Journal of Adhesion and Adhesives. 25, (2005), 87–91.

4- U. Meier-Westhues, (2007). Polyurethanes: Coatings, Adhesives and Sealants. Hannover: Vincentz Network.

5- M. De Fátima Poças, T. Hogg. Trends in Food Science & Technology. 18, (2007), 219–230.

6- K. Ellendt, B. Gutsche, G. Steiner. Deutsche Lebensmittel-Rundschau. 99, (2003), 131–136.

7- P. Vineis, R. Pirastu. Cancer Causes & Control. 8, (1997), 346–355.

8- U.S. Food and Drugs Administration. Indirect food additives: polymers, Pub. L. No. Title 21, Part 177 (2000). United States.

9- European Commission. Commission Regulation (EC) No 10/2011 of 17 January on plastic materials and articles intended to come into contact with food, Official Journal of the European Union (2011). European Union: http://eur-lex.europa.eu/.

10- B. Brauer, T. Funke. Deutsche Lebensmittel-Rundschau. 87, (1991), 280–281.

11- M. Aznar, E. Canellas, C. Nerín. Journal of Chromatography A. 1216, (2009), 5176–5181.

12- M. Akyüz, Ş. Ata. Journal of Pharmaceutical and Biomedical Analysis. 47, (2008), 68–80.

13- V. Andrisano, R. Gotti, A. M. Di Pietra, V. Cavrini. Chromatographia. 39, (1994), 138–145.

14- R. Noguerol-Cal, J. M. López-Vilariño, G. Fernández-Martínez, L. Barral-Losada, M. V. González-Rodríguez. Journal of Chromatography A. 1179, (2008), 152–160.

15- M. Shelke, S. K. Sanghi, A. Asthana, S. Lamba, M. Sharma. Journal of Chromatography A. 1089, (2005), 52–58.

16- M. Mattarozzi, F. Lambertini, M. Suman, M. Careri. Journal of Chromatography. A. 1320, (2013), 96–102.

17- Pezo, D., Fedeli, M., Bosetti, O., & Nerín, C. (2012). Analytica Chimica Acta, 756, 49–59.

18- C. Brede, I. Skjevrak, H. Herikstad. Journal of Chromatography A. 983, (2003), 35–42.

19- European Commission. Commission Regulation (EC) No 2023/2006 of 22 December 2006 on good manufacturing practice for materials and articles intended to come into contact with food, Official Journal of the European Union (2006). European Union: http://eur-lex.europa.eu/.

20- Flexible Packaging Europe. (2008). Code for good manufacturing practices for flexible and fiber-based packaging for food. Retrieved from http://www.flexpack-europe.org/tl_files/FPE/downloads/FPE_GMP_Code_6.0.pdf
21- M. Wirts, D. Grunwald, D. Schulze, E. Uhde, T. Salthammer. Atmospheric Environment. 37, (2003), 5467–5475.
22- D. S. Lee, K. L. Yam, L. Piergiovanni. (2008). Food Packaging Science and Technology. Press, Boca Raton, FL: CRC Press.
23- M. Ionescu. (2005). Chemistry and Technology of Polyols for Polyurethanes. Shawbury, Shrewsbury, Shropshire, U.K: Rapra Technology, Ltd.
24- H. J. Fabris. (1976). Thermal and oxidative stability of urethanes. In K. C. Frisch & S. L. Reegen (Eds.), Advances in Urethane Science and Technology, Vol. 6 (pp. 89–111). Westport (CT): Technomic Publishing Co.
25- Szycher, M. (2012). Szycher's Handbook of Polyurethanes. (2nd ed.). Boca Raton, CRC Press.
26- W. P. Yang, C. W. Macosko, S. T. Wellinghoff. Polymer. 27, (1986), 1235–1240.
27- A. M. Schiller, (1973). Soviet Urethane Technology. Technomic Publishing Company.
28- G. R. Griffin, L. J. Willwerth. I&EC Product Research and Development. 1, (1962), 265–268.
29- I. C. Kogon. Journal of Organic Chemistry. 24, (1959), 83–86.
30- K. Dušek, M. Ilavský, L. Matějka. Polymer Bulletin. 40, (1984), 33–40.
31- A. Lapprand, F. Boisson, F. Delolme, F. Méchin, J.-P. Pascault. Polymer Degradation and Stability. 90, (2005), 363–373.
32- E. Delebecq, J.-P. Pascault, B. Boutevin, F. Ganachaud. Chemical Reviews. 113, (2013), 80−118.
33- I. C. Kogon. Journal of Organic Chemistry. 23, (1958), 1594–1594.
34- N. Yoshitake, M. Furukawa. Journal of Analytical and Applied Pyrolysis. 33, (1995), 269–281.
35- D. B. Malpass. (2010). Introduction to Industrial Polyethylene: Properties, Catalysts, and Processes. Hoboken (NJ): Wiley & Sons
36- G. Avar, U. Meier-Westhues, H. Casselmann, D. Achten. Polyurethanes. Polymer Science: A Comprehensive Reference. 10, (2012), 411–441.
37- D. K. Chattopadhyay, K. V. S. N. Raju. Progress in Polymer Science. 32, (2007), 352–418.

4. CHAPTER 2

Determination of 2,4-diaminotoluene by a bionanocomposite modified glassy carbon electrode

In the present work, we report for the first time on the development of an electrochemical nanosensor for the quantitative determination of 2,4-diaminotoluene (TDA), which is one of the main PAAs that can be formed in food packaging materials that contain aromatic PU adhesives. The main goal of this work was to demonstrate how a "nano" approach is a key to achieve high selectivity, high sensitivity, and a lower limit of detection of the final device, with simultaneous prevention of surface fouling. To this scope, we decided to modify the electrode with gold nanoparticles (AuNPs), multi-walled carbon nanotubes (MWCNTs), and the polycation chitosan (CS) as the main polymer phase. Full electrochemical characterization of the AuNPs/MWCNTs-CS/GCE was carried out, and the arising electrochemical properties were described. A potential application of the developed sensor on real food systems was eventually investigated by preliminary trials using a conventional packaging material.

4.1. Experimental part

4.1.1. Preparation of modified electrodes

MWCNTs (0.5 mg) were added in 1 g EGMe solution, and the mixture was ultrasonicated by means of a UP400S ($power_{max}$ = 400 W; frequency = 24 kHz) ultrasonic device (Hielscher, Teltow, Germany) equipped with a cone frustum titanium sonotrode (mod. H3, tip Ø 3 mm, $amplitude_{max}$ = 210 μm; acoustic power density = 460 W cm^{-2}) under the following conditions: 0.5 cycle and 50% amplitude, for a period of 10 minutes. Afterward, 600 μL of the MWCNTs-EGMe solution was mixed with 150 μL of a chitosan solution (1 wt% in acidic water). Finally, this mixture was again ultrasonicated for 3 minutes to obtain a homogeneous MWCNTs-CS solution.

Before modification, a bare GCE was mechanically polished to a mirror finish with alumina powder on a polishing cloth and rinsed with double-distilled water. To prepare the MWCNTs-CS/GC electrode, 15 μL of the MWCNTs-CS solution was poured onto the GCE surface and dried with a double-bulb infrared lamp (type B, 1440 W) (Helios Italquartz srl, Cambiago, Italy) at a distance of 40 cm for 10 minutes. Subsequently, the AuNPs/MWCNTs-CS/GC electrode was prepared by dropping 5 μL of AuNPs solution (16.5×10^{12} particles/mL) on the surface of the MWCNTs-CS/GC electrode and again dried as before. The electrode was then washed with double-distilled water and stored at 4 °C when not in use. The MWCNTs/GC electrode and the AuNPs/GC electrode were prepared according to the same procedure, with the exception of chitosan preparation.

4.1.2. Morphological characterization of the electrodes' surface

A field emission scanning electron microscope (FE-SEM), Hitachi S-4800 (Schaumburg, IL), was used for electrode surface imaging. MWCNTs-coated, MWCNTs/CS-coated, AuNPs-coated, and MWCNTs-CS/AuNPs-coated GCE specimens were mounted with carbon tape on stubs and their surfaces observed after sputtering with Pt/Pd (60/40) under argon for 20 s at a current of 80 mA. The samples were observed using an acceleration voltage of 1-5 kV, and an electrode current of 10 μA.

4.1.3. Real sample analysis

Thermo-sealed bags of 1 dm^2 of surface area per side were prepared using a multilayer packaging material (Castagna Univel Spa, Guardamiglio, Italy) consisting of polyethylene terephthalate (PET, 12 μm thick), polyvinilidene chloride coating (PVDC, 6 μm thick), and low-density polyethylene (LDPE, 50 μm thick) whereby a PU adhesive was used to join together PET to the remaining part of the film. Each bag was filled with 100 mL of food simulant B (i.e., acetic acid water solution, 3 w/v %) (1), which represents the worst-case condition to evaluate potential PAA migration from PU-based multilayer packaging materials (2). The test was conducted at 121 ˚C for 20 minutes in an

autoclave (Asal 760, Steroglass srl, Perugia, Italy). After this time, 10 mL of simulant B was diluted with 10 mL PBS followed by the addition of specific amounts of TDA monitored by amperometry. From the quantitative determination of TDA, the final recovery (%) was determined.

4.2. Results and discussion

4.2.1. Morphological characterization of modified GCEs

Some representative FE-SEM images of the surface morphology of the electrochemical sensors are reported in Figure 1. Figure 1a shows the marked change in morphology after modification of the bare GCE with MWCNTs. A worm-like morphology due to the presence of carbon nanotubes of approximately 12 nm average diameter and 15–20 μm in length yielded a considerably higher specific surface area compared to the bare electrode. When the MWCNTs were loaded in the main polymer phase (Figure 1b), they were no longer clearly visible due to the flattening effect of chitosan, although the still highly rough surface of the modified GCE confirmed their presence (see the inset of Figure 1b).

The addition of AuNPs can be easily detected on the bare GCE, where they appear as small particles clustered in larger domains of 500 nm to 1.0 μm size (Figure 1c). However, when AuNPs are deposited on top of the MWCNTs-CS surface, they are hardly visible (Figure 1d and inset). This is probably due to the swelling of the chitosan matrix caused by the solvent (PBS) used for the AuNPs, which are eventually wrapped by the main biopolymer phase.

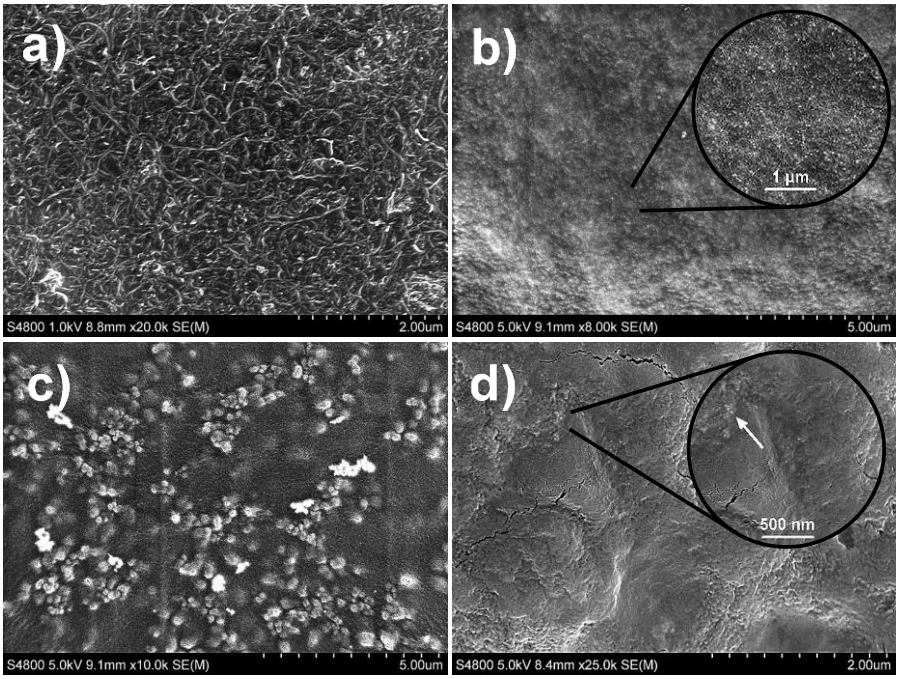

Figure 1. FE-SEM surface images of (a) MWCNTs/GCE, (b) MWCNTs-CS/GCE, (c) AuNPs/GCE, and (d) AuNPs/MWCNTs-CS/GCE.

4.2.2. Electrochemical behavior of TDA on electrode surface

The electrochemical behavior of TDA on the surface of both bare and modified electrodes was investigated by cyclic voltammetry (CV). Figure 2 depicts the CV response obtained for the bare GCE (a) and the electrode modified according with different degrees of complexity; MWCNTs/GCE (b), MWCNTs-CS/GCE (c), and AuNPs/MWCNTs-CS/GCE (d), in the presence of 500 μM TDA in PBS at a scan rate of 50 mV/s. At first glance, it can be clearly seen that the higher the degree of complexity of the modification, the higher the current recorded at the electrode's surface. More specifically, the bare electrode (Figure 2, trace a) showed a weak oxidation peak current response of 1.39 μA for TDA at 510 mV (Table 1). The first type of modification with only MWCNTs (Figure 2, trace b) yielded a higher oxidation peak current response of 2.79 μA at the same voltage compared to the bare electrode (Table 1). This can be plausibly explained in consideration of both the increased surface area of the electrode and the enhanced conductivity ensuing from the addition of MWCNTs.

The next step of modification, in which chitosan was included as the main polymer phase (Figure 2, trace c), led to an additional shift of the peak current toward higher values (9.43 μA) (Table 1). Such a dramatic increase in the peak current can be explained in terms of a co-continuous conductive composite network arising from the addition of chitosan incorporated with MWCNTs. The excellent adhesion properties of chitosan on the glassy surface of the electrode might also have played a role in increasing the catalytic performance of the MWCNTs/GC electrode. The best performance was eventually achieved by the deposition of AuNPs on the MWCNTs-CS/GCE surface (Figure 2, trace d). As shown in Table 1, the AuNP/MWCNTs-CS/GCE reached the maximum current response (9.87 μA) as assessed by CV. This shows the extra benefit that arose from the addition of Au nanoparticles, which increased both the surface area exposed to the medium and the electrical conductivity of the electrode due to the topological electrical contact points throughout the matrix. A similar dual phase conductive element approach was previously reported using silver nanowires to successfully interconnect a carbon nanotubes network (3,4).

Table 1. Comparison of the electrocatalytic oxidation peak current (I_p) of TDA (500 µM) at pH 7.0 on the bare GC electrode according to the different surface modifications (see the main text for details).

Electrode	Oxidation peak current (µA)	Drying method
Bare GCE	1.39	–
MWCNTs/GCE	2.79	IR lamp
MWCNTs-CS/GCE	9.43	IR lamp
AuNPs/MWCNTs-CS/GCE	9.87	IR lamp

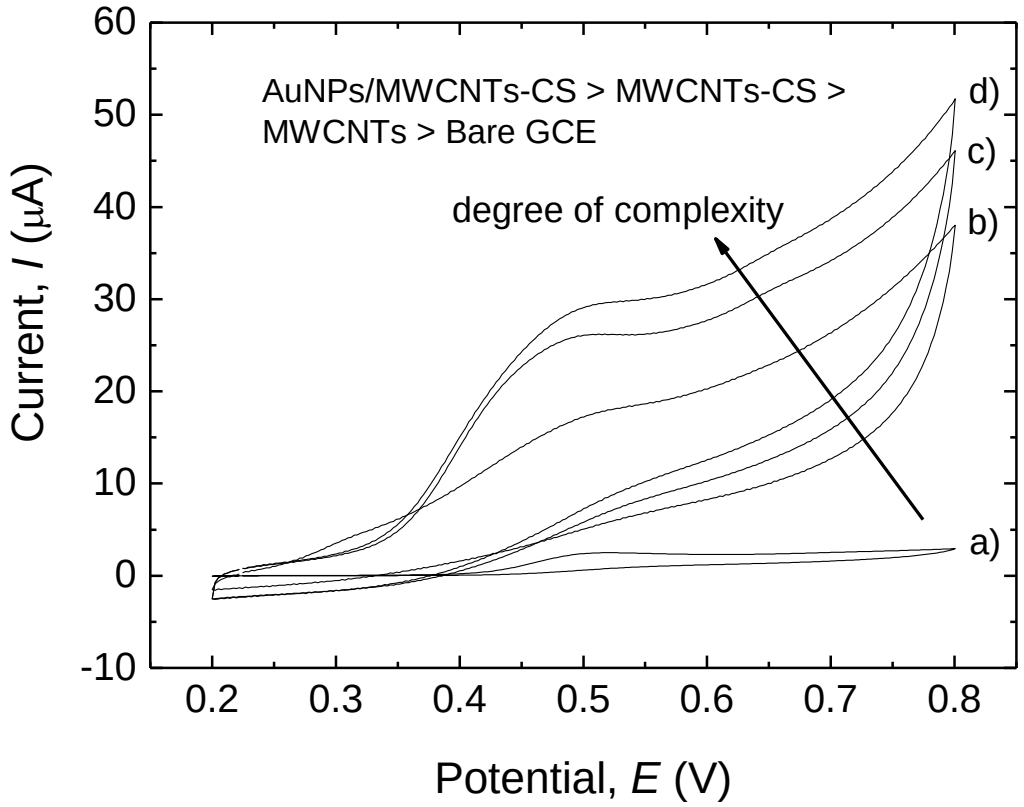

Figure 2. Cyclic voltammograms in phosphate buffer (pH 7.0) at a 50 mV/s scan rate of (from down-right to up-left direction) (a) bare GCE, (b) MWCNTs/GCE, (c) MWCNTs-CS/GCE, and (d) AuNPs/MWCNTs-CS/GCE in the presence of 500 µM TDA.

4.2.3. Influence of scan rate

The influence of the scan rate on the electrocatalytic oxidation of TDA at the AuNPs/MWCNTs-CS/GCE surface was investigated by CV within a range of 100–800 mV/s at a TDA concentration of 500 µM (Figure 3). The oxidation peak current (I_p) drawn from each scan rate setting was then plotted against the square root of the scan rate (inset of Figure 3). The linearity of the ensuing plot suggests

that the catalytic reaction of the analyte at the electrode's surface is diffusion-limited, that is, no absorption of the analyte within the nanocomposite polymer network occurs before oxidation.

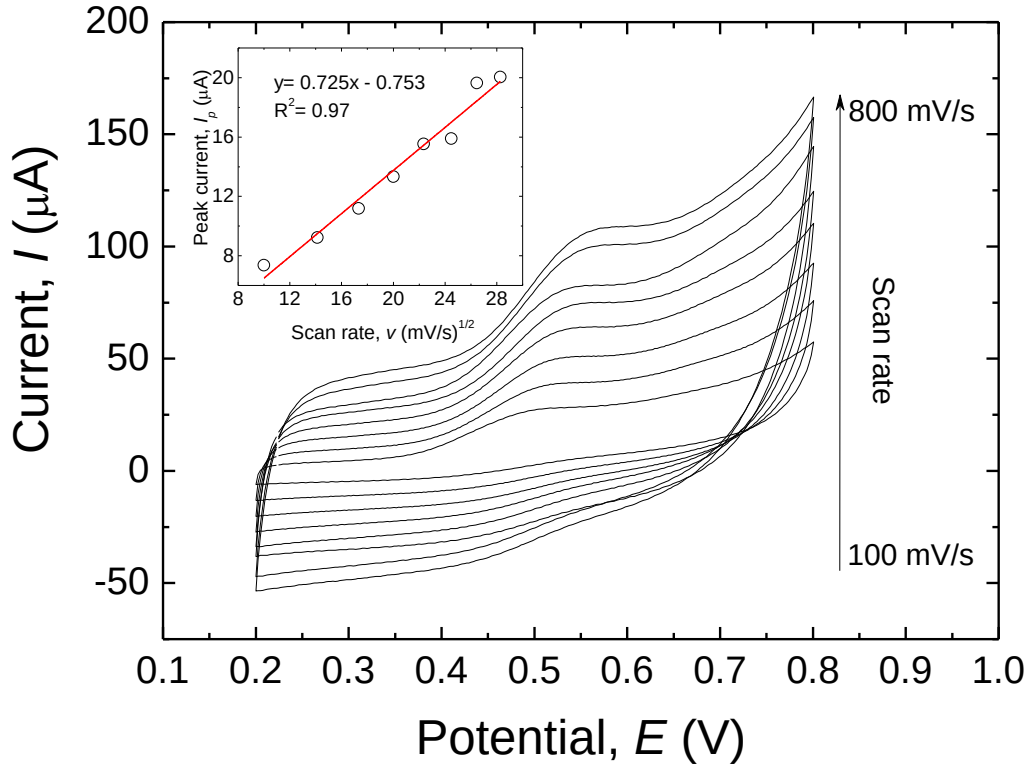

Figure 3. Cyclic voltammograms of AuNPs/MWCNTs-CS/GCE in a phosphate buffer (pH 7.0) containing 500 µM TDA at different scan rates (100–800 mV/s). The electrocatalytic peak current (I_p) variation as a function of the square root of sweep rate is shown in the inset.

In the following step, Tafel's theory was used to gather information on the rate-determining step of the electro-oxidation of TDA (5). To this scope, the Tafel region of the cyclic voltammogram obtained at 100 mV/s was considered (Figure 4) and the related slope determined (Figure 4, inset) according to equation 1 (6):

$$Tafel_{slope} = \frac{(1-\alpha)n_{\alpha}F}{2.3RT} \quad (1)$$

where α is the electron transfer coefficient, n_{α} is the number of electrons transferred until the end of the rate-determining step (up to and including the rate-determining step), F is Faraday's constant, R is gas constant (8.314 J mol^{-1} K^{-1}), and T the temperature (K).

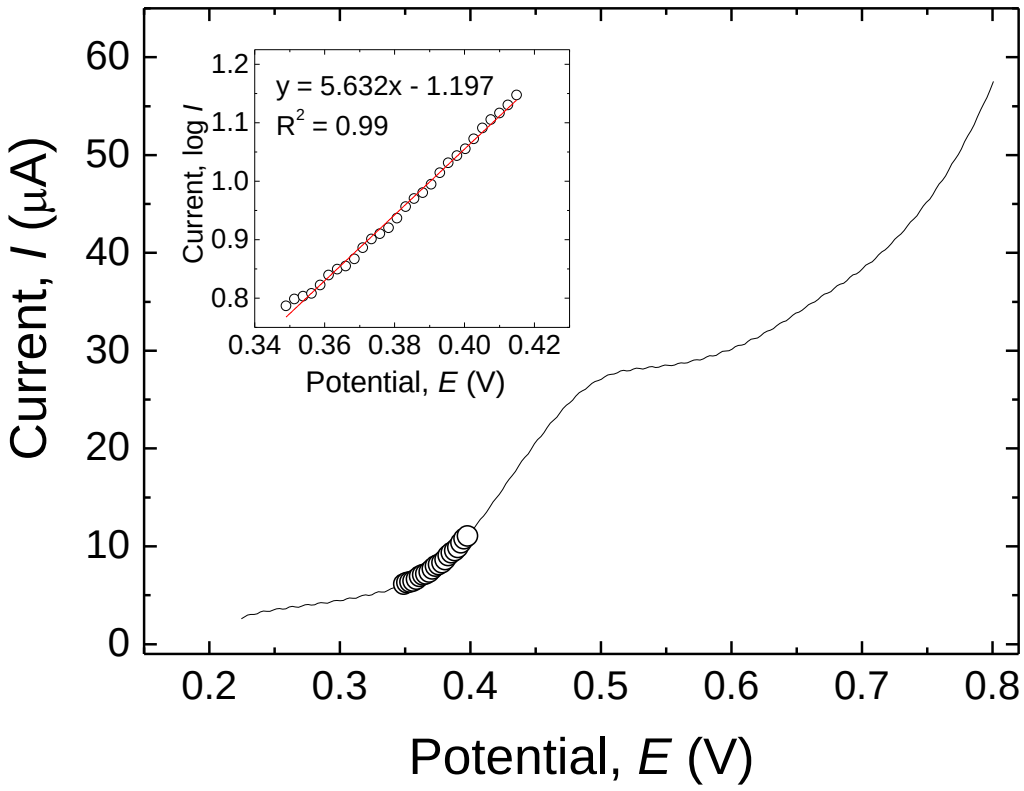

Figure 4. Linear sweep voltammogram of AuNPs/MWCNTs-CS/GCE in a phosphate buffer solution (pH 7.0) containing 500 µM TDA at 100 mV/s. The Tafel plot derived from the linear sweep voltammogram is shown in the inset.

The calculated slope of 5.632 V^{-1} yields an electron (or charge) transfer coefficient of $\alpha \approx 0.6$, if the rate-determining step of the electrode process includes a number of electron transfer ≈ 1. Therefore, a quantitative estimation of n_α involved in the oxidation reaction of TDA was performed using equation 2 (7):

$$\left|E_p - E_{p/2}\right| = \frac{47.7}{\alpha \times n_\alpha} \qquad (2)$$

where E_p is the peak potential (oxidation, in our case) of a selected CV trace (800 mV/s in this study) and $E_{p/2}$ is the half-peak potential, i.e., the potential (V) at the half-peak current ($I_p/2$). Because in our system $|E_p\text{-}E_{p/2}|$ = 60 mV and α = 0.58, a final n_α of ca. 1.35 for TDA oxidation was eventually calculated, which is slightly higher than the theoretical value of ≈ 1 assumed by eq. 1. From the intercept of the Tafel plot, it was also possible to extract the average value of the exchange current (i_0) and the exchange current density (j_0) (6). The values of i_0 and j_0 for TDA were found to be 0.063 µA and 2.019 µA cm^{-2}, respectively.

The total number of electrons (n) involved in the overall catalytic reaction was gathered through Laviron's theory, which is used to investigate the kinetic mechanism of the electrode toward the

analyte. Accordingly, for a totally irreversible electrode process, the anodic peak potential (E_{pa}) and the natural logarithm of the scan rate ln(v) can be defined by the following equation (8):

$$E_{pa} = E^0 + \left(\frac{RT}{\alpha nF}\right) ln\left(\frac{RTK^0}{\alpha nF}\right) + \left(\frac{RT}{\alpha nF}\right) lnv \quad (3)$$

where α is the transfer coefficient, K^0 is the standard rate constant of the reaction, n is the electron transfer number, υ is the scanning rate, E^0 is the formal redox potential, R is the gas constant, T is the absolute temperature, and F the Faraday constant. Using the raw voltammograms as reported in Figure 3, a linear relationship between E_{pa} and ln(v) was obtained as expressed by the equation E_p (V) = 0.0273 ln v (mV/s) + 0.3603 (Figure 5). According to Laviron's equation, the electron transfer number (n) can be calculated from the slope of E_{pa} versus ln(v), that is, RT/αnF. After appropriate substitutions, a final value of n 1.62 ≈ 2 was obtained, indicating that the electrochemical oxidation of TDA at the AuNP/MWCNTs-CS composite modified GCE is a two-electron transfer process.

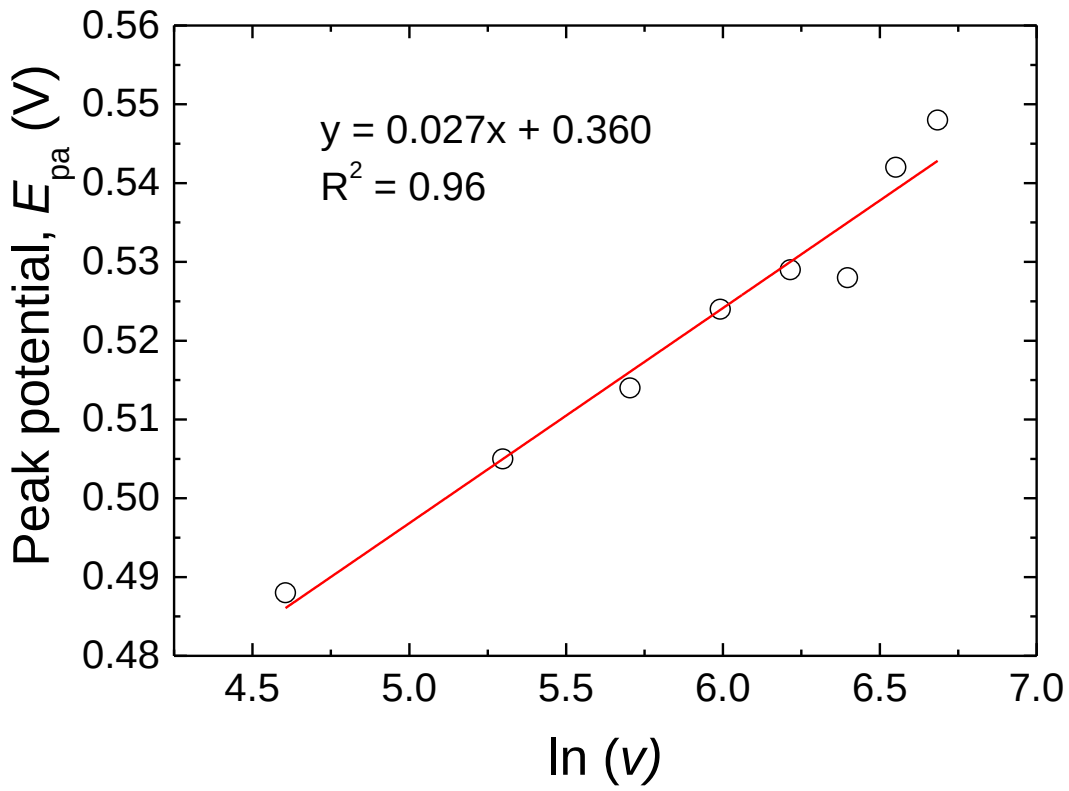

Figure 5. Experimental data (black dots) and linear regression of anodic peak potential (E_{pa}) versus natural logarithm of the scan rate [ln(v)].

4.2.4. Effect of pH

The pH value of the medium generally has great impact on the overall performance of the electrode, with special reference to its sensitivity. The effect of the pH on the redox reaction at the analyte/electrode interface was evaluated by differential pulse voltammetry at different pH values from 3 to 11 in a 0.1 M Britton-Robinson buffer solution.

As shown in Figure 6, the oxidation of TDA at the AuNPs/MWCNTs-CS/GCE surface is dramatically influenced by the pH of the electrolyte solution. In particular, the sensitivity of the electrode for the quantification of TDA reached its maximum at pH 7, which was thereby selected for the following experiments. At the same time, the oxidation potential decreased linearly with increasing pH. One may assume that this behavior is possibly due to the change in phase of AuNPs due to the pH variation. However, looking at the E-pH diagram (also known as a Pourbaix diagram) for Au in aqueous medium, only the Au(s) is expected within the sweet spot defined by the experimental E and pH conditions used in this work (9). Thus, neither ionic nor oxide species formed on the electrode surface. Rather, the decrease in potential following a pH decrease is typical of those reactions in which H^+ ions take part (10). The fact that protons were directly involved in the oxidation of TDA was demonstrated by the linear relationship between the potential (E) and pH and expressed as: E_{pa} (V) = –22.66 pH+624.22. According to the Nernst equation, a slope approaching 59.20/2 indicates an electron-to-proton proportion equal to 2:1 (11). Therefore, because in our study the slope of the regression line is |22.66|≈29.60, one proton every two electrons was involved in the electrochemical oxidation of TDA.

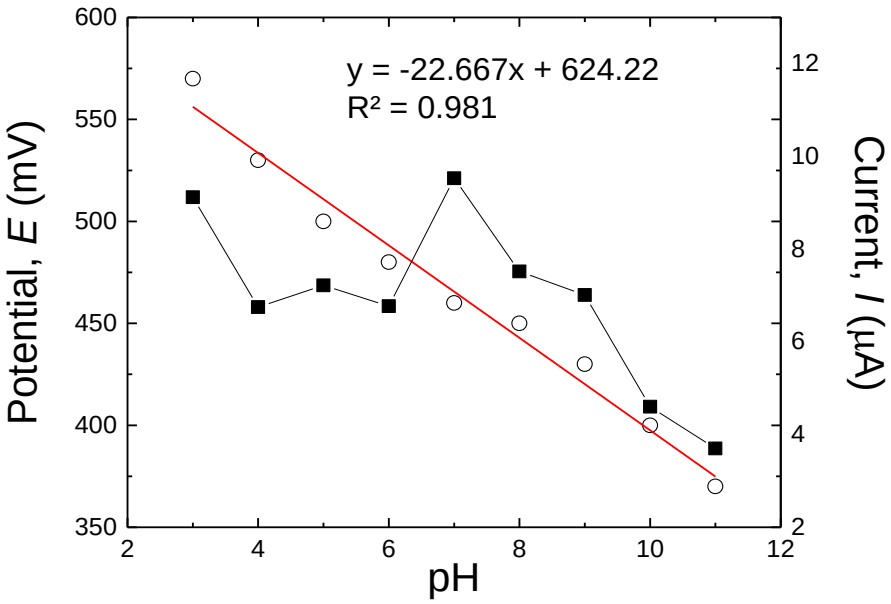

Figure 6. Effect of pH (solution containing 500 µM of TDA in 0.1 M Britton-Robinson buffer) on the anodic peak potential (E, –□–) and current (I, –●–) on the AuNPs/MWCNTs-CS/GCE.

4.2.5. Chronoamperometry measurements

The chronoamperometric investigation was carried out by setting the potential of the AuNPs/MWCNTs-CS/GCE at 570 mV and varying the concentration of TDA in PBS from 0.04 mM to 4.0 mM (Figure 7). The current response (I) for diffusion-limited electrocatalytic processes of electroactive materials (such as TDA) can be described by Cottrell's equation (6):

$$I = \frac{nFAD^{1/2}C_b}{\pi^{1/2}t^{1/2}} \quad (4)$$

where n is the number of electrons (2) exchanged per reactant molecule, F is the Faraday constant (9.648×10^4 C mol^{-1}), A is the geometric area of the electrode (0.0314 cm^2), C_b is the bulk concentration of the analyte (mol cm^{-3}), and D (cm^2 s^{-1}) is the diffusion coefficient of the analyte.

From the raw chronoamperometric traces, a linear curve was obtained for the different concentrations of TDA by plotting I against $t^{-1/2}$ (Figure 7, inset a). By plotting the slope of each individual straight line, the overall slope of the best-fit line (Figure 7, inset b) can be defined from equation 4 as

$$It^{1/2} = \frac{nFAD^{1/2}C_b}{\pi^{1/2}} \quad (5)$$

D can be thus drawn from

$$D = \frac{(slope)^2\pi}{(nFAC_b)^2} \quad (6)$$

The average diffusion coefficient (D) of TDA was eventually estimated to be 6.47×10^{-4} cm^2 s^{-1}.

Chronoamperometry was also used to calculate the catalytic rate constant (k) for the chemical reaction between TDA and AuNPs/MWCNTs-CS/GCE, according to the following equation (12):

$$\frac{I_{cat}}{I_l} = \gamma^{1/2}\left[\pi^{1/2}erf\left(\gamma^{1/2}\right) + exp\frac{(-\gamma)}{\gamma^{1/2}}\right] \quad (7)$$

where I_{cat} is the catalytic current of TDA at the AuNPs/MWCNTs-CS/GCE surface, I_l is the limited current in the absence of TDA, and $\gamma = kC_bt$ is the argument of the error function (C_b is the bulk concentration of TDA). For $\gamma > 2$, the error function ≈ 1. The above equation can thus be written as

$$\frac{I_{cat}}{I_l} = \gamma^{1/2}\pi^{1/2} = \pi^{1/2}(kC_bt)^{1/2} \quad (8)$$

Using eq. 8, k can be calculated from the slope of the I_{cat}/I_l vs. $t^{1/2}$ plots for the different TDA concentrations (Figure 7, inset c). Accordingly, the average value of k was calculated to be 3.01×10^4 M^{-1} s^{-1}.

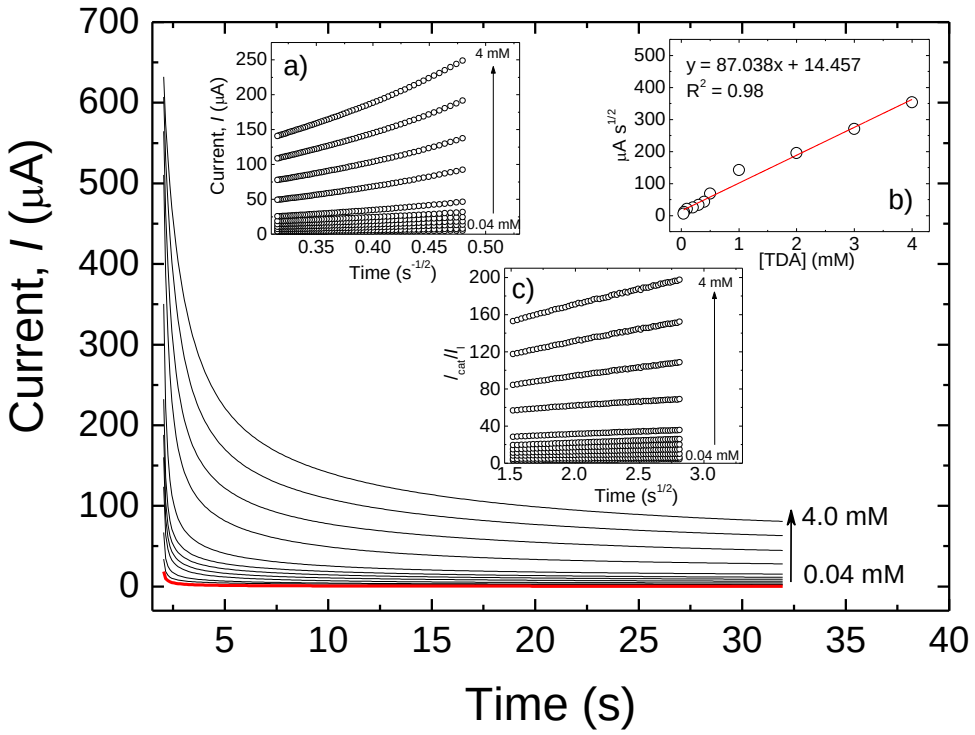

Figure 7. Chronoamperograms obtained at AuNPs/MWCNTs-CS/GCE in PBS (pH 7.0) for different concentrations of TDA (0.04–4.0 mM) of TDA. The red-marked chronoamperogram is the blank (i.e., obtained in the absence of TDA). Insets: (a) Plots of I vs. $t^{-1/2}$ obtained from the chronoamperograms (TDA concentration 0.04–4.0 mM). (b) Plot of the slope of the straight lines against TDA concentration. (c) Dependence of I_{cat}/I_l on $t^{1/2}$ derived from the chronoamperograms (TDA concentration 0.04–4.0 mM).

4.2.6. Amperometric tests

The sensitivity of the electrochemical nanosensor was investigated by amperometry. Although differential pulse voltammetry (DPV) could also be used to this scope, amperometry has been proposed as a more effective method due to the way of transfer of the analyte to the electrode surface. In fact, both diffusion and convection occur in amperometry experiments whereas only diffusion applies in the case of DPV. Eventually, this crucial difference allows for a lower concentration of the analyte to be detected, that is, a lower detection limit to be determined (13). Amperometry was thus used to extract the detection limit of TDA and measure the linear range at the surface of the working electrode. Figure 8 shows the amperometric response of the AuNPs/MWCNTs-CS/GCE after the dropwise addition of TDA at different concentrations (from 0.44 to 819.56 μM) into the 20 mL PBS at a working potential of 570 mV. The current response increased with increasing the TDA

concentration according to a linear relationship that specifically applied for two wide concentration ranges, i.e., 0.44–53.60 μM (Figure 7, panel a) and 53.60–819.56 μM (Figure 7, panel b).

Noticeably, the current response of the electrode held stable for ~ 1300 s (Figure 7, panel c) regardless of the concentration of TDA, demonstrating that both TDA and TDA's oxidation products did not adsorb on the surface of the electrode. This fact can be explained considering the use of MWCNTs and AuNPs, which are well-known for their antifouling properties (14). In addition, the observed stability clearly indicates that neither the solvent (PBS) nor the agitation impaired the modification of the bare electrode during the 1200 s time frame.

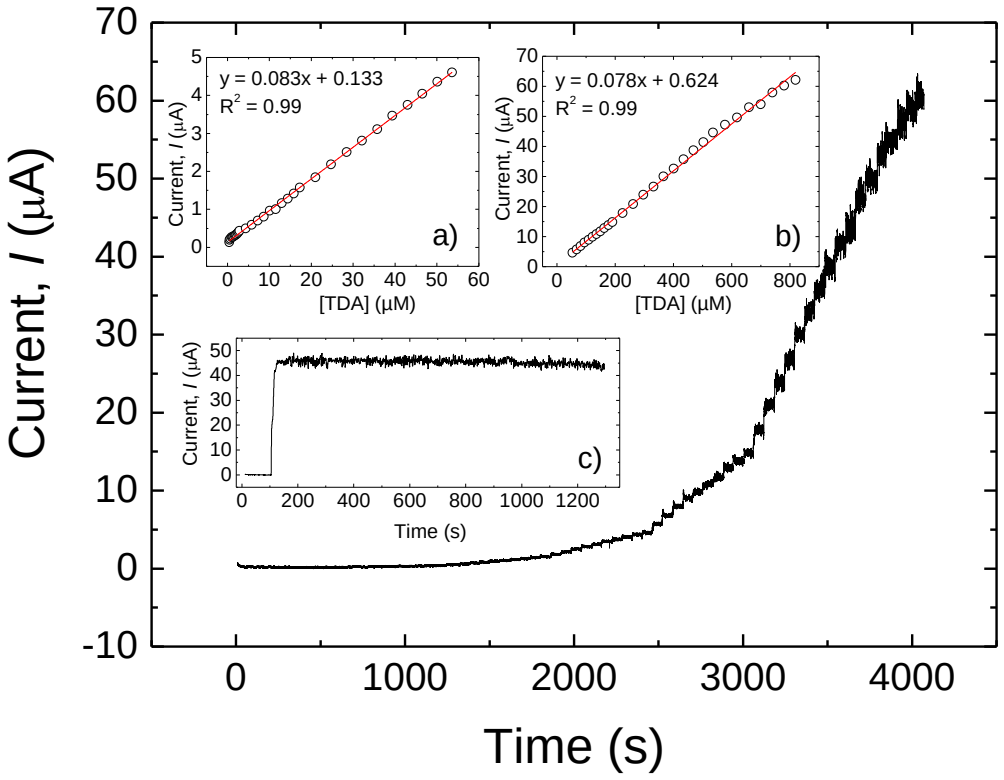

Figure 8. Amperometric response at the rotating AuNPs/MWCNTs-CS/GCE at 570 mV in 20 mL phosphate buffer (pH 7) (TDA concentration 0.44–819.56 μM). The variation of the amperometric current against the TDA concentration is shown in insets (a) (0.44–53.60 μM) and (b) (53.60–819.56 μM). Inset (c) shows the stability of the response of the AuNPs/MWCNTs-CS/GCE for ~ 1300 s (TDA concentration 550 μM).

The sensitivity of the modified electrode for TDA, calculated as the slope of the lower linear range in the amperometric plot, was 0.0835 μA $(\mu M)^{-1}$, from which the limit of detection (LOD) was calculated according to the following equation (15):

$$C_m = \frac{3S_{bl}}{m} \quad (9)$$

where S_{bl} is the standard deviation of the blank response (μA) obtained from 10 replicates of the blank solution (0.001) and m is the slope of the aforementioned lower linear range in the amperometric plot. A final LOD value of 35 nM was eventually calculated for the AuNPs/MWCNTs-CS/GC electrode.

4.2.7. Potential interference of other compounds

In real systems, one of the main issues that can impair the functionality in terms of selectivity of electrochemical sensors is the interference due to electroactive species concomitantly present with the targeted analyte. In our system (PU-based multilayer packaging materials), typical interfering compounds could be represented by other primary aromatic amines and additives commonly included during the manufacturing process (e.g., during extrusion).

In this work, we thus decided to investigate the influence of various substances as potential interfering compounds on TDA determination under optimum conditions at the AuNPs/MWCNTs-CS/GCE surface. The anti-interference ability of the modified electrode was first tested against two other PAAs, that is, aniline and 4,4'-diaminodiphenylmethane (MDA), which were added to the TDA-containing solution in the same concentration (85 μM) as TDA. As shown by the amperometry traces (Figure 9), no increase in the current response was observed for MDA and aniline, indicating that these two amines do not affect the detection of TDA on the AuNPs/MWCNTs-CS/GCE surface. The same procedure was then adopted for two additives widely used as antioxidant and processing stabilizers of polyolefins, i.e., Irganox® 1010 and Irgafos® 168, respectively. Also in this case, the addition of these two additives (85 μM) did not yield any electrochemical signal; that is, their addition did not affect the overall behavior of the AuNPs/MWCNTs-CS/GC electrode toward TDA (Figure 9). These results demonstrate that the developed electrode is appropriate for the selective quantification of TDA.

4.3. Real sample analysis

The suitability of the AuNPs/MWCNTs-CS/GCE as an analytical device for TDA determination in real samples was tested by performing a migration test under typical sterilization conditions (121 °C for 20 minutes). The results on the recovery of TDA determined by amperometry after the addition of TDA in the buffered food simulant B (acetic acid water solution, 3 w/v %) are reported in Table 2. The high recovery (96–110%) suggests that the modified electrode as prepared in this work is well suited for the quantification of PAAs possibly migrating from food packaging materials exposed to extensive thermal treatments (e.g., sous-vide cooking, pasteurizations, and sterilization).

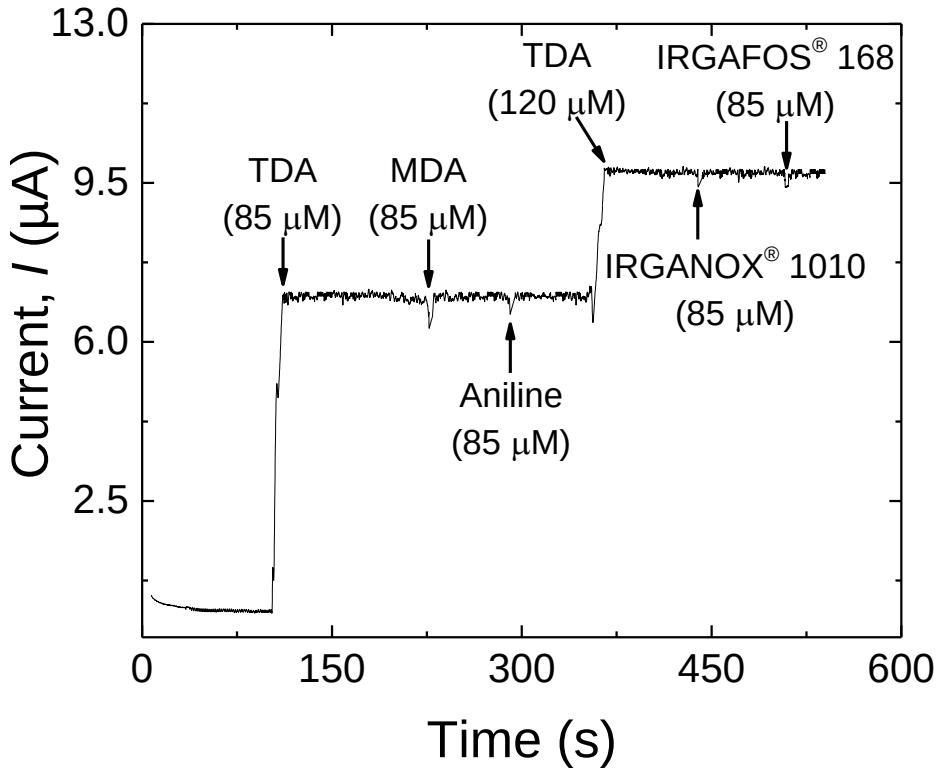

Figure 9. Amperometric trace displaying the current response of the AuNPs/MWCNTs-CS/GC electrode after the sequential addition of the PAAs TDA, MDA, aniline, and the two additives Irganox® 1010 and Irgafos® 168.

Table 2. Amount of added (spiked) and measured TDA at the AuNPs/MWCNTs-CS/GCE surface, with the resulting recovery percentage after the migration test using the acidic food simulant (simulant B) at typical sterilization conditions (121 °C for 20 minutes).

Sample	Spiked (μM)	Found (μM)	Recovery (%)
Laminate structure (PET/EVOH/PE) including a PU adhesive	0	–	–
	15	14.45	96
	30	29.06	96
	50	55.29	110

4.4. Conclusion

We successfully developed a glassy carbon electrochemical sensor for the selective and highly sensitive quantification of TDA, which is one of the two most representative PAAs possibly migrating from multilayer packaging materials made of PU adhesives. The electrocatalytic behavior of the sensor toward TDA revealed the key role of both MWCNTs and AuNPs in increasing the sensitivity of the sensor and decreasing the fouling phenomenon on the surface of electrode. Concurrently, CS

contributed to increase the sensitivity of the sensor due to its electroactive behavior as well as improving the adhesion of the MWCNTs on the surface of electrode. The best sensitivity of the electrode for TDA was achieved at neutral pH, with an ultimate detection limit of 35 nM. The AuNPs/MWCNTs-CS/GCE sensor exhibited high stability over a reasonably extended temporal window without suffering interference. The tests conducted on real samples indicated that the modified sensor allows reliable quantification of TDA, suggesting that this new analytical device can be considered a valid alternative to the most common available analytical techniques for the determination of TDA.

4.5. References

1- European Commission. Commission Regulation (EC) No 10/2011 of 17 January on plastic materials and articles intended to come into contact with food, Official Journal of the European Union (2011). European Union: http://eur-lex.europa.eu/.

2- D. Pezo, M. Fedeli, O. Bosetti, C. Nerín. Analytica Chimica Acta. 756, (2012), 49–59.

3- S. K. Raman Pillai, J. Wang, Y. Wang, M. M. Sk, A. B. Prakoso, Rusli; M. B. Chan-Park. Scientific Reports. 6, (2016), 38453–38465.

4- A. J. Stapleton, R. A. Afre, A. V. Ellis, J. G. Shapter, G. G. Andersson, J. S. Quinton, D. A. Lewis. Science and Technology of Advanced Materials. 14, (2013), 14, 035004–035012.

5- H. Karimi-Maleh, P. Biparva, M. Hatami. Biosensors and Bioelectronics. 48, (2013), 270–275.

6- A. J. Bard, L. R. Faulkner, (2001). Electrochemical Methods: Fundamentals and Applications. United States of America: John Wiley & Sons.

7- S. Erdoğan Kablan, N. Özaltın. Journal of Electroanalytical Chemistry. 785, (2017), 144–151.

8- E. Laviron. Electroanalytical Chemistry and Interracial Electrochemistry. 52, (1974), 355–393.

9- N. Takeno, (2005). Atlas of Eh-pH diagrams: Intercomparison of thermodynamic databases. Japan: National Institute of Advanced Industrial Science and Technology.

10- H. Wang, H. Zhai, Z. Chen, Z. Liang, S. Wang, Q. Zhou, Y. Pan. RSC Advances. 6, (2016), 71351–71359.

11- N. Chen, L. Chen, Y. Cheng, K. Zhao, X. Wu, Y. Xian. Talanta. 132, (2015), 155–161.

12- G. Karim-Nezhad, L. Samandari. Analytical and Bionalytical Electrochemistry. 6, (2014), 545–558.

13- J. Wang, (2001). Analytical Electrochemistry. New Jersey: John Wiley & Sons.

14- B. L. Hanssen, S. Siraj, D. K. Y. Wong. Review in Analytical Chemistry. 35, (2016), 1−28.

15- D. A. Skoog, D. M. West, S. R. Crouch, F. J. Holler, (2014). Fundamentals of analytical chemistry. California: Brooks/Cole, Cengage Learning.

5. CHAPTER 3

Bionanocomposite modified glassy carbon electrode for the determination of 4,4’-methylene diphenyl diamine

In this study, we have initially introduced and described a new bionanocomposite modified electrode based on MWCNTs, chitosan, and gold nanoparticles for electrocatalytic determination of 4,4’-methylene diphenyl diamine (MDA), which is one of the most important PAAs that can migrate form packaging material to the foodstuff. Then, the analytical performance of the sensor is investigated. The results show that a combination of MWCNT, chitosan and AuNPs remarkably improves the current response. Based on our findings the modified electrode has advantages compared to the other analytical methods in terms of repeatability, stability, reproducibility, and technical feasibility for the MDA determination. Full electrochemical characterization of the modified electrode was carried out and the arising electrochemical properties described.

5.1. Experimental part

5.1.1. Preparation of modified electrodes

In order to prepare MWCNTs solution, 0.5 mg of MWCNTs were added into 1 g of EGMe solution and the mixture thereof was treated by ultrasonication to make a homogeneous MWCNTs suspension. Subsequently, 600 µl MWCNTs-EGMe were mixed with 150 µl of chitosan and then were ultrasonicated for 3 minutes to achieve a completely homogeneous MWCNTs-CS suspension. 500 µl of MWCNTs-CS suspension were eventually mixed with 200 µl of gold nanoparticles (AuNPs) and the solution ultrasonicated for 3 minutes to make the suspension homogeneous.

Before applying the bionanocomposite modifier, the GCE surface was polished with alumina abrasive slurry (mean particle size 0.05 µm) on a polishing cloth and then rinsed with double distilled water. To prepare the final "multi walled carbon nanotubes-chitosan-gold nanoparticles modified glassy carbon electrode" (MWCNTs-CS-Au/GCE), 15 µL of MWCNTs-CS-Au solution were placed directly onto the GCE surface and dried with an infrared lamp for 10 minutes. The "multi walled carbon nanotubes-chitosan modified glassy carbon electrode" (MWCNTs-CS/GCE) was made by dropping 15 µl of MWCNTs-CS on the surface of electrode and drying for 10 minutes.

5.2. Results and discussion

5.2.1. Characterization of the MWCNTs-CS-AuNPs composite

Scanning electron microscopy (SEM) was employed to characterize the surface morphology of different electrodes, as shown in Figure 1. MWCNTs were uniformly distributed on the surface of the GCE to form a three-dimensional (3D) network increasing the specific surface area of the electrode (Figure 1a). Figure 1(b) shows the surface of the electrode after modification with MWCNTs-CS. This capacity of chitosan to improve the adhesion of the nanotubes on the surface of the electrode is highlighted. Figure 1 (c) shows a flat surface made of MWCNTs, CS, and AuNPs, the latter hardly visible at the magnification of the analysis and most likely encased within the main biopolymer network.

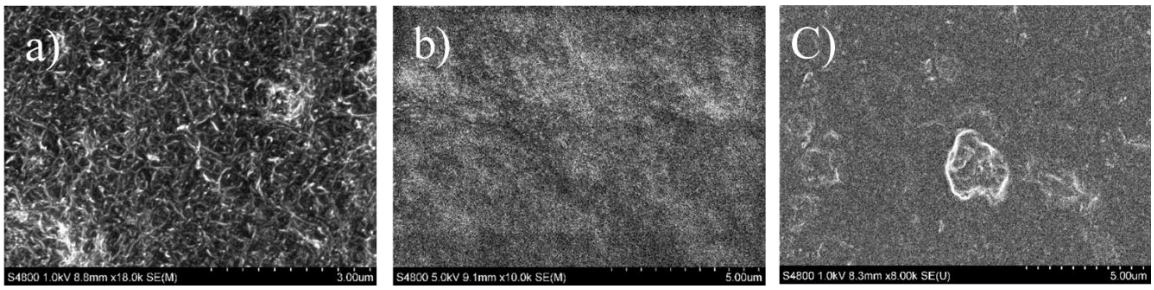

Figure 1. SEM images observed for (a) MWCNTs, (b) MWCNTs-CS and (c) MWCNTs-Cs-AuNPs.

5.2.2. Electrochemical behavior of MDA on MWCNTs-CS-AuNPs/GCE

The electrochemical behavior of the modified electrodes was examined using cyclic voltammetry (CV). The voltammograms of the MWCNTs-CS-AuNPs/GCE (a), MWCNTs-CS/GCE (b), MWCNTs/GCE (c), and bare GCE (d) were obtained in a Britton–Robinson (B–R) universal buffer solution (pH 10) containing 500 µM MDA at 50 mV/s from 0.35 V to 0.8 V. The bare GCE showed a weak oxidation peak with extremely low current (trace a, Figure 2). According to the Figure 2(b), the oxidation peak current increased remarkably after modification with MWCNTs, suggesting that MWCNTs could enhance the electron transfer rate while increasing the electrochemical surface area of the electrode (1). In order to improve the modification of the electrode, in the next step the electrode was modified using a mixture of chitosan and MWCNT. As shown in Figure 2, trace c, the peak current increased dramatically compared to the MWCNTs modified electrode. It was inferred that chitosan could effectively improve the performance of MWCNTs through its film forming ability and good adhesion, resulting in the amplification of the current response (2). Ultimately, in order to upsurge the sensitivity of the sensor, the MWCNT-CS solution was mixed with AuNPs and the electrode was modified with the MWCNT-CS-AuNPs bionanocomposite solution. The final voltammogram showed that the peak current further increased compared to the MWCNT-CS/GCE. The main reasons of this sensitivity increment could be the increase of the conductivity of the electrode by adding gold nano particles to the modifier. The electrocatalytic oxidation characteristics of MDA at different modified electrodes are summarized in Table 1.

Table 1. Comparison of the electrocatalytic oxidation peak current (I_p) of MDA (500 µM) on various electrode surfaces at pH 10.0

Electrode	Oxidation peak current (µA)	Modifier	Drying method
Bare GCE	0.01	-	-
MWCNTs/GCE	14.66	15 µl MWCNTs	IR lamp
MWCNTs-CS/GCE	23.47	15 µl MWCNTs-CS	IR lamp
MWCNTs-CS-AuNPs/GCE	27.50	15 µl (MWCNTs-CS/AuNPs)	IR lamp

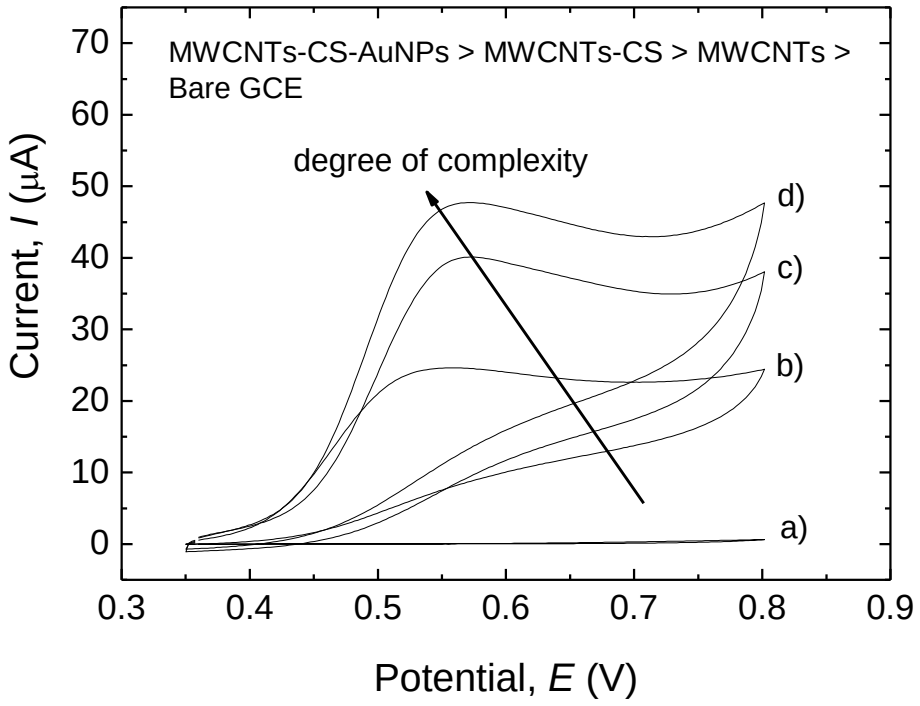

Figure 2. Cyclic voltammograms in B-R buffer (pH 10) at a scan rate of 50 mV/s in the presence of 500 µM of MDA: (a) bare GCE, (b) MWCNTs/GCE, (c) MWCNTs-CS/GCE, (d) MWCNTs-CS-AuNPs/GCE.

5.2.3. Effect of pH value

The effect of the pH on the electrochemical behavior of MDA was studied by CV at the MWCNTs-CS-AuNPs/GCE surface at different pH values (from 2 to 11) in 0.1 M B-R buffer solutions containing 500 µM of MDA (Figure 3).

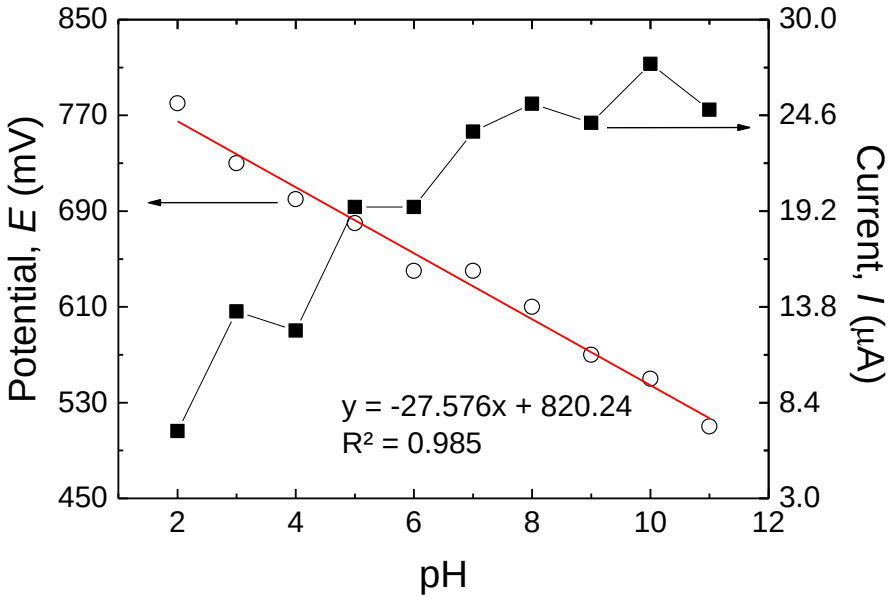

Figure 3. Effect of the pH on the oxidation peak current and oxidation peak potential in a 500 µM of MDA (B-R solution 0.1 M) on the surface of the MWCNTs-CS-AuNPs/GCE.

With increasing the pH value from 2 to 10, the oxidation peak current increased until an apparent steady condition was achieved (Figure 3). It could be inferred that the electrochemical behavior of MDA is pH-dependent and also the sensitivity of the sensor can be improved by increasing the pH. The sensor has the highest sensitivity when the pH of electrolyte is 10 (Figure 3). Moreover, E_{pa} shifted to negative values with increasing the pH, indicating that protons were involved in the oxidation reaction. The linear relationship was established between the oxidation peak potential and the pH value of the solution with the following linear regression equation: $E_{pa} = -27.576x + 820.24$ ($R^2 = 0.985$). The potential negatively shifted by 27.576 mV per pH unit, indicating that one proton per two electrons were involved in the electrochemical reaction.

5.2.4. Electrocatalytic oxidation of MDA at the MWCNTs-CS-AuNPs/GCE

The effect of scan rate (υ) on the electro-oxidation current of MWCNTs-CS-AuNPs/GCE in the presence of MDA was also examined by CV (Figure 4). Figure 4 (inset) shows the dependence of the oxidation peak current (I_p) of 500 µM MDA versus the square root of the potential scan rate ($\upsilon^{1/2}$) in the range of 5–40 mV/s, at the MWCNTs-CS-AuNPs/GCE surface. The plot of the peak current versus the square root of the sweep rate had a linear trend, suggesting that the reaction is diffusion-limited (3).

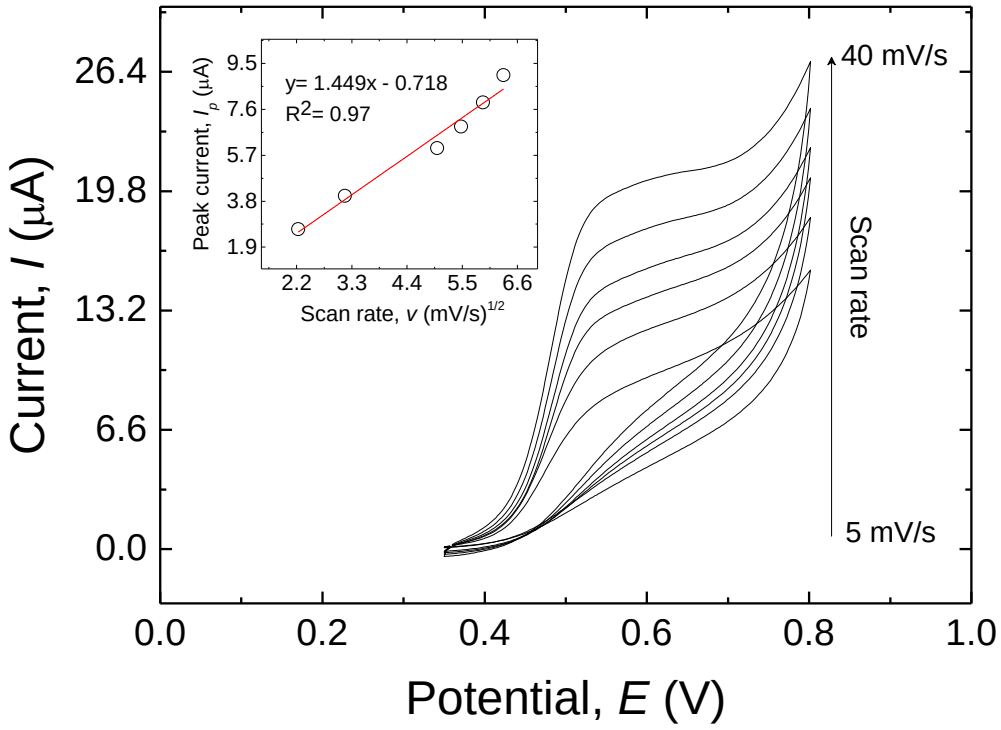

Figure 4. 6 cyclic voltammograms of MWCNTs-CS-AuNPs/GCE in a Britton-Robinson buffer solution (pH 10.0) containing 500 µM MDA at different scan rates (5–40 mV/s). Electrocatalytic peak current (I_p) variation as a function of the square root of sweep rate (inset).

Figure 5 displays the linear sweep voltammograms obtained applying different scan rates (25–40 mV/s) to obtain information on the rate-determining step. The inset of Figure 5 shows the Tafel regions obtained from the linear sweep voltammograms. The average of the Tafel slopes is 11.8 V^{-1} (Figure 5, inset). Referring to equation 1 (4), if the rate-determining step of the electrode process includes one electron transfer, the charge transfer coefficient (α) is 0.50.

$$Tafel_{Slope} = \frac{(1-\alpha)n_{\alpha}F}{2.3RT} \qquad (1)$$

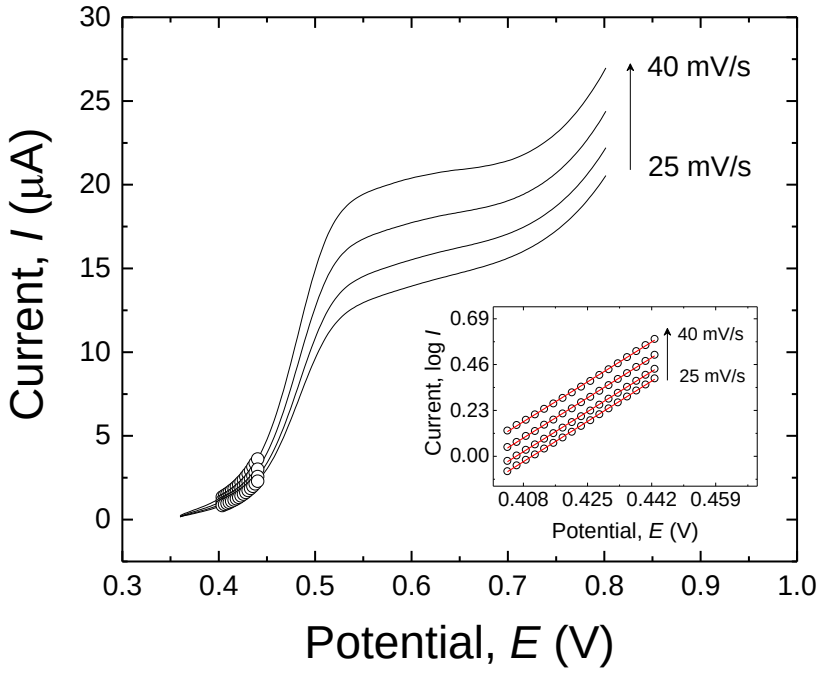

Figure 5. Linear sweep voltammogram of MWCNTs-CS-AuNPs/GCE in a Britton-Robinson buffer solution (pH 10.0) containing 500 µM MDA at 25–40 mV/s. Inset shows tafel plot derived from the linear sweep voltammograms.

By CV, the number of electrons involved in the rate-determining step of the reaction was calculated. E_p-$E_{p/2}$ value was calculated to be 68 mV. This value was then substituted in the following equation to obtain 'n_α' value (5):

$$\left|E_p - E_{p/2}\right| = \frac{47.7}{\alpha \times n_\alpha} \qquad (2)$$

Solving this Eq. (2), the αn_a value is found to be 0.701. Now, for a totally irreversible reaction, the electron transfer coefficient (α) is assumed to be 0.50. Therefore, by substitution of the value of α in the above equation provides the number of electrons to be ca. 1.39 ≈ 1 for the oxidation of MDA.

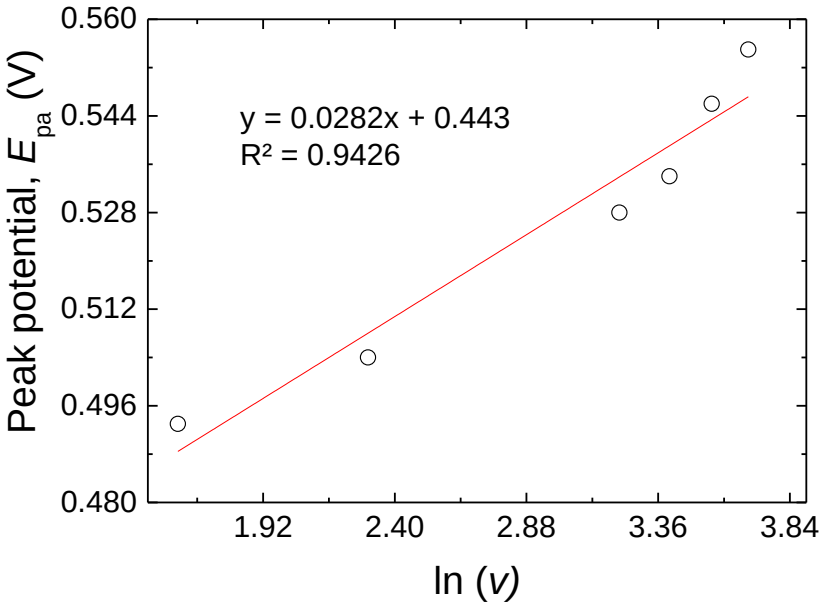

Figure 6. Experimental data (black dots) and linear regression of anodic peak potential (E_{pa}) versus natural logarithm of the scan rate [ln(v)].

In the meantime, a proper linear relationship between the oxidation peak potential (E) and natural logarithm of scan rate (ln) was gained in Figure 6. The equation was: E_p (V) = 0.0282 ln v (mV/s) + 0.443. This phenomenon could be explained by Laviron's theory are the related equation (6):

$$E_{pa} = E^0 + (\frac{RT}{\alpha nF})Ln(\frac{RTK^0}{\alpha nF}) + (\frac{RT}{\alpha nF})Ln\, v \qquad (3)$$

where E° is formal redox potential, T is the absolute temperature, R is the gas constant, n is electron transfer number, α is transfer coefficient , K° is standard rate constant of the reaction, F is the Faraday constant, and v is scan rate. According to the above linear correlation of E_{pa} vs. ln v, the slope is equal to RT/αnF. Thus, the electron transfer number (n) is estimated to be about 1.83 ≈ 2 (α = 0.54, T = 298, R = 8.314, and F = 96.480).

5.2.5. Chronoamperometric Measurements

The electrochemical oxidation of MDA at the surface of MWCNTs-CS-Au/GCE was studied at a potential of 700 mV by chronoamperometry (Figure 7). To measure the diffusion coefficient (D) of MDA at the surface of electrode, different concentrations of MDA were used. MDA diffusion occurs in a diffusion layer located between the electrode surface and the bulk

solution. For an electroactive material with a diffusion coefficient D, the current response under diffusion control is described by the Cottrell equation (4):

$$I = \frac{nFAD^{1/2}C_b}{\pi^{1/2}t^{1/2}} \qquad (4)$$

which can be explicated as:

$$D^{1/2} = \frac{\pi^{1/2}}{nFA} \times m \qquad (5)$$

where D and C are the diffusion coefficient ($cm^2\ s^{-1}$) and the bulk concentration (mol cm^{-3}) of the analyte, respectively. According to the Cottrell equation, the plot of I versus $t^{-1/2}$ is expected to be linear. Fig 7(a) shows the experimental plots with the best straight lines for the different concentrations of MDA employed. The slope values of the resulting straight lines were then plotted versus the concentration of MDA (Figure 7, inset b). The overall slope (33.32 µA $s^{1/2}$ mM^{-1}) was used within the Cottrell equation, to eventually obtain a diffusion coefficient of 9.49×10^{-5} $cm^2\ s^{-1}$.

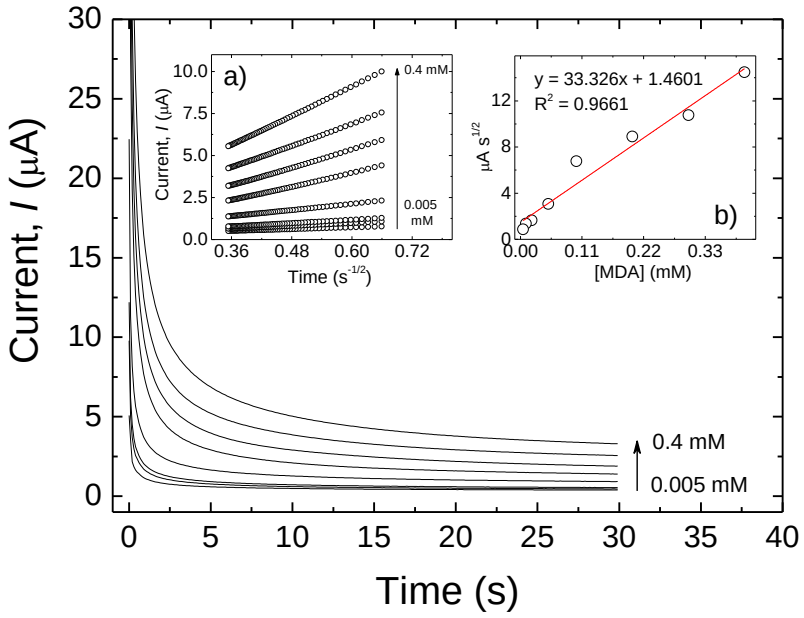

Figure 7. Current response over time of the MWCNTs-CS-AuNPs/GCE in 0.1 M B-R buffer solution (pH 10.0) containing different concentrations of MDA (0.005 – 0.4 mM) by chronoamperometric measurements (potential 700 mV). Numbers 1–8 correspond to the different MDA concentrations. Insets: (a) chronoamperograms of the intensity (I) as a function of the reciprocal square root of time ($t^{-1/2}$); (b) linear plot of the slopes of the eight straight lines in the inset (a) against the MDA concentration.

5.2.6. Amperometric studies of the electrocatalytic oxidation of MDA at the MWCNTs-CS-AuNPs/GCE surface

Amperometry is a well-known technique to be more sensitive with higher accuracy than other voltammetric procedures due to stirring condition of this method (7). Thus, the amperometric i-t response was employed for the detection and determination of MDA using the MWCNTs-CS-AuNPs modified electrode. Figure 8 shows the amperogram obtained for a rotating MWCNTs-CS-AuNPs/GCE, at a fixed potential of 700 mV in a 0.1 M B-R buffer solution (pH 10.0) containing different concentrations of MDA.

As shown in Figure 8, during successive additions of MDA, a well-defined stairs-like current versus time plot was obtained. The calibration plot was linear in three concentration ranges, i.e., 0.49-10.14 µM (Figure 8, inset a), 10.14-94.9 µM (Figure 8, inset b), and 94.9-261.18 µM (Figure 8, inset c) of MDA. The linear least square calibration curve over the latter range had a slope of 0.1509 µA $(\mu M)^{-1}$ (sensitivity) and a correlation coefficient of 0.9982. According to the method mentioned in the reference (8), the lower detection limit, LOD, was obtained to be 20 nM by using the following equation:

$$C_m = \frac{3 \times S_{bl}}{m} \qquad (6)$$

where s_{bl} is the standard deviation of the blank response (µA) obtained from 10 replicates of the blank solution (0.00101), and m is the slope of the calibration plot 0.1509 µA $(\mu M)^{-1}$. The operational stability of MWCNTs-CS-AuNPs/GCE composite modified electrode was further examined by amperometry and the results are shown in inset (d) of Figure 8. The amperometric current response of MDA was almost unchanged when continuously run up to 3310 s in 5 µM MDA containing B-R buffer. This observation shows that, throughout the monitored time span, there was no inhibition effect due to the adsorption of MDA and MDA's oxidation products on the modified electrode surface.

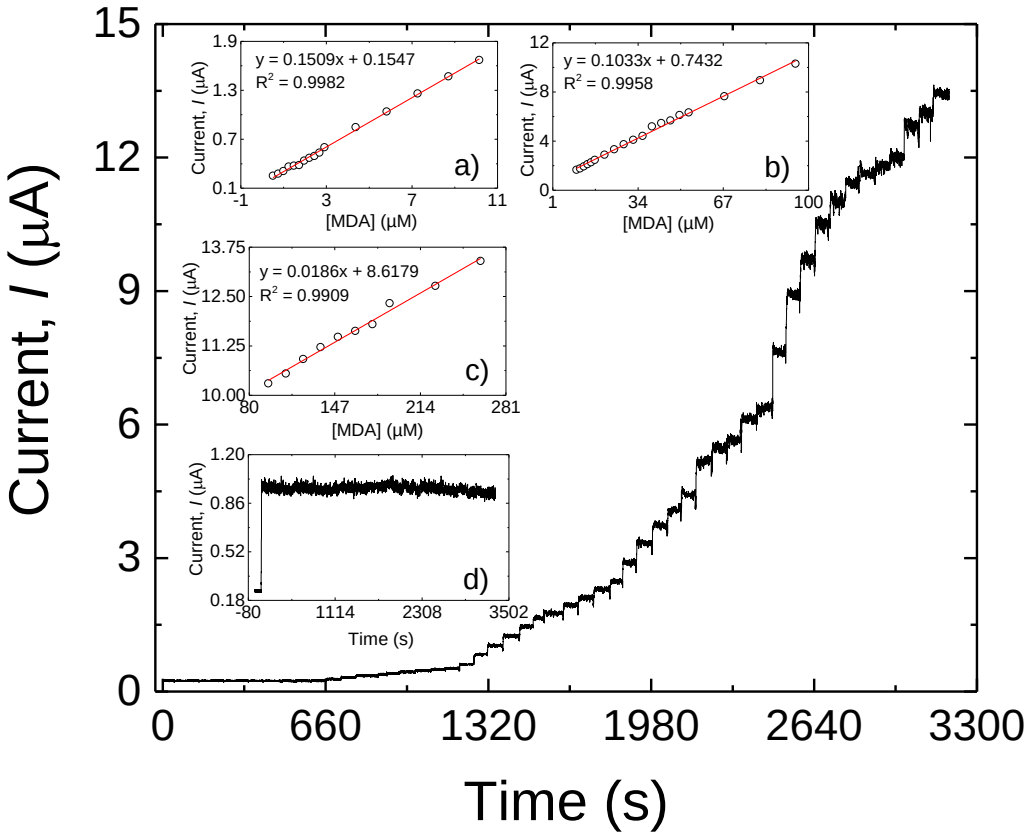

Figure 8. Amperometric responses at a rotating MWCNTs-CS-AuNPs/GCE held at 700 mV in different concentrations of 0.49 to 261.18 µM of MDA. The variation of amperometric current vs. MDA concentration in the range of 0.49–10.14 µM (inset a), 10.14–94.9 µM (inset b) and 94.90–261.18 µM (inset c). Inset d shows the stability of the response of MWCNTs-CS-AuNPs/GCE to 5 µM MDA during 3310 s.

5.2.7. Real sample analysis

In this experiment, we have attempted to determine the MDA concentration that had possibly migrated from the PU-based food packaging material into the food simulant. The food simulant B, i.e. acetic acid 3% (w/v), was used for the analysis because this simulant represents the worst-case scenario to evaluate the PAAs migration. In order to investigate the migration in real samples, a thermos-sealed bag (1 dm^2) was filled with 100 mL of food simulant B, and kept at 121 ˚C for 20 minutes in an autoclave (to simulate typical sterilization conditions), according with the EU regulation n. 10/2011. Then, 10 mL of the sample was diluted with 10 mL B-R buffer solution (0.1 M, pH 10.0) and used for the analysis. The standard addition method was used to evaluate the potential application of the MWCNTs-CS-AuNPs/GCE in real samples by using the recovery method. The range of the recovery was from 98.1 to 101.1%.

These results suggest that the modified electrode as prepared in this work is well suited for the quantification of MDA possibly migrating from food packaging materials exposed to extensive thermal treatments.

Table 2. Amount of added (spiked) and measured MDA at the MWCNTs-CS-AuNPs/GCE surface, with the resulting recovery percentage after the migration test using the acidic food simulant (simulant B) at typical sterilization conditions (121 ˚C for 20 minutes).

Samples	Spiked (µM)	Found (µM)	Recovery (%)
Laminate structure (PET/EVOH/PE) including a PU adhesive	0	-	-
	3.5	3.54	101.1
	5	4.93	98.6
	5.5	5.4	98.1

5.3. Conclusion

A new electrochemical sensor with high level of sensitivity and low limit of detection was developed for the quantification of the MDA which is one of the most important Primary aromatic amines that can migrate from food packaging material into foodstuff. The sensor was developed by use of MWCNTs-CS-AuNPs bionanocomposite to modify surface of electrode. Synergic effect of MWCNTs, chitosan and AuNPs in exhibiting electrocatalytic effect for the electro-oxidation of MDA, was found as the chief factor in the success of the established sensor. By use of cyclic voltammetry the transfer coefficient, α, and the overall number of electrons involved in the catalytic oxidation of MDA at MWCNTs-CS-AuNPs/GCE were determined. The pH dependence of the MDA oxidation is 27.576 mV pH^{-1}. By use of chronoamperometry method the diffusion coefficient of MDA was calculated as 9.49×10^{-5} cm^2 s^{-1}. Finally, in amperometric determination, the limit of detection of MDA was estimated to be in the order of 20 nM and the calibration plot was linear in the ranges of 0.49–10.14 µM, 10.14–94.9 µM and 94.90–261.18 µM.

5.4. References

1. H. Wang, S. Yao, Y. Liu, S. Wei, J. Su, G. Hu. Biosensors and Bioelectronics. 87, (2017), 417–421.
2. Jialei Bai, Xiaoyan Zhang, Yuan Peng, Xiaodi Hong, Yuanyuan Liu, Suiyi Jiang, Baoan Ning, Zhixian Gao. Sensors and Actuators B. 238, (2017), 420–426.
3. Navid Nasirizadeh, Zahra Shekari. Ionics. 20, (2014), 275–285.
4. A. J. Bard, L. R. Faulkner, (2001). Electrochemical Methods: Fundamentals and Applications. United States of America: John Wiley & Sons.Journal of Electroanalytical Chemistry 785 (2017) 144–151
5. Sevilay Erdoğan Kablan, Nuran Özaltın. Journal of Electroanalytical Chemistry. 785, (2017), 144–151.
6. E. Laviron, Adsorption, autoinhibition and autocatalysis in polarography and in linear potential sweep voltammetry, J. Electroanal. Chem. 52 (1974) 355–393.
7. J. Wang, (2001). Analytical Electrochemistry. New Jersey: John Wiley & Sons.
8. D. A. Skoog, D. M. West, S. R. Crouch, F. J. Holler, (2014). Fundamentals of analytical chemistry. United States of America: Cengage Learning.

6. CHAPTER 4

Development of a new electrochemical sensor obtained by electropolymerization of nanocomposite molecularly imprinted biopolymer for determination of 4,4’-methylene diphenyl diamine

The main goal of this investigation was to prepare a new, selective, and sensitive analytical device for determining 4,4’-methylene diphenyl diamine (MDA), which is one of the most important PAAs that can possibly migrate from PU-based multilayer packaging materials to the packaged food. Conductive MWCNTs were used both to increase the surface area of the electrode and to improve its resistance to fouling. We also used the electropolymerization technique to fabricate chitosan molecularly imprinted polymer (MIP) layer on the surface of electrode in order to increase the selectivity of the sensor. The analytical performance of the sensor was thoroughly investigated by differential pulse voltammetry (DPV). The experimental parameters possibly affecting the performance of the MIP sensor were studied and optimized, and the potential application of the developed sensor in real samples was eventually examined by preliminary trials.

6.1. Experimental part

6.1.1. Fabrication of MWCNTs modified GCE

MWCNTs (0.5 mg) was added into 1 g DMF solution and the mixture was ultrasonicated for 3 minutes to form a homogeneous MWCNTs suspension.

A GCE was polished with an Al_2O_3 slurry and then rinsed with doubly distilled water. To fabricate the MWCNTs modified GCE (MWCNT/GCE), 15.0 µL of MWCNTs-DMF solution were placed directly onto the GCE surface and dried with infrared lamp for 10 minutes to form a MWCNTs layer.

6.1.2. Preparation of MIP and non-imprinted modified electrodes

Chitosan powder (0.1 g) was added to hydrochloric acid 1 M (0.52 g) and water (9.38 g). The mixture was then left under stirring for 15 minutes at room temperature. A 10 mM solution of MDA was separately prepared in ethanol. Subsequently, the chitosan solution, MDA, the supporting electrolyte, and water were mixed together to prepare the modifying solution. MIPs were prepared by electrodepositing chitosan and the analyte (MDA) on the surface of the MWCNTs/GCE. The MIP modified electrode, denoted as MIP/MWCNTs/GCE, was prepared by cyclic voltammetry (CV) in the range of -0.5 V to 1.5 V and at a scan rate of 50 mV S^{-1} in the modifying solution. After the electrodeposition, the MIP/MWCNTs/GCE was immersed in an eluent solution to remove the MDA template molecules. A non-imprinted polymer (NIP) sensor, denoted as NIP/MWCNTs/GCE, was prepared similarly to the MIP/MWCNTs/GCE except that the template molecules were absent in the electrodeposition step.

6.2. Result and discussion

6.2.1. Surface Morphology

Scanning electron microscopy (SEM) was allowed to investigate the surface morphology of the electrode modified with MWCNTs (MWCNTs/GCE). Figure 1 shows the MWCNTs on the surface of electrode at two different magnifications. At it can be seen, the nanotubes were evenly distributed throughout the surface of the electrode, thereby contributing to an obvious increase the surface of the electrode exposed to the surrounding medium.

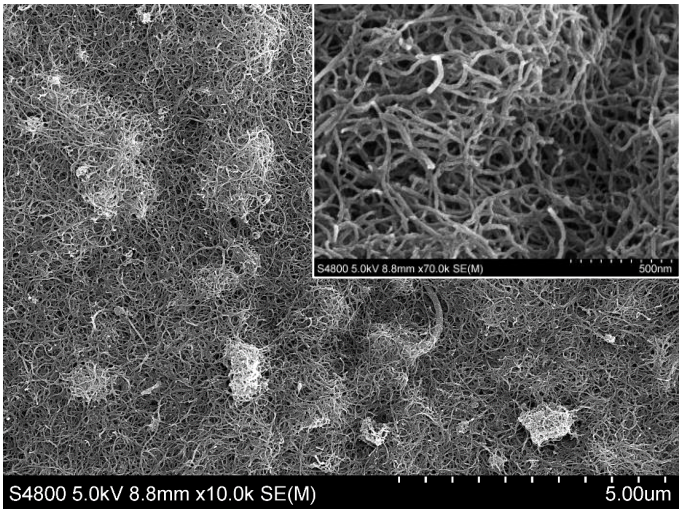

Figure 1. SEM image of multi-walled carbon nanotubes-modified glassy carbon electrode (MWCNTs/GCE). A zoomed area is shown in the inset.

6.2.2. Electrochemical responses

Figure 2 shows the DPV responses of the MIP/MWCNTs/GCE with and without template. An obvious current peak was detected in the presence of the template encased in the main biopolymer network (trace a). However, when the MIP/MWCNTs/GCE was eluted with a solution of ethanol and NaOH, no peak was observed (trace b). This demonstrated that the ethanol-NaOH solution is an efficient solvent for extracting MDA, thus to generate the final MIP structure.

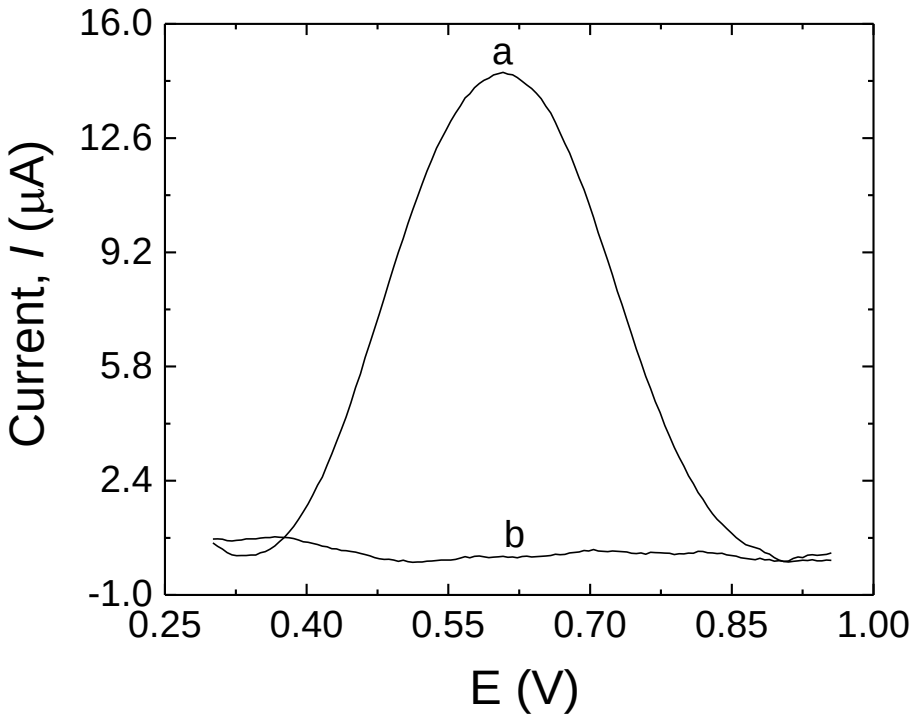

Figure 2. DPV responses of the MIP/MWCNTs/GCE before extraction (trace a) and after extraction (trace b).

The electrochemical behavior of MDA at the MIP/MWCNTs/GCE (a), NIP/MWCNTs/GCE (b), MIP/GCE (c), and bare electrode (d) was investigated by DPV, as shown in Figure 3. The peak current at the modified GCE varied according to the following order: MIP/GCE < bare electrode < NIP /MWCNTs/GCE < MIP/MWCNTs/GCE. MIP/GCE (trace d, Figure 3), which can be explained in terms of fouling occurred during the electropolymerization on the surface of the bare electrode as well as to the low sensitivity to low analyte concentrations of the bare electrode probably due to the low surface area of the electrode. The bare electrode (trace c, Figure 3) showed a peak with higher current compared to MIP/GCE, which could be due to the fact that the electrode was in contact with the analyte for a short time (the electropolymerization was not done in this case). NIP/MWCNTs/GCE (trace b, Figure 3) showed a peak with higher current than the discussed electrodes, which could be attributed to the antifouling effect of MWCNT and also to the high conductivity and high surface area of the nanotubes, which can result in an increased sensitivity the sensor. Furthermore, the peak current at the MIP/MWCNTs/GCE (trace a, Figure 3) is higher than the others, implying that the elution of the analyte occurred succesfully and MDA molecules have extracted from the MIP structure. As a result, cavities were made properly in the MIP structure, which was the reason for the higher performance for this electrode. The nanoporous, templated

structure of MIP helped MDA molecules to migrate easier to the surface of electrode, thus enhancing the analyte oxidation and thereby its detection. These results demonstrate that MWCNTs can amplify the response signal while taking advantage of the imprinting process for the identification of MDA. The electrocatalytic oxidation characteristics of MDA at various electrode surfaces at pH 11.0 are summarized in Table 1.

Table 1. Comparison of the electrocatalytic oxidation peak current (Ip) of MDA (500 µM) on various electrode surfaces at pH 11.0

Electrode	Oxidation peak current (µA)	Modifier
Bare GCE	1.13	-
MIP/GCE	0.01	Cs-MDA electrodeposited
NIP/MWCNTs/GCE	8.05	Cs electrodeposited
MIP/MWCNTs/GCE	29.47	Cs-MDA electrodeposited

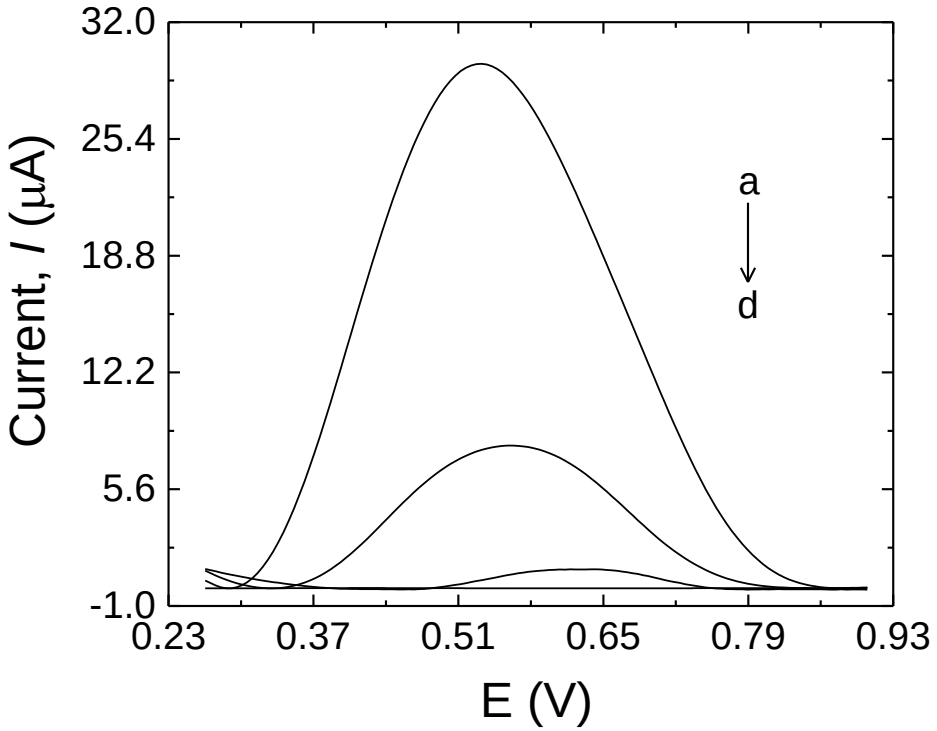

Figure 3. MIP/MWCNTs/GCE (a), NIP/MWCNTs/GCE (b), bare GCE (c), and MIP/GCE (d) in 20 mL B-R buffer (pH 11) containing 500 µM MDA.

6.2.3. Optimization of analytical conditions

6.2.3.1. Effect of scan cycles

Working with MIPs, film thickness is one of the most important parameters to take into account in order to maximize the sensitivity and stability of the sensor (1). More specifically, in the case of too thin imprinted membranes, the main drawback is associated to the low number of imprinted sites can be formed on the surface of electrode. In turn, this may result in low sensitivity of the sensor. Conversely, when the imprinted layer is too thick, low sensitivity of the sensor may be due to two main aspects: i) it is almost impossible to remove the template molecules that are located in the bulk of the membrane; ii) due to the high mass-transfer resistance, accessing the imprinted sites located in the bulk of the membrane is hard for the target analyte. The simplest approach to control the thickness of the polymer membrane is to monitor the number of scan cycles throughout the electropolymerization process (2). In this work, in order to control the thickness of the imprinted film, various scanning cycles (10, 20, 30, and 40) were used for the electrodeposition process. As shown in Figure 4, the peak current response to MDA increased with the cycle numbers, reaching its maximum at 30 cycle numbers. The steeping part of the plot is plausibly due to the progressive increase in the MDA-binding sites, whereas the descending part of the plot might be due to the thick sensing layer with less approachable imprinted sites. Because the peak current response reached its maximum at 30 scanning cycles, this setup was selected to obtain the best performance of the MIP layer (3,4).

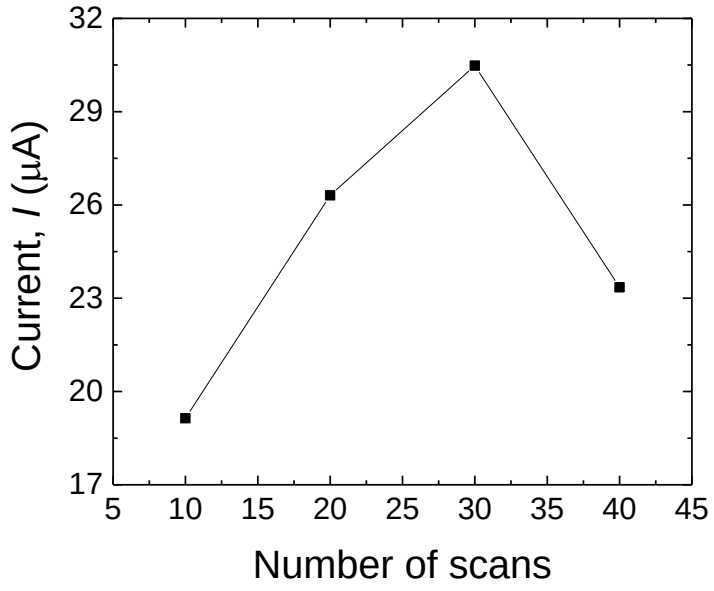

Figure 4. Effect of different number of cycles in electropolymerization process on the anodic peak currents of MDA (500 μM).

6.2.3.2. Effect of elution time

The elution of the template is a crucial step during the MIP formation, as it can directly affect the selectivity and the sensitivity of the sensor by successful removal of the template from the surface of the electrode and making the cavities instead. The template removal was performed in 0.5 M NaOH solution containing 200 µl of ethanol during a period of 2 min, 5 min, 10 min, 15 min, and 20 min. As shown in Figure 5, after 20 minutes the peak current approached zero, which means that almost all of the MDA molecules were removed from the surface of the electrode and the electrode has the highest porosity to be used in the solution containing the target analyte. Therefore, an elution time of 20 minutes was selected in this work.

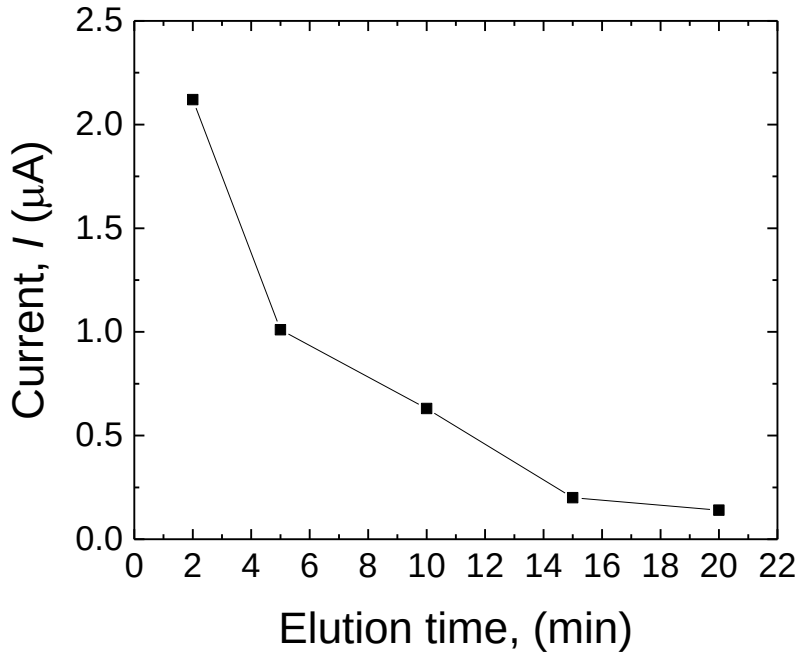

Figure 5. Effect of elution time (2 min, 5 min, 10 min, 15 min, and 20 min) on the current response of the sensor to MDA in the MIP layer.

6.2.3.3. Effect of incubation time

The effect of the incubation time on the response of the sensor toward MDA was investigated with the goal of optimizing the adsorption of the analyte in the MIP layer. To this scope, the modified electrode (after the template extraction) was incubated in 500 µM MDA for 5 min, 10 min, 15 min, 20 min and 30 min. As shown in Figure 6, the peak current progressively increased with prolonged incubation time and achieved its highest value after 20

minutes, indicating that after this period the highest amount of MDA adsorption was achieved. After 20 minutes, the current response tended to decrease slightly, suggesting that the MIP layer approached its saturation. Consequently, the incubation time of the MIP sensor was set at 20 minutes.

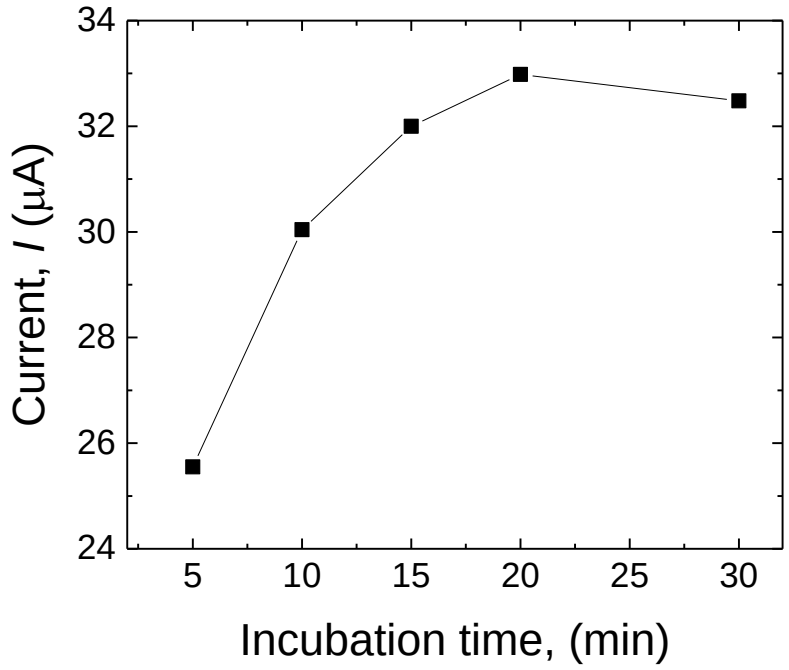

Figure 6. Effect of incubation time (5 min, 10 min, 15 min, 20 min, and 30 min) on the current response of the sensor to MDA (500 μM).

6.2.3.4. Effect of the 'template:biopolymer' molar ratio

The performance of the MIP sensor is also affected by the molar ratio between the template and the biopolymer in the polymerization process (5). The molar ratio of MDA to CS was investigating by varying the MDA:CS molar ratio as it follows: 1:1, 2:1, 2.5:1, 3:1, and 4:1. As shown in Figure 7, the peak current increased as the ratio increased, and a maximum value was reached at 2.5:1, after which the peak current decreased gradually. Based on this result, it can be said that the sensor is less sensitive at lower template concentrations, in agreement with a lower number of recognition sites made in the biopolymer matrix. Concurrently, a low sensitivity was observed for high concentrations of the template, which can be explained considering the tendency of MDA molecules to make a complex, thus reducing the probability for entrapment of the template molecule in the tri-dimensional biopolymer matrix (6).

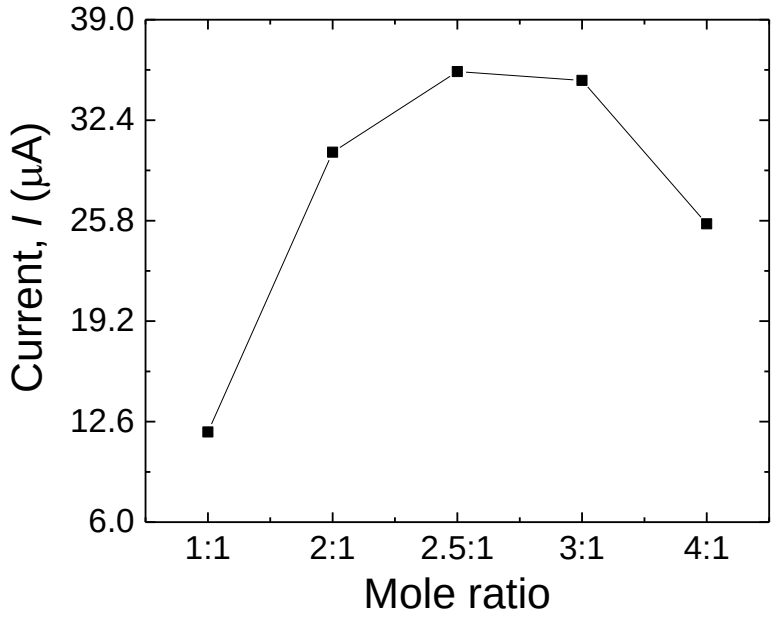

Figure 7. Effect of the 'template:biopolymer' molar ratio during the electropolymerization process on the current response of the sensor to MDA (500 µM).

6.2.3.5. Effect of the pH

One of the most important parameters on the performance of the MIP sensors is the pH, not only because of its influence on the oxidation rate, but also because it may affect both the shape of the target molecules and the function and structure of the imprinted polymer (7). The impact of the pH on the peak potential (E_{pa}) and peak current (I_{pa}) was investigated by DPV using 500 µM ofMDA sin the pH range of 6-11 (Figure 8). As the pH increased from 6 to 10, the peak current of the imprinted sensor increased progressively. Conversely, when the pH changed from 10 to 11, the peak current declined, probably due to the impact of the high pH on the oxidation of MDA on the surface of the modified electrode (8). The linear relationship between Ep and pH can be expressed by the equation: $E_{pa}(V) = -23\ pH+756$. The potential negatively shifts by 23 mV per pH unit, demonstrating that one proton every two electrons was involved in the electrochemical reaction (9).

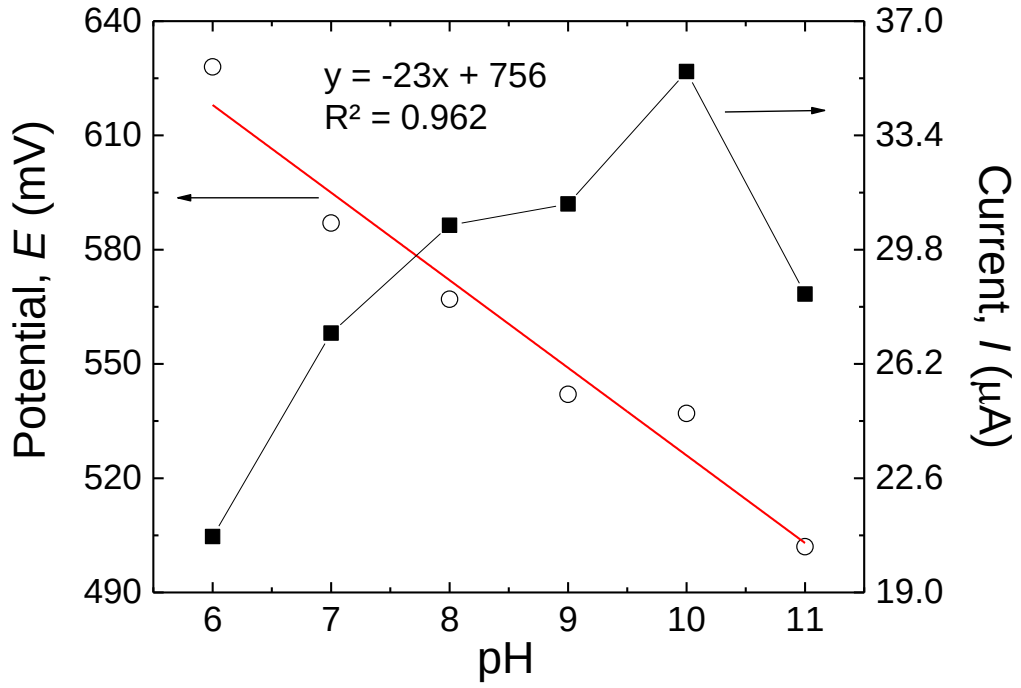

Figure 8. Effect of the pH solution. The pH effects on the anodic peak potentials and currents of 500 µM of MDA in Britton-Robinson buffer solution on the MIP/MWCNTs/GCE

Finally, in order to select the best medium for MDA monitoring, Britton–Robinson buffer (B-R) and phosphate buffer (Na_2HPO_4–NaH_2PO_4) were compared as supporting electrolytes. The best peak shape and higher peak current were gained from the B–R buffer. Hence, the BR buffer solution with pH = 10 was selected as the best electrolyte to achieve the best sensitivity in all the measurements.

6.2.4. Performance of the imprinted MIP/MWCNTs/GCE sensor

6.2.4.1. Sensitivity

The sensitivity of the MIP/MWCNTs modified electrode to MDA was assessed by DPV according to the optimized conditions discussed before. Figure 9a shows that the oxidation peak was centered at +0.53 V and there is a proportional relationship between MDA concentration and the peak current intensity. A linear calibration curve was obtained in the range of 0.5 - 100 µM (Figure 9b) with the following linear regression equation: $I_p = 1.1509 + 0.1956x$ ($R^2 = 0.9982$). The ultimate limit of detection of the sensor was calculated to be 15 nM, according with a method reported by Skoog et al. (10),

$$\mathrm{LOD} = \frac{3 \times \sigma_{\mathrm{bl}}}{\mathrm{m}} \qquad (1)$$

In this equation, σ_{bl} is the standard deviation of the blank response (μA), which is 0.001 in this case; and m is the slope of the calibration plot (0.1956 μA μM^{-1}).

Another important parameter that is used to describe the analytical performance of the electrode is the imprinting factor (IF), which shows the recognition performance of the imprinted sensor. This factor can be calculated by the fitting parameters of I_{pm}.

$$IF = \frac{I_{pm}\ (MIP)}{I_{pm}\ (NIP)} \quad (2)$$

where I_{pm} (MIP) is the peak current of the MIP/MWCNTs/GCE toward the analyte, and I_{pm} (NIP) is related to the NIP/MWCNTs/GCE. A higher IF means an improved selectivity of the MIP/MWCNTs/GCE. In this experiment IF is equal to 3.66, which shows a high selectivity performance of the MIP. This is another indirect evidence of the presence of cavities on the surface of the electrode (11). According to our literature review, there is only one paper reporting on the measurement of MDA concentration using a graphene-based MIP electrochemical sensor. The linear range and slope of the calibration curve of that sensor were 1-15 μM and 0.0352, respectively. These two values show clearly the advantages of our sensor over the previous work (9).

6.2.4.2. Selectivity and reproducibility

A problem that may occur during the analyte detection by electrochemical sensors in real samples is the interference in the measurement of the target analyte due to other electroactive species. The selectivity of the MIP sensor toward MDA was investigated by assessing the interference of some potential compounds (Aniline, TDA, IRGAFOS® 168, IRGANOX 1010) that may be present in real food packaging samples. The results (data not shown) demonstrated that these compounds had no effect on the MDA measurement.

Successively, in order to check for the reproducibility of the proposed sensor, three different MIP/MWCNTs /GCE sensors were prepared independently and used in the same way for the determination of 50 μM MDA. For three successive runs, the relative standard deviation (RSD) was about 4.13%. This result indicates the satisfactory reproducibility for the proposed electrode.

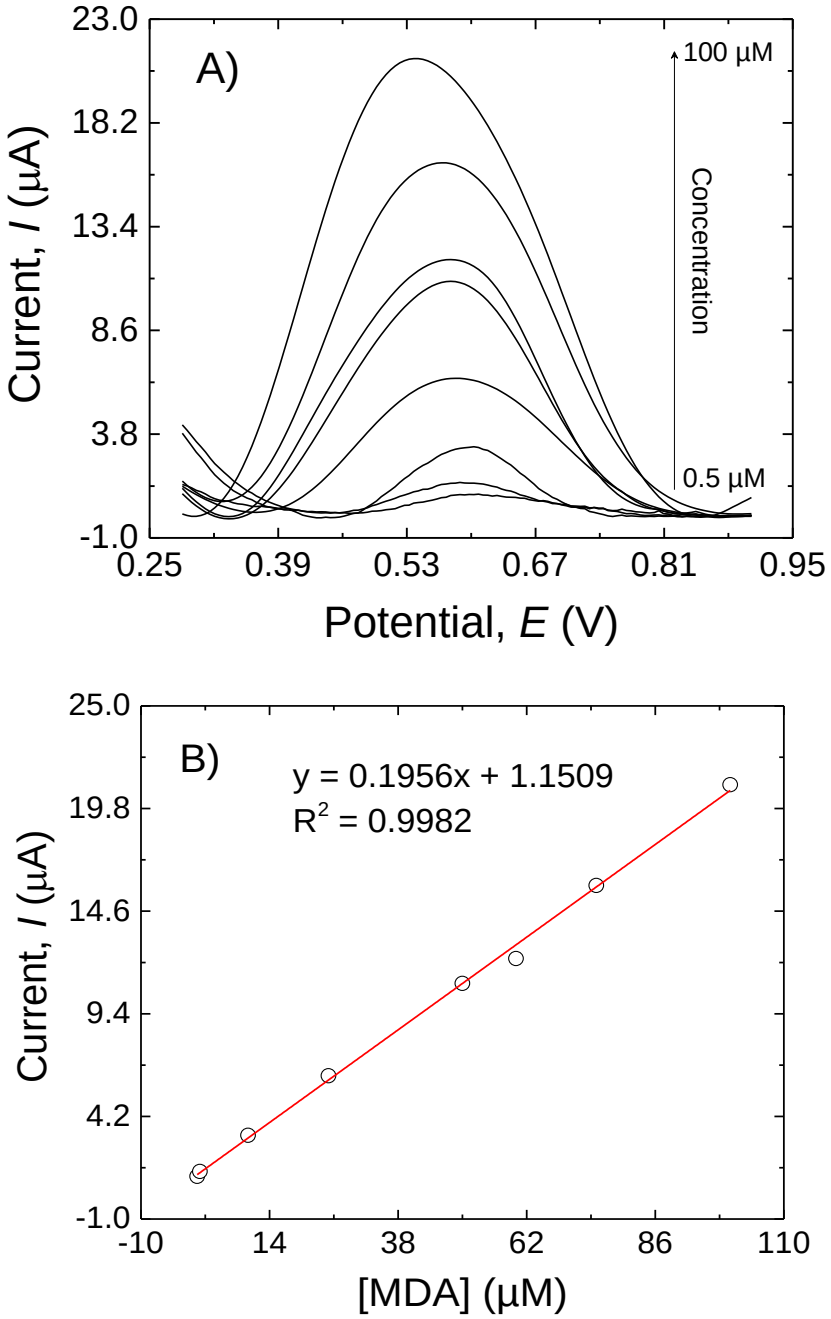

Figure 9. (A) DPV responses of the MIP/MWCNTs/GCE. MDA concentrations: 0.5, 1, 10, 10, 25, 50, 60, 75 and 100 µM. (B) the calibration line of the response peak current vs. the MDA concentration.

6.2.5. Real sample analysis

The practical application of the MIP/MWCNTs /GCE was evaluated by using the modified electrode to determine MDA in real samples. The food simulant B (acetic acid 3% w/v) was used as per legislative provisions for worst-case scenario with PU-based packaging materials

(EU reg. 10/2011). In a first step, a thermos-sealed bag (1 dm^2) was prepared and subsequently filled with 100 mL of food simulant B. The package was kept at 121 ˚C for 20 minutes. It should be noted that to apply the sterilization conditions, the filled bags were immersed in an autoclave. For the electrochemical measurements, 10 mL of the sample were used for the incubation step. However, no MDA was detected in the sample. Therefore, the standard addition method was used to evaluate the potential application of MIP/MWCNTs/GCE for real applications. The results obtained by the proposed method were certified with the calibration curve of MDA. The results (Table 2) show that the recoveries are in the range of 94.10 to 106.76 %.

Table 2. Amount of added (spiked) and measured MDA at the MIP/MWCNTs/GCE surface, with the resulting recovery percentage after the migration test using the acidic food simulant (simulant B) at typical sterilization conditions (121 °C for 20 minutes).

Samples	Spiked (µM)	Found (µM)	Recovery (%)
Laminate structure (PET/EVOH/PE) including a PU adhesive	0	-	-
	15	15.37	102.46
	30	32.03	106.76
	50	47.05	94.10

6.3. Conclusions

A novel molecularly imprinted electrochemical sensor with high selectivity and sensitivity was proposed. The results showed that the electrode modification with MWCNTs enhanced significantly the surface area and the conductivity of the electrode, resulting in the improvement of the sensitivity of the sensor. The use of the nanoparticles was also beneficial because of their antifouling properties. The electrodeposited MIP layer exhibited excellent electrochemical response due to the excellent film forming ability of CS and also to the bonding of CS to the target molecule. The response of the sensor to the MDA was linear in the concentration range of 0.5 µM– 100 µM, and the calculated LOD was 15 nM. This sensor displayed a low limit of detection, wide linear concentration range, excellent selectivity and satisfactory reproducibility. High recoveries (94.10 to 106.76 %) were obtained with this sensor during the detection of MDA in real samples. As a result, MIP/MWCNTs/GCE is a highly promising device for the monitoring of trace amounts of MDA.

6.4. References

1. H. Wang, S. Yao, Y. Liu, S. Wei, J. Su, G. Hu. Biosensors and Bioelectronics. 87, (2017), 417–421.
2. H. Raoa, M. Chena, H. Ge, Z. Lu, X. Liu, P. Zou, X. Wang, H. He, X. Zeng, Y. Wang. Biosensors and Bioelectronics. 87, (2017), 1029–1035.
3. B. Rezaei, M. Hamedian Esfahani, Ali A. Ensafi. IEEE SENSORS JOURNAL. 16, (2016), 7037–7044.
4. Y. Yun, M. Pan, G. Fang, Y. Yang, T. Guo, J. Deng, B. Liu, S. Wang. Sensors and Actuators B. 238, (2017), 32–39.
5. H. Rao, M. Chen, H. Ge, Z. Lu, X. Liu, P. Zou, X. Wang, H. He, X. Zeng, Y. Wang. Biosensors and Bioelectronics. 87, (2017), 1029–1035.
6. K. Kor, K. Zarei. Talanta. 146, (2016), 181–187.
7. T. Li, T. Yao, C. Zhang, G. Liu, Y. She, M. Jin, F. Jin, S. Wang, H. Shaoa, J. Wang. RSC Advances. 6, (2016), 66949–66956.
8. W.-R. Zhao, T.-F. Kang, L.-P. Lu, F.-X. Shen, S.-Y. Cheng. Journal of Electroanalytical Chemistry. 786, (2017), 102–111.
9. N. Chen, L. Chen, Y. Cheng, K. Zhao, X. Wu, Y. Xian. Talanta. 132, (2015), 155–161.
10. D. A. Skoog, D. M. West, S. R. Crouch, F. J. Holler, (2014). Fundamentals of analytical chemistry. United States of America: Cengage Learning.
11. L. Chen, H.-T. Lian, X.-Y. Sun, B. Liu. Analytical Biochemistry. 526, (2017), 58–65.

7. Conclusions

Controlling and measuring the migration of PAAs from food packaging materials to the packaged food is one of the most critical subjects in the food sector and, more specifically, for food packaging companies and especially converters. Due to the provisions of the current legislation (EU reg. 10/2011), the potential migration of PAAs must be assessed according to the worst foreseeable scenario, that is, in consideration of all the critical steps that the package might undergo before it enters the market. Among these steps, the heat treatments (such as pasteurization and sterilization) have been oftentimes underestimated, while representing a potential route for the formation of PAAs. To make this assessment 'easy-to-access' by all the food packaging players, "updating" the analytical tools for PAAs determination is necessary. Well-established techniques (spectrometric and chromatographic techniques, for example), while robust and sensitive, have some main disadvantages (e.g., high costs, sample preparation, time-consuming operations, need of specialized personnel, etc.) that restrict their use to the academia or highly qualified agencies. Reliable, high sensitive and selective, user-friendly, and cost-efficient tools are sought especially for quality control in the companies' lines.

Electrochemical sensors with wide linear ranges and low limit of detections showed a great potential for the selective detection of primary aromatic amines. Within this PhD project, it has been possible to demonstrate that merging analytical/electrochemical concepts with polymer science theory and nanotechnology schemes in a synergistic way, electrochemical sensors with enhanced sensitivity and, more generally, with outstanding analytical performance were obtained.

8. Materials & Methods

8.1. Reagents

2,4-Diaminotoluene (analytical grade 98%, molar mass 122.17 g mol^{-1}), 4,4′-Diaminodiphenylmethane (analytical grade 98%, molar mass 198.26 g mol^{-1}), Multi walled carbon nanotube (≥98% carbon basis), Gold nanoparticles (5 nm diameter), Chitosan (≥75%, deacetylated), Boric acid (99.99% trace metals basis), Phosphoric acid (85-90%), Acetic acid, Aniline (≥99.5%), and Phosphate buffer solution (pH 7.0) were purchased from Sigma Aldrich (Milan, Italy). Ethylene glycol monomethyl ether (EGMe) was bought from Merck (Milan, Italy). Irgafos® 168 [tris (2,4-ditert-butylphenyl)phosphite] and Irganox® 1010 [pentaerythritol tetrakis(3-(3,5-di-tert-butyl-4-hydroxyphenyl)propionate)] were purchased from BASF (Pontecchio Marconi, Italy). Alumina Powder (type DX, 0.05µm average size) was bought from EMS (Hatfield, PA, U.S.). Britton–Robinson (B–R) universal buffer (0.04 M boric acid, 0.04 M acetic acid and 0.04 M phosphoric acid) was prepared in deionized water.

8.2. Apparatus and methods

Electrochemical experiments were performed at 25 ± 0.5 °C using a PGSTAT 302N potentiostat (Metrohm, Herisau, Switzerland), equipped with a three-electrode electrochemical cell mounting a modified glassy carbon (working) electrode, a platinum (counter/auxiliary) electrode, and an Ag/AgCl (reference) electrode, all immersed in a double-jacket 80 mL glass cell (Bio-Logic, Claix, France). The software Nova 2.0 was used throughout the electrochemical experiments. pH measurements were performed with a pH-meter BASIC 20 + (Crison Instruments, S.A. Barcelona, Spain). The electrochemical methods that have been used in these analysis were: cyclic voltammetry, differential pulse voltammetry, chronoamperometry and amperometry.

APPENDIX 1

CONFERENCE ABSTRACTS

1. M. Ghaani, N. Nasirizadeh, F. Zare Mehrjardi, S. Farris. (2015). Gallic acid determination by using a novel electrochemical nano-sensor. Innovations in Food Packaging, Shelf Life and Food Safety. 15–17, September, 2015. Erding, Germany.

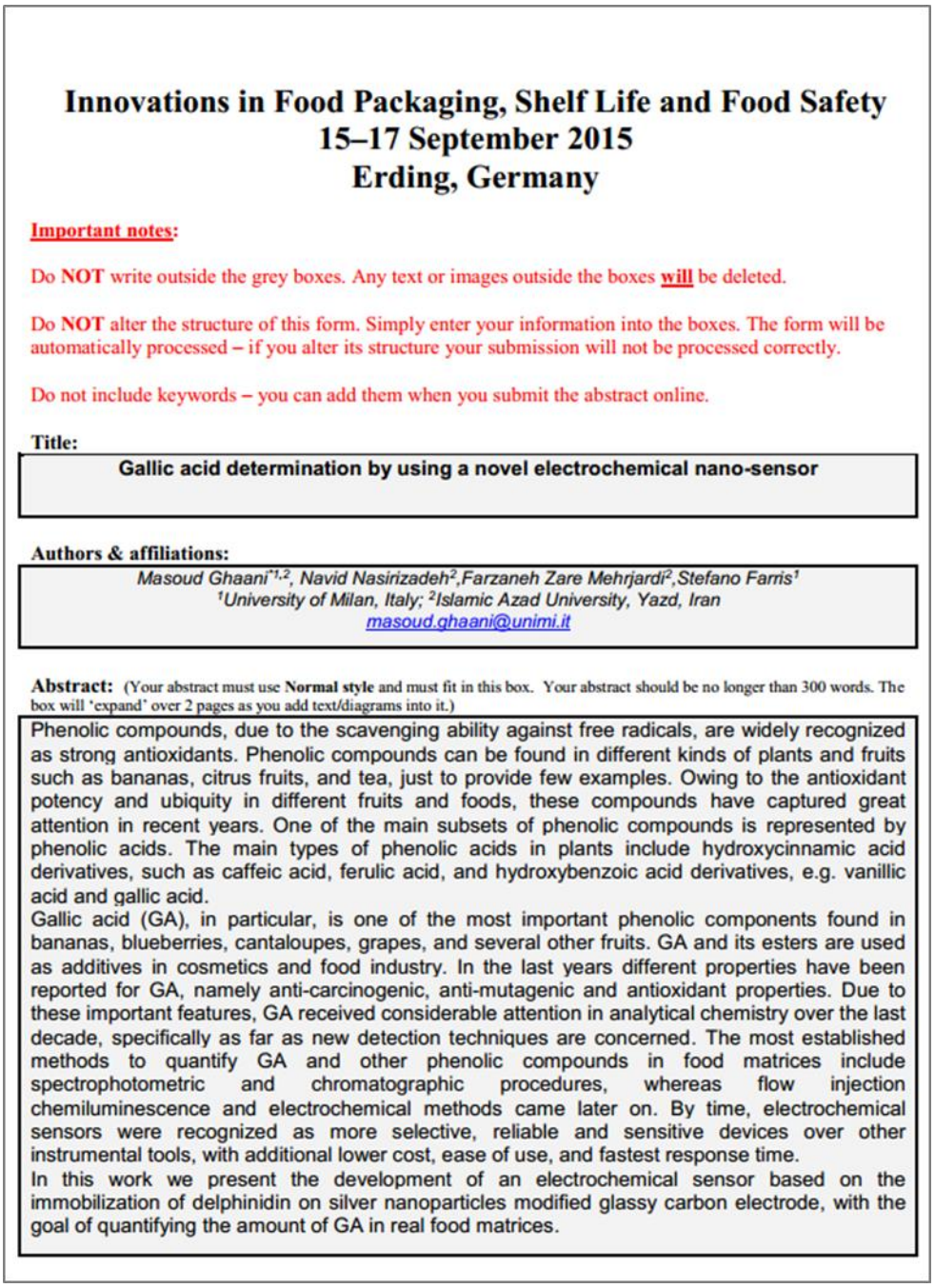

Innovations in Food Packaging, Shelf Life and Food Safety
15–17 September 2015
Erding, Germany

Important notes:

Do **NOT** write outside the grey boxes. Any text or images outside the boxes **will** be deleted.

Do **NOT** alter the structure of this form. Simply enter your information into the boxes. The form will be automatically processed – if you alter its structure your submission will not be processed correctly.

Do not include keywords – you can add them when you submit the abstract online.

Title:

Gallic acid determination by using a novel electrochemical nano-sensor

Authors & affiliations:

*Masoud Ghaani[*1,2], Navid Nasirizadeh[2], Farzaneh Zare Mehrjardi[2], Stefano Farris[1]*
[1]University of Milan, Italy; [2]Islamic Azad University, Yazd, Iran
masoud.ghaani@unimi.it

Abstract: (Your abstract must use **Normal style** and must fit in this box. Your abstract should be no longer than 300 words. The box will 'expand' over 2 pages as you add text/diagrams into it.)

Phenolic compounds, due to the scavenging ability against free radicals, are widely recognized as strong antioxidants. Phenolic compounds can be found in different kinds of plants and fruits such as bananas, citrus fruits, and tea, just to provide few examples. Owing to the antioxidant potency and ubiquity in different fruits and foods, these compounds have captured great attention in recent years. One of the main subsets of phenolic compounds is represented by phenolic acids. The main types of phenolic acids in plants include hydroxycinnamic acid derivatives, such as caffeic acid, ferulic acid, and hydroxybenzoic acid derivatives, e.g. vanillic acid and gallic acid.

Gallic acid (GA), in particular, is one of the most important phenolic components found in bananas, blueberries, cantaloupes, grapes, and several other fruits. GA and its esters are used as additives in cosmetics and food industry. In the last years different properties have been reported for GA, namely anti-carcinogenic, anti-mutagenic and antioxidant properties. Due to these important features, GA received considerable attention in analytical chemistry over the last decade, specifically as far as new detection techniques are concerned. The most established methods to quantify GA and other phenolic compounds in food matrices include spectrophotometric and chromatographic procedures, whereas flow injection chemiluminescence and electrochemical methods came later on. By time, electrochemical sensors were recognized as more selective, reliable and sensitive devices over other instrumental tools, with additional lower cost, ease of use, and fastest response time.

In this work we present the development of an electrochemical sensor based on the immobilization of delphinidin on silver nanoparticles modified glassy carbon electrode, with the goal of quantifying the amount of GA in real food matrices.

2. M. Ghaani, S. Farris. (2016). MIP electrochemical sensor for the quantification of primary aromatic amines. IXth ECNP International Conference on Nanostructured Polymers and Nanocomposites. 19–21, September, 2016. Rome, Italy.

IXth ECNP International Conference on Nanostructured Polymers and Nanocomposites
Rome, Italy, September 19 to 21, 2016

MIP ELECTROCHEMICAL SENSOR FOR THE QUANTIFICATION OF PRIMARY AROMATIC AMINES

Masoud Ghaani, Stefano Farris

DeFENS, Department of Food, Environmental and Nutritional Sciences—Packaging Division, University of Milan, via Celoria 2 – 20133 Milan, Italy (masoud.ghaani@unimi.it; stefano.farris@unimi.it)

Introduction

Molecular imprinting is a process that allows for the synthesis of artificial receptors for a given target molecule based on synthetic polymers [1]. Molecularly imprinted polymers (MIPs) are known as polymer systems produced by the polymerization of a monomer mixture in the presence of both an inert solvent and a template. In many cases, the template is the analyte itself, which originates the imprinted layout after its removal from the polymer network [2]. According to the type of binding interactions (covalent or non-covalent) that occur during pre-assembly, two main approaches can be distinguished. The subsequent step of template removal leaves complementary cavities that, in theory, should be capable of rebinding the template (i.e., the analyte) [3].

Primary aromatic amines (PAAs) are substances that can be transferred from the packaging materials into foodstuffs and are "possibly carcinogenic to humans". All food packaging materials must therefore comply with current legislation limits (10 ng g^{-1} of food). The formation of PAAs from multilayer packaging materials consisting of aromatic polyurethane (PU) adhesives occurs from the reaction between residual isocyanic monomers that have migrated to the surface of the inner layer of the package and water molecules making contact with the same plastic surface [4]. Nowadays, the detection of PAAs occurs through high-cost, sophisticated, and offline analytical methods, especially chromatography and spectroscopy methods. Therefore, finding a sensitive and selective instrument, which is also affordable to detect very low amounts of PAAs, represents a great step forward for packaging companies, especially converters that are directly involved in the lamination process to obtain multilayer packaging structures.

Over the recent years, electrochemistry has attracted much attention as a promising approach for the development of alternative analytical methods. Electrochemical sensors, in particular, seem to open unprecedented possibilities in terms of sensitivity and selectivity over other techniques. A sensor is a device or system that includes control and processing electronics, interconnection networks, and software. Such a sensor responds to a chemical or physical quantity to make an output that is quantifiable and is proportional to the measure. Most sensors include four major components: (1) the receptor, i.e. a sampling area where the surface chemistry occurs; (2) the transducer, i.e. the component able to 'sense' the quantity variation arising from the surface chemistry (e.g., pH change, electron transfer, thermal variation, etc.); (3) signal processing electronics, i.e. all the electronic elements enabling the shift of the raw quantity change into an electronic signal; and (4) a signal display unit, which shows a digital output readily available for the operator (Fig.1) [5]. Electrochemical sensors represent an important subclass of chemical sensors in which an electrode is the transduction element. Such devices hold a leading position among sensors presently available, have reached the commercial stage, and have found a vast range of important applications in the fields of food, clinical, industrial, environmental, and agricultural analyses [6].

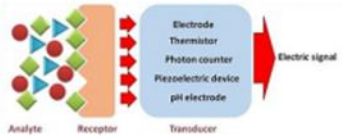

3. M. Ghaani, M. Scampicchio, S. Farris. (2017). Development of an electrochemical sensor for the quantification of primary aromatic amines. MATBIM 2017, 4th international meeting on Material/Bioproduct Interaction. 26–28, April. Porto, Portugal.

MATBIM 2017, 4th international meeting on Material/Bioproduct Interaction
Porto, Portugal, April 26 to 28, 2017

DEVELOPMENT OF AN ELECTROCHEMICAL SENSOR FOR THE QUANTIFICATION OF PRIMARY AROMATIC AMINES

Masoud Ghaani, Matteo Scampicchio, Stefano Farris

DeFENS, Department of Food, Environmental and Nutritional Sciences—Packaging Division, University of Milan, via Celoria 2 – 20133 Milan, Italy (masoud.ghaani@unimi.it; stefano.farris@unimi.it)
Free University of Bolzano, Piazza Università 1– 39100 Bolzano, Italy (matteo.scampicchio@unibz.it)

Introduction

Primary aromatic amines (PAAs) are substances that can be transferred from the packaging materials into foodstuffs and are "possibly carcinogenic to humans". All food packaging materials must therefore comply with current legislation limits (10 ng g^{-1} of food). The formation of PAAs from multilayer packaging materials consisting of aromatic polyurethane (PU) adhesives occurs from the reaction between residual isocyanic monomers that have migrated to the surface of the inner layer of the package and water molecules making contact with the same plastic surface [1]. Nowadays, the detection of PAAs occurs through high-cost, sophisticated, and offline analytical methods, especially chromatography and spectroscopy methods. Therefore, finding a sensitive and selective instrument, which is also affordable to detect very low amounts of PAAs, represents a great step forward for packaging companies, especially converters that are directly involved in the lamination process to obtain multilayer packaging structures.

Over the recent years, electrochemistry has attracted much attention as a promising approach for the development of alternative analytical methods. Electrochemical sensors, in particular, seem to open unprecedented possibilities in terms of sensitivity and selectivity over other techniques. A sensor is a device or system that includes control and processing electronics, interconnection networks, and software. Such a sensor responds to a chemical or physical quantity to make an output that is quantifiable and is proportional to the measure. Most sensors include four major components: (1) the receptor, i.e. a sampling area where the surface chemistry occurs; (2) the transducer, i.e. the component able to 'sense' the quantity variation arising from the surface chemistry (e.g., pH change, electron transfer, thermal variation, etc.); (3) signal processing electronics, i.e. all the electronic elements enabling the shift of the raw quantity change into an electronic signal; and (4) a signal display unit, which shows a digital output readily available for the operator (Fig.1) [2]. Electrochemical sensors represent an important subclass of chemical sensors in which an electrode is the transduction element.

4. M. Ghaani. (2015). Development of nanostructured electrochemical sensors for food packaging applications. 20th Workshop on the Developments in the Italian PhD Research on Food Science Technology and Biotechnology. 23–25, September, University of Perugia, Perugia.

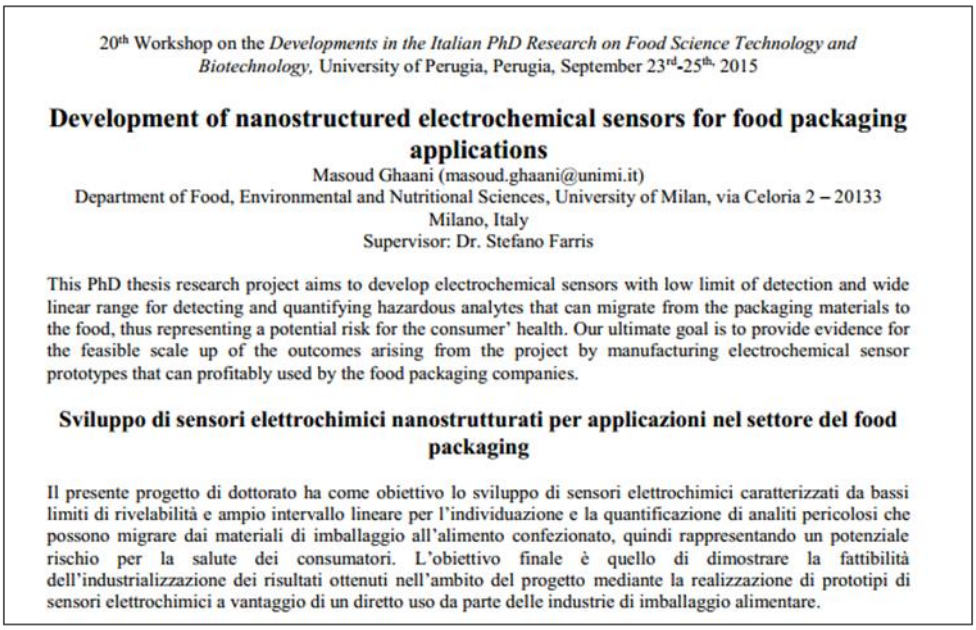

20th Workshop on the *Developments in the Italian PhD Research on Food Science Technology and Biotechnology,* University of Perugia, Perugia, September 23rd-25th, 2015

Development of nanostructured electrochemical sensors for food packaging applications

Masoud Ghaani (masoud.ghaani@unimi.it)
Department of Food, Environmental and Nutritional Sciences, University of Milan, via Celoria 2 – 20133 Milano, Italy
Supervisor: Dr. Stefano Farris

This PhD thesis research project aims to develop electrochemical sensors with low limit of detection and wide linear range for detecting and quantifying hazardous analytes that can migrate from the packaging materials to the food, thus representing a potential risk for the consumer' health. Our ultimate goal is to provide evidence for the feasible scale up of the outcomes arising from the project by manufacturing electrochemical sensor prototypes that can profitably used by the food packaging companies.

Sviluppo di sensori elettrochimici nanostrutturati per applicazioni nel settore del food packaging

Il presente progetto di dottorato ha come obiettivo lo sviluppo di sensori elettrochimici caratterizzati da bassi limiti di rivelabilità e ampio intervallo lineare per l'individuazione e la quantificazione di analiti pericolosi che possono migrare dai materiali di imballaggio all'alimento confezionato, quindi rappresentando un potenziale rischio per la salute dei consumatori. L'obiettivo finale è quello di dimostrare la fattibilità dell'industrializzazione dei risultati ottenuti nell'ambito del progetto mediante la realizzazione di prototipi di sensori elettrochimici a vantaggio di un diretto uso da parte delle industrie di imballaggio alimentare.

5. M. Ghaani. (2016). Development of nanostructured electrochemical sensors for food packaging applications. 21th Workshop on the Developments in the Italian PhD Research on Food Science Technology and Biotechnology. 14–16, September, Portici.

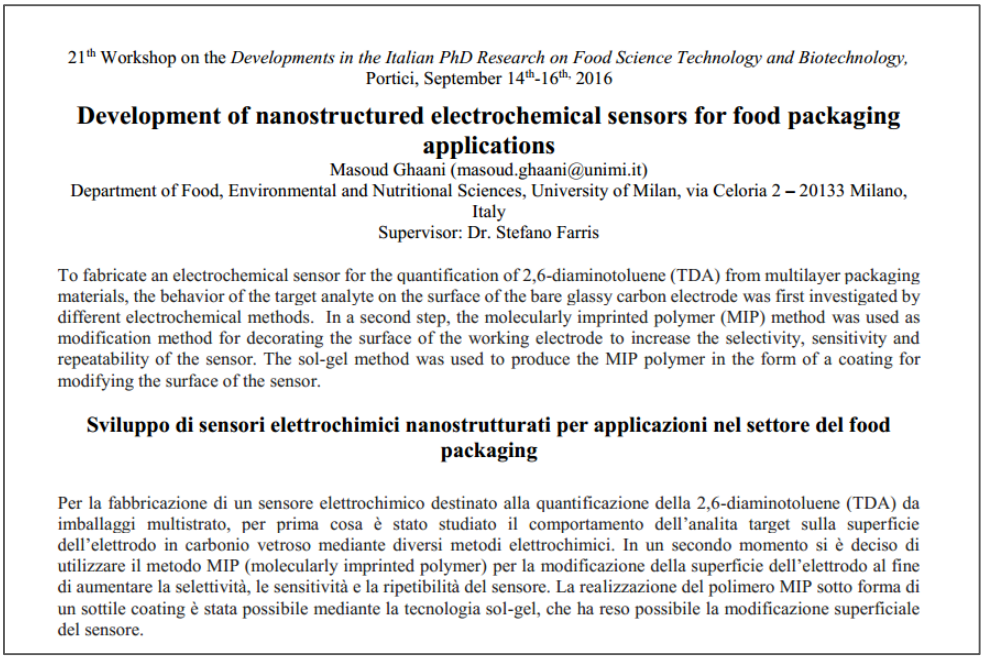

21th Workshop on the *Developments in the Italian PhD Research on Food Science Technology and Biotechnology,* Portici, September 14th-16th, 2016

Development of nanostructured electrochemical sensors for food packaging applications

Masoud Ghaani (masoud.ghaani@unimi.it)
Department of Food, Environmental and Nutritional Sciences, University of Milan, via Celoria 2 – 20133 Milano, Italy
Supervisor: Dr. Stefano Farris

To fabricate an electrochemical sensor for the quantification of 2,6-diaminotoluene (TDA) from multilayer packaging materials, the behavior of the target analyte on the surface of the bare glassy carbon electrode was first investigated by different electrochemical methods. In a second step, the molecularly imprinted polymer (MIP) method was used as modification method for decorating the surface of the working electrode to increase the selectivity, sensitivity and repeatability of the sensor. The sol-gel method was used to produce the MIP polymer in the form of a coating for modifying the surface of the sensor.

Sviluppo di sensori elettrochimici nanostrutturati per applicazioni nel settore del food packaging

Per la fabbricazione di un sensore elettrochimico destinato alla quantificazione della 2,6-diaminotoluene (TDA) da imballaggi multistrato, per prima cosa è stato studiato il comportamento dell'analita target sulla superficie dell'elettrodo in carbonio vetroso mediante diversi metodi elettrochimici. In un secondo momento si è deciso di utilizzare il metodo MIP (molecularly imprinted polymer) per la modificazione della superficie dell'elettrodo al fine di aumentare la selettività, le sensitività e la ripetibilità del sensore. La realizzazione del polimero MIP sotto forma di un sottile coating è stata possibile mediante la tecnologia sol-gel, che ha reso possibile la modificazione superficiale del sensore.

APPENDIX 2

Publications

1- M. Ghaani, N. Nasirizadeh, S. A. Yasini Ardakani, F. Zare Mehrjardi, M. Scampicchio, Stefano Farris. Development of an electrochemical nanosensor for the determination of gallic acid in food. Analytical Methods. 8, (2016), 1103–1110.

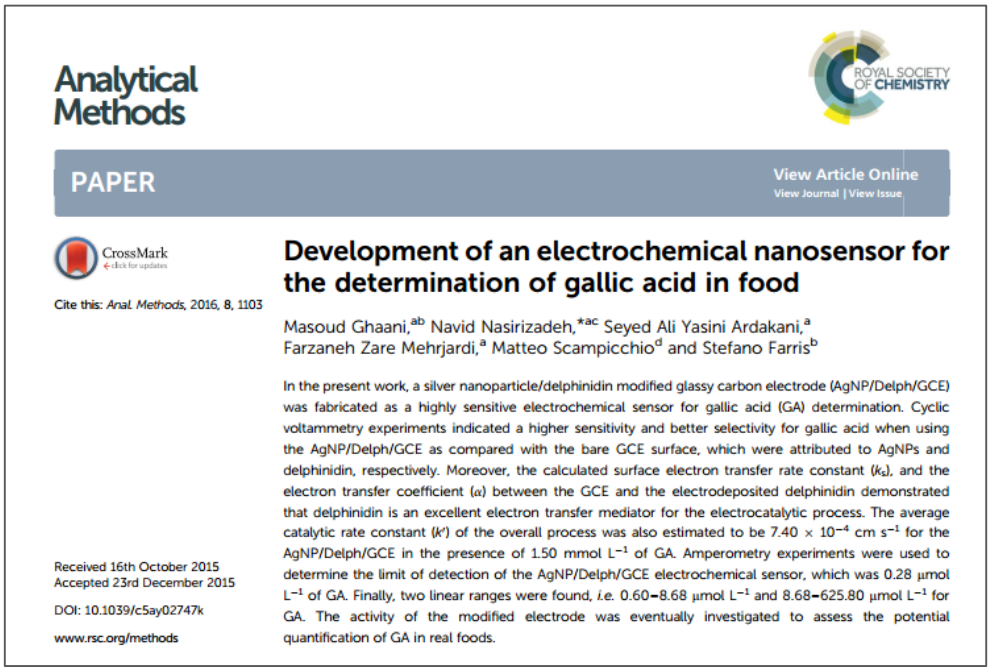

Analytical Methods

PAPER

View Article Online
View Journal | View Issue

CrossMark

Cite this: *Anal. Methods*, 2016, 8, 1103

Development of an electrochemical nanosensor for the determination of gallic acid in food

Masoud Ghaani,[ab] Navid Nasirizadeh,*[ac] Seyed Ali Yasini Ardakani,[a] Farzaneh Zare Mehrjardi,[a] Matteo Scampicchio[d] and Stefano Farris[b]

In the present work, a silver nanoparticle/delphinidin modified glassy carbon electrode (AgNP/Delph/GCE) was fabricated as a highly sensitive electrochemical sensor for gallic acid (GA) determination. Cyclic voltammetry experiments indicated a higher sensitivity and better selectivity for gallic acid when using the AgNP/Delph/GCE as compared with the bare GCE surface, which were attributed to AgNPs and delphinidin, respectively. Moreover, the calculated surface electron transfer rate constant (k_s), and the electron transfer coefficient (α) between the GCE and the electrodeposited delphinidin demonstrated that delphinidin is an excellent electron transfer mediator for the electrocatalytic process. The average catalytic rate constant (k') of the overall process was also estimated to be 7.40×10^{-4} cm s^{-1} for the AgNP/Delph/GCE in the presence of 1.50 mmol L^{-1} of GA. Amperometry experiments were used to determine the limit of detection of the AgNP/Delph/GCE electrochemical sensor, which was 0.28 μmol L^{-1} of GA. Finally, two linear ranges were found, *i.e.* 0.60–8.68 μmol L^{-1} and 8.68–625.80 μmol L^{-1} for GA. The activity of the modified electrode was eventually investigated to assess the potential quantification of GA in real foods.

Received 16th October 2015
Accepted 23rd December 2015

DOI: 10.1039/c5ay02747k

www.rsc.org/methods

2- M. Ghaani, C. A. Cozzolino, G. Castelli, S. Farris. An overview of the intelligent packaging technologies in the food sector. Trends in Food Science and Technology. 51, (2016), 1–11.

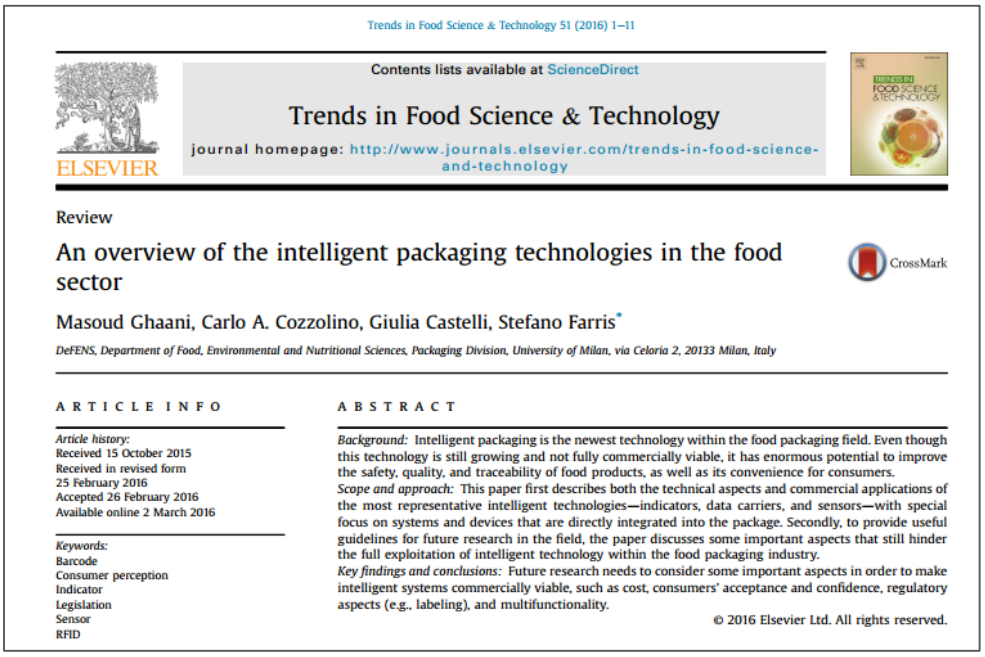

Trends in Food Science & Technology 51 (2016) 1–11

Contents lists available at ScienceDirect

Trends in Food Science & Technology

journal homepage: http://www.journals.elsevier.com/trends-in-food-science-and-technology

Review

An overview of the intelligent packaging technologies in the food sector

Masoud Ghaani, Carlo A. Cozzolino, Giulia Castelli, Stefano Farris*

DeFENS, Department of Food, Environmental and Nutritional Sciences, Packaging Division, University of Milan, via Celoria 2, 20133 Milan, Italy

ARTICLE INFO

Article history:
Received 15 October 2015
Received in revised form
25 February 2016
Accepted 26 February 2016
Available online 2 March 2016

Keywords:
Barcode
Consumer perception
Indicator
Legislation
Sensor
RFID

ABSTRACT

Background: Intelligent packaging is the newest technology within the food packaging field. Even though this technology is still growing and not fully commercially viable, it has enormous potential to improve the safety, quality, and traceability of food products, as well as its convenience for consumers.
Scope and approach: This paper first describes both the technical aspects and commercial applications of the most representative intelligent technologies—indicators, data carriers, and sensors—with special focus on systems and devices that are directly integrated into the package. Secondly, to provide useful guidelines for future research in the field, the paper discusses some important aspects that still hinder the full exploitation of intelligent technology within the food packaging industry.
Key findings and conclusions: Future research needs to consider some important aspects in order to make intelligent systems commercially viable, such as cost, consumers' acceptance and confidence, regulatory aspects (e.g., labeling), and multifunctionality.

3- G. Campanella, M. Ghaani, G. Quetti, S. Farris. On the origin of primary aromatic amines in food packaging materials. Trends in Food Science and Technology. 46, (2015), 137–143.

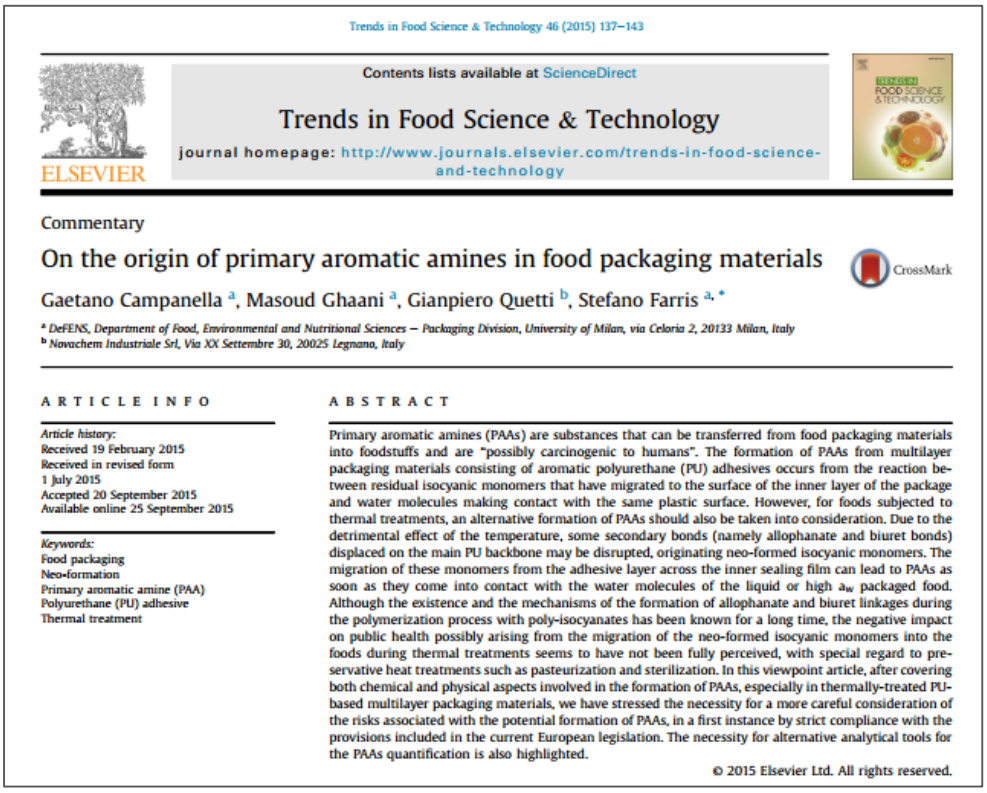

Trends in Food Science & Technology 46 (2015) 137–143

Contents lists available at ScienceDirect

Trends in Food Science & Technology

journal homepage: http://www.journals.elsevier.com/trends-in-food-science-and-technology

Commentary

On the origin of primary aromatic amines in food packaging materials

Gaetano Campanella [a], Masoud Ghaani [a], Gianpiero Quetti [b], Stefano Farris [a, *]

[a] DeFENS, Department of Food, Environmental and Nutritional Sciences – Packaging Division, University of Milan, via Celoria 2, 20133 Milan, Italy
[b] Novachem Industriale Srl, Via XX Settembre 30, 20025 Legnano, Italy

ARTICLE INFO

Article history:
Received 19 February 2015
Received in revised form
1 July 2015
Accepted 20 September 2015
Available online 25 September 2015

Keywords:
Food packaging
Neo-formation
Primary aromatic amine (PAA)
Polyurethane (PU) adhesive
Thermal treatment

ABSTRACT

Primary aromatic amines (PAAs) are substances that can be transferred from food packaging materials into foodstuffs and are "possibly carcinogenic to humans". The formation of PAAs from multilayer packaging materials consisting of aromatic polyurethane (PU) adhesives occurs from the reaction between residual isocyanic monomers that have migrated to the surface of the inner layer of the package and water molecules making contact with the same plastic surface. However, for foods subjected to thermal treatments, an alternative formation of PAAs should also be taken into consideration. Due to the detrimental effect of the temperature, some secondary bonds (namely allophanate and biuret bonds) displaced on the main PU backbone may be disrupted, originating neo-formed isocyanic monomers. The migration of these monomers from the adhesive layer across the inner sealing film can lead to PAAs as soon as they come into contact with the water molecules of the liquid or high a_w packaged food. Although the existence and the mechanisms of the formation of allophanate and biuret linkages during the polymerization process with poly-isocyanates has been known for a long time, the negative impact on public health possibly arising from the migration of the neo-formed isocyanic monomers into the foods during thermal treatments seems to have not been fully perceived, with special regard to preservative heat treatments such as pasteurization and sterilization. In this viewpoint article, after covering both chemical and physical aspects involved in the formation of PAAs, especially in thermally-treated PU-based multilayer packaging materials, we have stressed the necessity for a more careful consideration of the risks associated with the potential formation of PAAs, in a first instance by strict compliance with the provisions included in the current European legislation. The necessity for alternative analytical tools for the PAAs quantification is also highlighted.

4- I. Uysal Unalan, D. Boyacı, M. Ghaani, S. Trabattoni, S. Farris. Graphene oxide bionanocomposite coatings with high oxygen barrier properties. Nanomaterials. 6, (2016), 244–253.

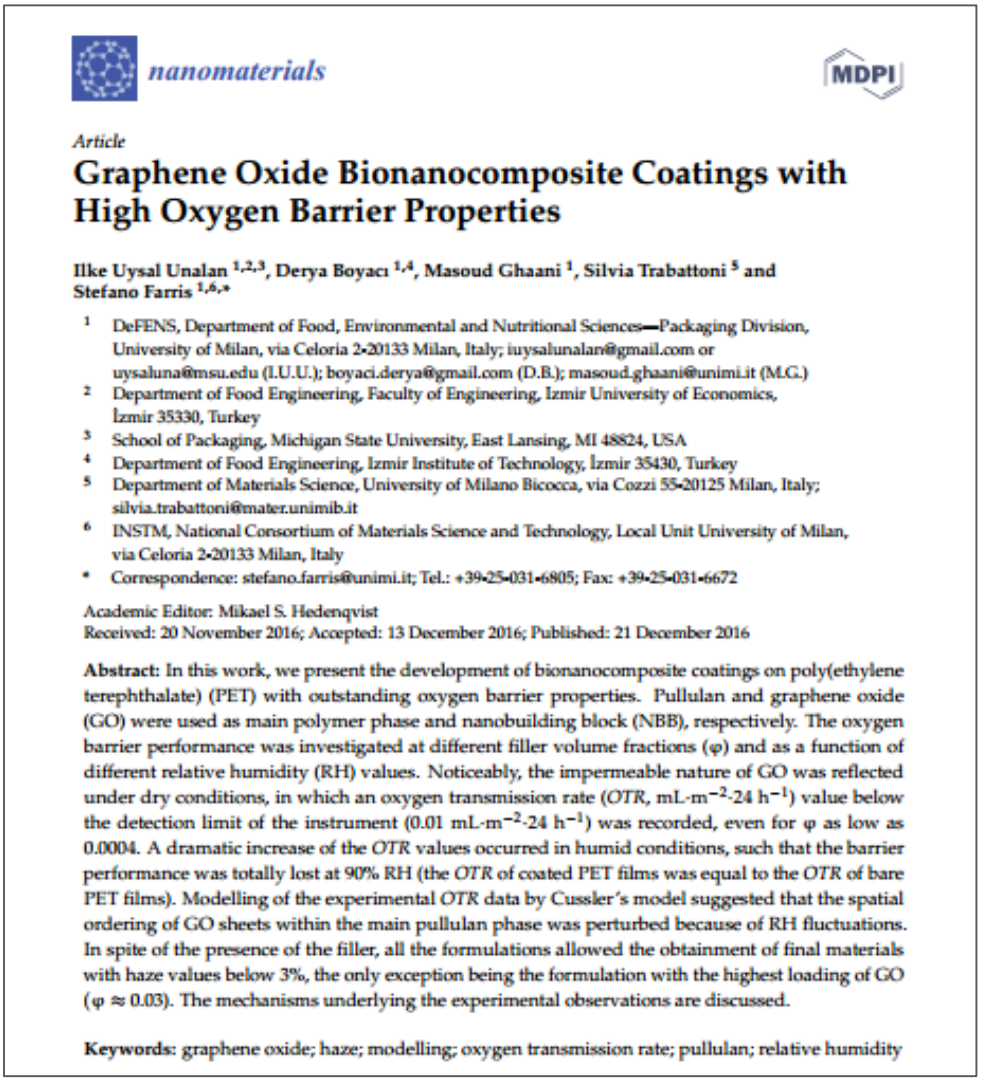

nanomaterials

MDPI

Article

Graphene Oxide Bionanocomposite Coatings with High Oxygen Barrier Properties

Ilke Uysal Unalan [1,2,3], Derya Boyacı [1,4], Masoud Ghaani [1], Silvia Trabattoni [5] and Stefano Farris [1,6,*]

1 DeFENS, Department of Food, Environmental and Nutritional Sciences—Packaging Division, University of Milan, via Celoria 2-20133 Milan, Italy; iuysalunalan@gmail.com or uysaluna@msu.edu (I.U.U.); boyaci.derya@gmail.com (D.B.); masoud.ghaani@unimi.it (M.G.)
2 Department of Food Engineering, Faculty of Engineering, Izmir University of Economics, İzmir 35330, Turkey
3 School of Packaging, Michigan State University, East Lansing, MI 48824, USA
4 Department of Food Engineering, Izmir Institute of Technology, İzmir 35430, Turkey
5 Department of Materials Science, University of Milano Bicocca, via Cozzi 55-20125 Milan, Italy; silvia.trabattoni@mater.unimib.it
6 INSTM, National Consortium of Materials Science and Technology, Local Unit University of Milan, via Celoria 2-20133 Milan, Italy
* Correspondence: stefano.farris@unimi.it; Tel.: +39-25-031-6805; Fax: +39-25-031-6672

Academic Editor: Mikael S. Hedenqvist
Received: 20 November 2016; Accepted: 13 December 2016; Published: 21 December 2016

Abstract: In this work, we present the development of bionanocomposite coatings on poly(ethylene terephthalate) (PET) with outstanding oxygen barrier properties. Pullulan and graphene oxide (GO) were used as main polymer phase and nanobuilding block (NBB), respectively. The oxygen barrier performance was investigated at different filler volume fractions (φ) and as a function of different relative humidity (RH) values. Noticeably, the impermeable nature of GO was reflected under dry conditions, in which an oxygen transmission rate (*OTR*, mL·m^{-2}·24 h^{-1}) value below the detection limit of the instrument (0.01 mL·m^{-2}·24 h^{-1}) was recorded, even for φ as low as 0.0004. A dramatic increase of the *OTR* values occurred in humid conditions, such that the barrier performance was totally lost at 90% RH (the *OTR* of coated PET films was equal to the *OTR* of bare PET films). Modelling of the experimental *OTR* data by Cussler's model suggested that the spatial ordering of GO sheets within the main pullulan phase was perturbed because of RH fluctuations. In spite of the presence of the filler, all the formulations allowed the obtainment of final materials with haze values below 3%, the only exception being the formulation with the highest loading of GO ($\varphi \approx 0.03$). The mechanisms underlying the experimental observations are discussed.

Keywords: graphene oxide; haze; modelling; oxygen transmission rate; pullulan; relative humidity

5- C. Rovera, C. A. Cozzolino, M. Ghaani, D. Morrone, R. T. Olsson, S. Farris. Mechanical behavior of biopolymer composite coatings on plastic films by depth-sensing indentation – A nanoscale study. Journal of Colloid and Interface Science. 512, (2018), 638–646.

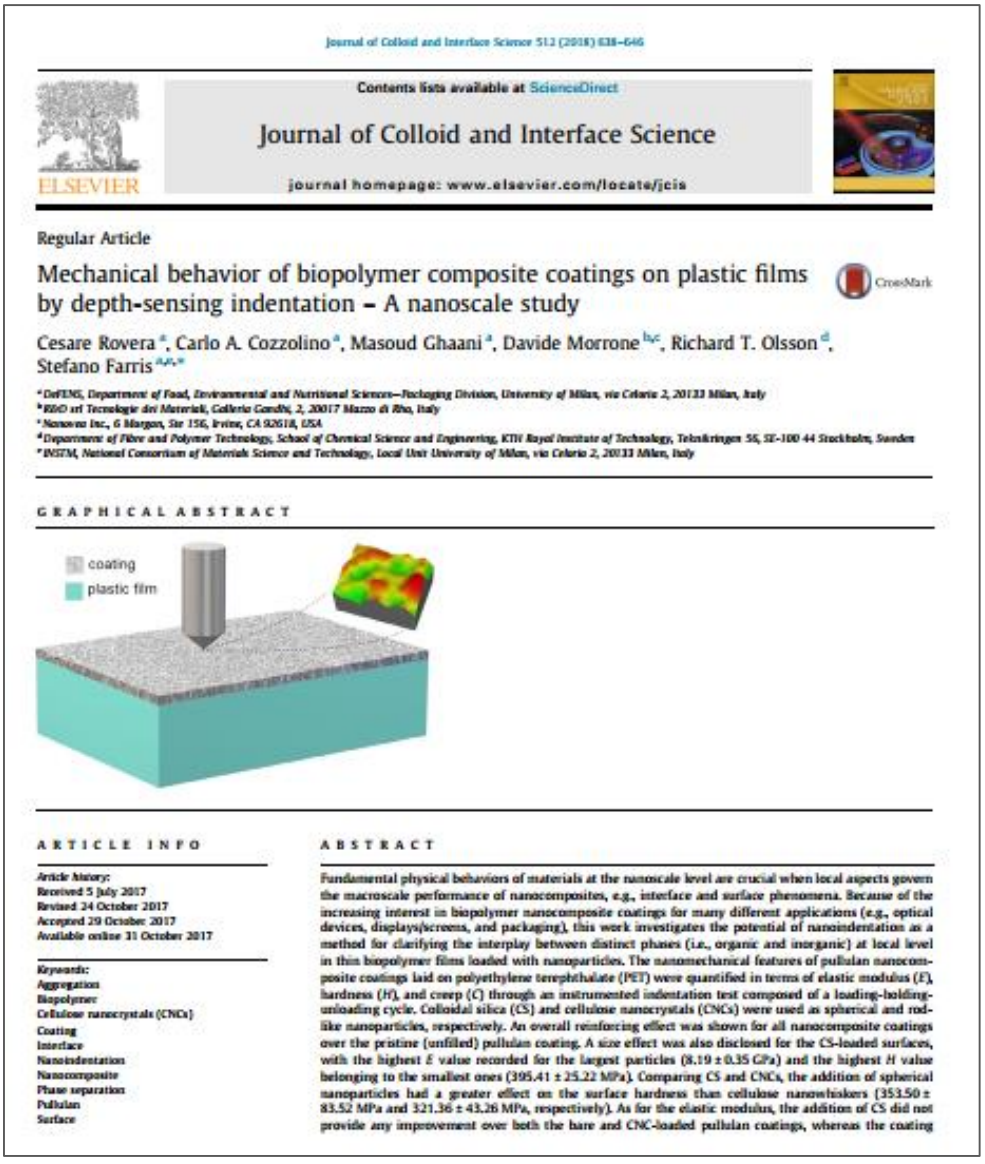

Journal of Colloid and Interface Science 512 (2018) 638–646

Contents lists available at ScienceDirect

Journal of Colloid and Interface Science

journal homepage: www.elsevier.com/locate/jcis

Regular Article

Mechanical behavior of biopolymer composite coatings on plastic films by depth-sensing indentation – A nanoscale study

Cesare Rovera [a], Carlo A. Cozzolino [a], Masoud Ghaani [a], Davide Morrone [b,c], Richard T. Olsson [d], Stefano Farris [a,e,*]

[a] DeFENS, Department of Food, Environmental and Nutritional Sciences—Packaging Division, University of Milan, via Celoria 2, 20133 Milan, Italy
[b] RISD srl Tecnologie dei Materiali, Galleria Gandhi, 2, 20017 Mazzo di Rho, Italy
[c] Nanovea Inc., 6 Morgan, Ste 156, Irvine, CA 92618, USA
[d] Department of Fibre and Polymer Technology, School of Chemical Science and Engineering, KTH Royal Institute of Technology, Teknikringen 56, SE-100 44 Stockholm, Sweden
[e] INSTM, National Consortium of Materials Science and Technology, Local Unit University of Milan, via Celoria 2, 20133 Milan, Italy

GRAPHICAL ABSTRACT

ARTICLE INFO

Article history:
Received 5 July 2017
Revised 24 October 2017
Accepted 29 October 2017
Available online 31 October 2017

Keywords:
Aggregation
Biopolymer
Cellulose nanocrystals (CNCs)
Coating
Interface
Nanoindentation
Nanocomposite
Phase separation
Pullulan
Surface

ABSTRACT

Fundamental physical behaviors of materials at the nanoscale level are crucial when local aspects govern the macroscale performance of nanocomposites, e.g., interface and surface phenomena. Because of the increasing interest in biopolymer nanocomposite coatings for many different applications (e.g., optical devices, displays/screens, and packaging), this work investigates the potential of nanoindentation as a method for clarifying the interplay between distinct phases (i.e., organic and inorganic) at local level in thin biopolymer films loaded with nanoparticles. The nanomechanical features of pullulan nanocomposite coatings laid on polyethylene terephthalate (PET) were quantified in terms of elastic modulus (E), hardness (H), and creep (C) through an instrumented indentation test composed of a loading-holding-unloading cycle. Colloidal silica (CS) and cellulose nanocrystals (CNCs) were used as spherical and rod-like nanoparticles, respectively. An overall reinforcing effect was shown for all nanocomposite coatings over the pristine (unfilled) pullulan coating. A size effect was also disclosed for the CS-loaded surfaces, with the highest E value recorded for the largest particles (8.19 ± 0.35 GPa) and the highest H value belonging to the smallest ones (395.41 ± 25.22 MPa). Comparing CS and CNCs, the addition of spherical nanoparticles had a greater effect on the surface hardness than cellulose nanowhiskers (353.50 ± 83.52 MPa and 321.36 ± 43.26 MPa, respectively). As for the elastic modulus, the addition of CS did not provide any improvement over both the bare and CNC-loaded pullulan coatings, whereas the coating

6- C. Rovera, M. Ghaani, N. Santo, S. Trabattoni, R. Olsson, D. Romano, S. Farris. Enzymatic hydrolysis in the green production of bacterial cellulose nanocrystals. ACS Sustainable Chemistry & Engineering, (Submitted).
7- M. Ghaani, C. Rovera, F. Pucillo, M. R. Ghaani, R. T. Olsson, M. Scampicchio, S. Farris. Determination of 2,4-diaminotoluene by a bionanocomposite modified glassy carbon electrode. ACS Journal of Agricultural and Food Chemistry, (Submitted).
8- M. Ghaani, M. Scampicchio, S. Farris. Bionanocomposite modified glassy carbon electrode for the determination of 4,4'-methylene diphenyl diamine (in preparation).
9- M. Ghaani, M. Scampicchio, S. Farris. Development of a new electrochemical sensor obtained by electropolymerization of nanocomposite gold nanoparticles-molecularly imprinted biopolymer for determination of 4,4'-methylene diphenyl diamine, (in preparation).